EUROPEAN ORGANIZATION FOR NUCLEAR RESEARCH

CERN/SPSC/84-33

SPSC/P200

May 16, 1984

THE LEPTON ASYMMETRY ANALYSER: A PROPOSAL

C. Alberini, M. Basile, J. Berbiers, G. Cara Romeo, L. Cifarelli,
A. Contin, G. D'Ali, C. Del Papa, M.I. Ferrero, D. Galli,
G. Iacubucci, P. Giusti, T. Massam, R. Meunier (*), R. Nania,
F. Palmonari, G. Rinaldi, F. Rohrbach, P. Rotelli,
G. Sartorelli, M. Spinetti, G. Susinno, L. Votano and A. Zichichi

Dipartimento di Fisica dell'Universita', Bologna, Italy
Istituto Nazionale di Fisica Nucleare, Bologna, Italy
CERN, Geneva, Switzerland
Istituto Nazionale di Fisica Nucleare, LNF, Frascati, Italy
Dipartimento di Fisica dell'Universita', Lecce, Italy

(*) Visitor C.E.N.S. - D.Ph.P.E.

ABSTRACT

A proposal to search for new heavy flavours produced in hadronic interactions at the CERN ($p\bar{p}$) Collider is presented.

The proposal is based on the measurement of the $\mu^{\pm}$ asymmetry in the proton and antiproton hemispheres. The sign of this leptonic asymmetry depends on the "up-like" or "down-like" nature of the new flavour. For a given heavy flavour, the sign of the asymmetry changes from the proton to the antiproton outgoing telescopes, thus allowing an important cross-check on the effect looked for.

Cases of simultaneous production of "up-like" and "down-like" new heavy flavours are considered, in addition to the simpler case of only one flavour, either "up-like" or "down-like".

The detailed description of the lepton asymmetry analyser is presented. It is shown that, if new heavy flavours are produced with masses above the present limit of 22 GeV/c^2, the lepton asymmetry should be clearly observable, with the expected integrated luminosity of 10 pb^{-1}, even for cross-section values ten times lower than the QCD extrapolations.

SUMMARY

1. INTRODUCTION

Our ISR studies have shown the importance of the "Leading" effect in hadronic interactions. These studies allow to conclude that the "Leading" effect has to be present, at least with the same strength, at the Collider energies. Using this as a starting point, we propose a new method to search for new heavy flavours carried by baryonic and antibaryonic states, produced in the "Leading" way and decaying semileptonically. For example, if a baryon is produced with "top" flavour, its semileptonic decay will produce an eccess of μ^+ on the outgoing proton side.

This new method is thus based on the measurement of the $\mu^\pm$ asymmetry in the proton and antiproton hemispheres. The sign of the asymmetry depends on the "up-like" or "down-like" nature of the new heavy flavour carried by the barionic state. An important feature of the asymmetry is that in the two hemispheres it has opposite sign.

Several possibilities have been studied in detail: for example, we have assumed, for the "top" mass, two values : 25 GeV/c^2 and 35 GeV/c^2. The asymmetry varies with p_T, according to the mass difference between the new heavy flavour and its nearest decay state. For the "top" case, the nearest state is "beauty".

On the other hand, the Collider energy opens a region of masses which could belong to heavy flavours above the third family. According to the present trend, the lightest state of the fourth family is expected to be "down-like". How far is away this new heavy flavour from the "top" mass is crucial for the $\mu^\pm$ asymmetry produced by the "top" and for its p_T dependence. Thus, we have studied the case where "top" and the "down-like" member of the fourth family ("superbeauty") are both produced. A specific case has been considered with "superbeauty" mass at 55 GeV/c^2 and "top" at 25 GeV/c^2.

The main parameters of the new method are the cross-section values for the production of the "Leading" baryons (antibaryons) and the background level. Both points have been studied to the best of present knowledge.

It turns out that the $\mu^{\pm}$ asymmetry looks a very powerful tool to investigate the existence of new heavy flavours and to establish their "up-like" or "down-like" nature.

The muon detector, positioned behind the forward/backward UA2 calorimeter consists of an iron hadron filter, tracking chambers, a system of Limited Streamer Tubes for triggering, and a 3.0 Tm iron toroid. The detector covers the full azimuthal angle in the polar angle intervals $5^{\circ} \leq \theta \leq 30^{\circ}$ and $150^{\circ} \leq \theta \leq 175^{\circ}$.

Muons are separated from hadrons with a rejection power of 10^{-3} at a transverse momentum p_T=3 GeV/c, increasing up to 10^{-4} at p_T=20 GeV/c. The momentum accuracy $\Delta p/p$ provided by the iron toroids is better than 20% up to p=150 GeV/c.

The detector is compatible, both for the mechanical and the trigger rate points of view, with the UA2 detector, even in its proposed upgraded version.

Apart from its main task, relative to the new heavy flavours detection, the proposed set-up allows the study of $(\mu^{\pm}\mu^{\mp})$ pairs produced in $(p\bar{p})$ interactions, and other processes where a well identified muon can be coupled to the event detected in the UA2 apparatus.

2. PHYSICS MOTIVATIONS.

The present status of our knowledge on quarks and leptons may be summarized as follows:

Families:	1^{st}	2^{nd}	3^{rd}
Quarks:	$\begin{pmatrix} u \\ d \end{pmatrix}$	$\begin{pmatrix} c \\ s \end{pmatrix}$	$\begin{pmatrix} ? \\ b \end{pmatrix}$
Leptons:	$\begin{pmatrix} \nu_e \\ e \end{pmatrix}$	$\begin{pmatrix} \nu_\mu \\ \mu \end{pmatrix}$	$\begin{pmatrix} \nu_\tau \\ \tau \end{pmatrix}$

There are very good reasons to believe that our knowledge is far from being complete and thus the search for new heavy flavours and the study of their family structure is one of the key problems in Subnuclear Physics.

Two "theoretical" arguments favour the need for new quarks. The Adler-Bell-Jackiw (ABJ) anomaly cancellation requires the number of leptons to be equal to the number of quarks. This means that a sixth quark is needed. Its natural location would be the "up-like" member of the 3^{rd} family, i.e. the "top" quark.

According to SuperSymmetry, a very heavy quark with a mass in the few 10^2 GeV/c^2 range is needed in order to produce radiatively (see Fig. 1) a gluino with a mass such as to avoid a conflict with existing lower limits [1]. None of the presently known quarks (s, c and b) is heavy enough for this purpose.

Apart from these theoretical arguments we should not underevaluate that Nature has often provided physicists with more regularities than needed (for example the equality between the proton and the electron charges, which took more than three decades to be understood).

We propose to consider the ratio between the masses of the known heavy quarks as a limit for the regularity in their masses. There are good reasons [2] to consider the strange quark heavy enough to be used in our argument.

At present we know that:

i) $(m_c / m_s) \cong (1.8 / .5) \cong 3.5 \sim 4$;

ii) $(m_b / m_s) \cong (5.5 / .5) \cong 11 \sim 10$.

Suppose that (i) and (ii) are of general validity, i.e. :

$$(m_c / m_s) = [m(\text{uplike quark}) / m(\text{downlike quark})] = 4 , \quad (1)$$

and:

$$(m_b / m_s) = [m(\text{family N+1}) / m(\text{family N})] = 10 . \quad (2)$$

We ignore the 1^{st} family (u,d) because of its very light mass. On the other hand, the ratios (1) and (2) would not be inconsistent with the various models used to derive from bound states the quark masses [2].

The validity of (1) and (2) would allow to conclude that the "top" mass is in the 20 GeV/c^2 range. This is too light for SuperSymmetric models to avoid a gluino mass in conflict with experimental data. On the other hand, SuperSymmetry tells us that the maximum number of flavours, n_f, allowed in order to have a consistent theory (for example: the unification limit not above the Planck mass) is n_f=8. This means that the maximum number of families is 4. In the theories that ignore SuperSymmetry, the asymptotic freedom is lost if n_f>16.

What is not forbidden, in Nature, does take place. Thus, the message from SuperSymmetry is twofold:

i) four families of quarks are allowed;

ii) quarks heavier than (d,u,s,c,b and t) are needed.

Formulas (1) and (2) tell us that the 4^{th} family would have the "up-like" mass wanted by SuperSymmetry. In fact, using (2), the heavy "down-like" quark (called, in the following, "superbeauty" or sb) would have a mass in the 50 GeV/c^2 range:

$$m(\text{down-4}^{th}\text{family}) = m(\text{"superbeauty"}) \simeq 10 \times 5.5 \simeq 55 \text{ GeV}/c^2 ,$$

but, using (1), the heavy "up-like" quark would have a mass in the 200 GeV/c^2 range:

$$m(\text{up-4}^{th}\text{family}) = m(\text{"supertruth"}) \simeq 55 \times 4 \simeq 220 \text{ GeV}/c^2 .$$

If SuperSymmetry and asymptotic freedom were Bible-like truths, this flavour should be the last ever to be discovered.

The four families are shown in Table I, where the main objectives of the present proposal are indicated by the dotted circles.

It should however be emphasized that the measurement of the lepton asymmetry is a tool open to the detection of any "up-like" or "down-like" new state in the mass range above the present limits: i.e. m(heavy-flavour)≥22 GeV/c^2.

Let us come to a key question: if "top" and "superbeauty" are accessible to ($p\bar{p}$) Collider energies, how can they be detected?

Many methods are in principle possible. For example:

i) detection of a hidden state with the study of the invariant mass of the lepton pairs;

ii) detection of an open state with the identification of hadronic decay channels;

iii) study of multilepton events;

iv) study of the inclusive transverse momentum spectrum of the leptons from semileptonic decays;

v) study of the transverse dilepton (ℓ,ν) and jets masses.

All of these methods present, in various degrees, experimental problems related to small production cross-sections, low global branching ratios, high background levels, poor experimental resolution of the quantities needed to be measured. Moreover, none of them, but (ii), is able to identify the "up-like"

or "down-like" nature of the new flavours. However, method (ii) seems out of present experimental reach.

We propose here a new method to observe the production of heavy mass states, either "up-like" ("top") or "down-like" ("superbeauty") which is based on the "Leading" production mechanism, extended to the the heaviest baryon and antibaryon states. In fact, due to this production mechanism, a charge asymmetry of the leptons (ℓ^+,ℓ^-), originating from these heavy flavours can be observed in a selected region of phase-space. Morever, this asymmetry will show a p_T dependence characteristic of the masses of the decaying states.

More precisely, the "top" baryonic state will decay semileptonically into ℓ^+ and produce a positive asymmetry in the outgoing proton hemisphere

$$A_p = (\ell^+-\ell^-)/(\ell^++\ell^-) = \text{positive} .$$

The "anti-top" antibaryonic state will produce a negative asymmetry in the outgoing antiproton hemisphere

$$A_{\bar{p}} = (\ell^+-\ell^-)/(\ell^++\ell^-) = \text{negative} .$$

The signs of these asymmetries will be reversed for the "superbeauty" case. Fig. 2 shows the main trend of the measurement we propose.

The p_T range where to measure the $\ell^{\pm}$ asymmetry, and the separation between the maxima and minima, depend on the parent-daughter mass difference in the decay of the two new flavours. Extending the validity of the Generalized Cabibbo Dominance (GCD) to the 4^{th} family, the mass differences in the "superbeauty" and "top" decays would be:

$$\Delta m = m(\text{top}) - m(\text{beauty}) \simeq 20 \text{ GeV}/c^2 ,$$

$$\Delta m = m(\text{superbeauty}) - m(\text{top}) \simeq 30 \text{ GeV}/c^2 .$$

The Asymmetry will change sign with increasing lepton p_T. Notice that this GCD condition, if not valid, would not spoil our method. It would shift the lepton p_T spectrum to higher values, thus making the measurement cleaner.

To check the validity of our new method, we have considered, not only the case with only one new flavour produced, but also the production of two new heavy flavours, one "up-like" and one "down-like". For this last case we have followed the mass extrapolations (1) and (2), i.e.:

$$m(\text{"top"}) = 25 \text{ GeV}/c^2$$
$$m(\text{"superbeauty"}) = 55 \text{ GeV}/c^2.$$

The single "up-like" case has been evaluated at

$$m(\text{"top"}) = 25 \text{ GeV}/c^2, \text{ and}$$
$$m(\text{"top"}) = 35 \text{ GeV}/c^2.$$

Note that present (e^+e^-) data impose a lower limit $m_t \geq 22$ GeV/c^2.

Let us emphasize a detail concerning the sequence of new heavy flavour masses. This sequence could be opposite to present expectations. If, for example:

$$m(\text{"down-like"}) = 25 \text{ or } 35 \text{ GeV}/c^2, \text{ and}$$
$$m(\text{"up-like"}) = 55 \text{ GeV}/c^2,$$

the asymmetry would still be there, with opposite sign and minor effects on the lepton p_T spectrum.

As we will see in section 2.4 and chapter 5, the amplitude of the effect depends on:

i) the "Leading" effect;

ii) the decay angular and momentum distributions;

iii) the branching ratios into semileptonic channels;

iv) the acceptance and rejection power of the experimental set-up designed to observe the leptons produced by these "new" flavours decay.

2.1 THE "LEADING" EFFECT.

A result which was theoretically unpredicted is the "Leading" effect which shows up in the production of heavy flavours.

A detailed study of (pp) interactions at the ISR showed that the Λ^+_c is produced in a "Leading" way [3].

After this experimental result was obtained, a series of theoretical proposals were presented, to account for the "Leading" Λ^+_c production. The longitudinal momentum distribution for Λ^+_c was in fact found at the ISR [3] to be:

$$E(d\sigma/d|x|) \sim (1-|x|)^{\alpha} \quad \text{with } \alpha \sim 0.$$

The results are shown in Fig. 3. The charmed meson production [4] was on the other hand measured to be "non-Leading", i.e.

$$E(d\sigma/d|x|) \sim (1-|x|)^{\alpha} \text{ with } \alpha \approx 3 \ .$$

This can "a posteriori" be qualitatively understood in terms of the Λ^+_c obtained by a recombination of the spectator c-quark with a valence (ud) pair in the proton; while the D production is given by the recombination of the spectator c-quark with at most one valence quark [5,7].

Figure 4a shows how the "Leading" Λ^+_c and Λ^0_s productions compare. This indicates that the "Leading" effect does not decrease with increasing flavour mass. Figure 4b shows the qualitative behaviour, as a function of the flavour mass, of the quantity (Leading/Total). This quantity will be defined in section

2.4.5 as the ratio between the inclusive cross-section for producing leading baryons with flavour "f" and the total cross-section for producing the same flavour "f". This figure shows that, at ISR energies, the (Leading/Total) production does not decrease with increasing flavour mass.

A more complete summary of "charm" production in purely hadronic interactions is reported in Table II [8]. There is no model which can fit all measured quantities [8].

The conclusion of this short review on the "charm" flavour production in (pp) interactions is therefore:

i) the cross-section values found are at least an order of magnitude above the "theoretical" predictions of perturbative QCD;

ii) the x-distribution for Λ^{+}_{c}, i.e. the "Leading" effect, was theoretically unpredicted;

iii) with "new" models (essentially flavour excitation [5,6] and non-perturbative QCD [7]) both cross-sections values and x-distributions can be "theoretically" derived.

All this should be quite a warning for QCD prediction on New Heavy Flavours production at extreme energies such as those of the ($p\bar{p}$) CERN Collider.

2.2 NOTE ON THE SEMI-LEPTONIC DECAY MODES: GENERALIZED CABIBBO DOMINANCE.

A fact of Nature is that the matrix which relates the "down-like" "weak" flavours "Cabibbo mixed"

$$\begin{pmatrix} d_c \\ s_c \\ b_c \end{pmatrix}$$

to the "strong" flavours

$$\begin{pmatrix} d \\ s \\ b \end{pmatrix}$$

is approximately a unit matrix

$$\begin{pmatrix} d_c \\ s_c \\ b_c \end{pmatrix} \approx \begin{pmatrix} 1 & 0 & 0 \\ 0 & 1 & 0 \\ 0 & 0 & 1 \end{pmatrix} \begin{pmatrix} d \\ s \\ b \end{pmatrix}$$

as shown in Figs. 5a and 5b.

In order to extend the generalized Cabibbo dominance to the 4^{th} Family, we make the following extrapolations:

i) all the generalized Cabibbo angles, even those coming from the existence of the 4^{th} family, are small;

ii) the flavour-changing neutral currents are forbidden to any order of family;

iii) the amplitude for the transition from family N to family N±α has a coefficient

$$\prod_{i=1,\alpha} (\sin\theta_i) .$$

As a consequence, the Cabibbo-favoured decay chains of flavours c, b, t and sb are:

$$c \to s$$

$$b \to c \to s$$

$$t \to b \to c \to s$$

$$sb \to t \to b \to c \to s.$$

A sequence $t \to b \to c \to s$ will be accompained by the semileptonic series giving rise to $\ell^+ \to \ell^- \to \ell^+$. For the antiquark sequence $\bar{t} \to \bar{b} \to \bar{c} \to \bar{s}$, the charges will be reversed ($\ell^- \to \ell^+ \to \ell^-$).

2.3 CROSS-SECTION ESTIMATES.

We will try to estimate the production cross-section for very high flavour masses using the QCD predictions from Halzen [9] for m_{top}=25 GeV/c^2 at Collider energies (σ_{top}~0.1 μb). For this extrapolation we make use of dimensionality and scaling:

$$\sigma(m) \sim (1/m^2) \times f(s/m^2) \qquad (3)$$

In order to check dimensionality and scaling, we have used:

i) the strangeness data to predict c and b;

ii) the "charm" data to predict b.

The results are shown in Figs. 6-7. There is no violent disagreement between extrapolated results and experimental findings.

2.4 THE STUDY OF THE LEPTON CHARGE ASYMMETRY AND ITS ENERGY DEPENDENCE AS A WAY TO DETECT NEW HEAVY FLAVOURED STATES (BARYONIC AND ANTIBARYONIC) AT THE ($p\bar{p}$) COLLIDER.

The leptonic decay chains, following the generalized Cabibbo dominance, for the various flavours c,b,t,sb, are shown in Fig. 8.

Once a particle-antiparticle pair has been produced, on the average the number of positive and negative leptons from its decay is equal. However we will

discuss under which conditions an asymmetry in the number of positive and negative leptons can be observed, due to the different longitudinal momentum production distribution for baryons and mesons, and to the dependence of the lepton p_T spectra from the product particle mass.

Let us define the Asymmetry parameter as

$$A^0\ (p_T,\theta_{cut}) = \frac{N(\ell^+) - N(\ell^-)}{N(\ell^+) + N(\ell^-)}$$

where $N(\ell^+) \equiv N(\ell^+;p_T,\theta_{cut})$ and $N(\ell^-) \equiv N(\ell^-;p_T,\theta_{cut})$ are the number of positive and negative leptons produced in the angular range $0^0<\theta<\theta_{cut}$ and with transverse momentum p_T.

The number of positive leptons ℓ^+ is expressed by

$$N(\ell^+) = L[n_{sb}(\ell^+)+n_t(\ell^+) +n_b(\ell^+)+n_c(\ell^+)]$$

where L is the total integrated luminosity and $n_f(\ell^+)$ (with f = sb,t,b,c) is the contribution from the direct production of sb,t,b,c states.

Analogously the number of negative leptons is given by

$$N(\ell^-) = L[n_{sb}(\ell^-)+n_t(\ell^-) +n_b(\ell^-)+n_c(\ell^-)]$$

The leptons originated by the decay of the various flavours and antiflavours are summarized in Tables III and IV.

In order to write down explicitly $n_f(\ell^+)$ let us define:

i) $\sigma_f^T \equiv$ total cross-section for the production of open $(f,\bar{f})$ pairs;

ii) $\rho_{Mf},\rho_{\bar{M}\bar{f}},\rho_{Bf},\rho_{\bar{B}\bar{f}} \equiv$ ratio between, the inclusive cross-section for producing [M = meson, $\bar{M}$ = antimeson, B = baryon, $\bar{B}$ = antibaryon] states with flavour "f", and the total cross section σ_f^T ;

iii) $BR_{Mf'}, BR_{\bar{M}\bar{f}'}, BR_{Bf'}, BR_{\bar{B}\bar{f}'}$ ≡ semileptonic branching ratio of the various states with flavour f' (f' = c,b,t,sb) ;

iv) $\varepsilon_{Mf}(\ell^{\pm}_{f'}), \varepsilon_{\bar{M}\bar{f}}(\ell^{\pm}_{\bar{f}'}), \varepsilon_{Bf}(\ell^{\pm}_{f'}), \varepsilon_{\bar{B}\bar{f}}(\ell^{\pm}_{\bar{f}'})$ ≡ acceptance for $\ell^{\pm}$ from the leptonic decay of the flavour f' produced in the decay chain of the state with flavour f. This acceptance is a function of the lepton p_T and of the cut $\theta < \theta_{cut}$ applied to the lepton polar angle.

Accordingly we have, for the case of "superbeauty":

$$
\begin{aligned}
n_{sb}(\ell^+) = \sigma_{sb}^{T} \{ & \rho_{Msb}[BR_{Mt}\varepsilon_{Msb}(\ell^+_t) + BR_{Mc}\varepsilon_{Msb}(\ell^+_c)] \\
& + \rho_{\bar{M}\bar{sb}}[BR_{\bar{M}\bar{sb}}\varepsilon_{\bar{M}\bar{sb}}(\ell^+_{\bar{sb}}) + BR_{\bar{M}\bar{b}}\varepsilon_{\bar{M}\bar{sb}}(\ell^+_{\bar{b}})] \\
& + \rho_{Bsb}[BR_{Bt}\varepsilon_{Bsb}(\ell^+_t) + BR_{Bc}\varepsilon_{Bsb}(\ell^+_c)] \\
& + \rho_{\bar{B}\bar{sb}}[BR_{\bar{B}\bar{sb}}\varepsilon_{\bar{B}\bar{sb}}(\ell^+_{\bar{sb}}) + BR_{\bar{B}\bar{b}}\varepsilon_{\bar{B}\bar{sb}}(\ell^+_{\bar{b}})]\}
\end{aligned}
$$

and

$$
\begin{aligned}
n_{sb}(\ell^-) = \sigma_{sb}^{T} \{ & \rho_{\bar{M}\bar{sb}}[BR_{\bar{M}\bar{t}}\varepsilon_{\bar{M}\bar{sb}}(\ell^-_{\bar{t}}) + BR_{\bar{M}\bar{c}}\varepsilon_{\bar{M}\bar{sb}}(\ell^-_{\bar{c}})] \\
& + \rho_{Msb}[BR_{Msb}\varepsilon_{Msb}(\ell^-_{sb}) + BR_{Mb}\varepsilon_{Msb}(\ell^-_b)] \\
& + \rho_{\bar{B}\bar{sb}}[BR_{\bar{B}\bar{t}}\varepsilon_{\bar{B}\bar{sb}}(\ell^-_{\bar{t}}) + BR_{\bar{B}\bar{c}}\varepsilon_{\bar{B}\bar{sb}}(\ell^-_{\bar{c}})] \\
& + \rho_{Bsb}[BR_{Bsb}\varepsilon_{Bsb}(\ell^-_{sb}) + BR_{Bb}\varepsilon_{Bsb}(\ell^-_b)]\}
\end{aligned}
$$

The analogous expressions for $n_t(\ell^{\pm})$, $n_b(\ell^{\pm})$, $n_c(\ell^{\pm})$ can be easily derived and are not reported here.

From the above formulae it can be seen that in order to evaluate the Asymmetry parameter A^0 one needs to know:

i) the total cross-sections : σ^T ;

ii) the decay branching ratios : BR ;

iii) the production distributions of the baryons or mesons states and the lepton distributions in the decays : ε ;

iv) the relative fraction of baryons and mesons : ρ ;

We will now discuss in some detail the assumptions made for these quantities.

2.4.1 The total cross-sections.

The total cross-sections for the heavy flavours at the ($p\bar{p}$) Collider ($\sqrt{s}$=540 GeV) are taken from perturbative QCD calculations [5,9]:

$$\sigma_c \sim 2000 \quad \mu b \ ,$$
$$\sigma_b \sim 10 \quad \mu b \ ,$$
$$\sigma_t \sim 0.1 \quad \mu b \ ,$$

where the "top" mass is taken to be m_t= 25 Gev/c^2.

To get consistent values for higher masses, for example m_{sb} = 55 Gev/c^2, we use dimensionality and scaling, as outlined in section 2.3. The result for m_{sb} = 55 Gev/c^2 is

$$\sigma_{sb} \sim 0.01 \ \mu b \ .$$

We will see that cross-section values even ten times lower that these QCD extrapolations give rise to a measurable Asymmetry.

2.4.2 The decay branching ratios.

Recent data from CLEO [16] give for the semileptonic branching ratio of the "beauty" mesons:

$$(M_b \to \ell^{\pm})/(M_b \to \text{all}) \approx 0.13 \ .$$

In our Monte Carlo we assume the known semileptonic branching ratios for "charm":

$$(D \to \ell^{\pm})/(D \to \text{all}) \approx 0.085 \ ,$$
$$(\Lambda^{+}_{c} \to \ell^{\pm})/(\Lambda^{+}_{c} \to \text{all}) \approx 0.045 \ ,$$

and the conservative value of 0.1 for all other heavier particles.

2.4.3 The production distributions of baryon and meson states.

The study of the reactions:

$$pp \to D + e^{-} + \text{anything} \ ,$$
$$pp \to \Lambda^{+}_{c} + e^{-} + \text{anything} \ ,$$
$$pp \to \Lambda^{0}_{b} + e^{+} + \text{anything} \ ,$$

at the ISR, indicate that in baryon-baryon collisions the heavy flavoured baryons are produced according to a rather flat x-distribution:

$$(d\sigma/dx) \sim \text{const.} \ ,$$

while the heavy flavoured mesons are produced with softer x-distribution of the type:

$$E(d\sigma/d|x|) \sim (1-|x|)^{3} \ .$$

These distributions will be assumed all along the following discussion, together with the p_T dependence:

$$(d\sigma/dp_T) \sim p_T \exp(-2.5p_T)$$

observed at the ISR in the production of heavy flavours [17, 18].

2.4.4 The lepton decay distributions.

The data from CLEO [19] show that in the semileptonic decay of "beauty" mesons, M_b, the magnitude of the mass recoiling with respect to the leptons is very near to the D mass:

$$M_b \rightarrow Xe\nu \ , \text{ with } M_X \sim M_D \approx 2.0 \text{ GeV}/c^2$$

Moreover, the mean charged multiplicity of the decay is 3.5, where the D contributes with 2.5 charged particles on the average. We can conclude that, even at values of the mass as high as the mass of the M_b, the semileptonic decay proceeds via a 3-body decay. On the contrary, the mean charged multiplicity in the hadronic decays of the M_b mesons is 6.3, i.e. the hadronic decay of the M_b produces, on the average, one D plus four charged particles plus two neutral particles:

$$M_b \rightarrow D + 6\text{-bodies} \ .$$

In the following we will assume that the total multiplicity of all semileptonic decays is 3 and the decay is $K_{\ell 3}$-like for mesons and phase-space for baryons, while the total multiplicity of all the hadronic decays have the known values for "charm" and "beauty" (~3 for "charm", ~charm+6 for "beauty"), and, for "top" and "superbeauty", the same multiplicity as "beauty".
It should be noted that this is already a conservative hypothesis, since the hadronic decays of "top" and "superbeauty" can be expected to produce more particles than "beauty". Higher values of multiplicity would dump the leptonic spectra of unwanted processes. The genuin asymmetry will thus remain unaffected.

2.4.5 The relative yield of meson and baryons.

From the data on strangeness production at the ISR, it can be assumed that, in (pp) collisions the following reactions dominate (L and C indicate "Leading" and "Central" production) :

$$(L)\ p_1p_2 \rightarrow \overline{M}_{Central} + (B_{Leading})_1 + anything \equiv \{\overline{M}_C;B_{L1}\}\ ,$$
$$(L)\ p_1p_2 \rightarrow \overline{M}_{Central} + (B_{Leading})_2 + anything \equiv \{\overline{M}_C;B_{L2}\}\ ,$$
$$(C)\ p_1p_2 \rightarrow \overline{M}_{Central} + M_{Central} + anything \equiv \{\overline{M}_C;M_C\}\ .$$

In $(p\bar{p})$ collisions, due to the the presence of an anti-flavoured antibaryonic state, another leading reaction can occur :

$$(L)\ p_1\bar{p}_2 \rightarrow \overline{M}_{Central} + (B_{Leading})_1 + anything \equiv \{\overline{M}_C;B_{L1}\}\ ,$$
$$(L)\ p_1\bar{p}_2 \rightarrow M_{Central} + (\overline{B}_{Leading})_2 + anything \equiv \{M_C;\overline{B}_{L2}\}\ ,$$
$$(L)\ p_1\bar{p}_2 \rightarrow (B_{Leading})_1 + (\overline{B}_{Leading})_2 + anything \equiv \{B_{L1};\overline{B}_{L2}\}\ .$$
$$(C)\ p_1\bar{p}_2 \rightarrow M_{Central} + \overline{M}_{Central} + anything \equiv \{M_C;\overline{M}_C\}\ .$$

The indices (1,2) are redundant in the $(p\bar{p})$ case and will be omitted from now on.

The ratio between the inclusive cross-sections for producing the four classes of particles M_C, $\overline{M}_C$, B_L and $\overline{B}_L$ and the total cross-sections are:

$$\rho_M = [\sigma\{M_C;\overline{B}_L\}+\sigma\{\overline{M}_C;M_C\}] \ / \ \sigma^T\ ,$$
$$\rho_{\overline{M}} = [\sigma\{\overline{M}_C;B_L\}+\sigma\{\overline{M}_C;M_C\}] \ / \ \sigma^T\ ,$$
$$\rho_B = [\sigma\{\overline{M}_C;B_L\}+\sigma\{B_L;\overline{B}_L\}] \ / \ \sigma^T\ ,$$
$$\rho_{\overline{B}} = [\sigma\{M_C;\overline{B}_L\}+\sigma\{B_L;\overline{B}_L\}] \ / \ \sigma^T\ ;$$

with:

$$\sigma^T = \sigma\{\overline{M}_C;B_L\}+\sigma\{M_C;\overline{B}_L\}+\sigma\{\overline{M}_C;M_C\}\ +\sigma\{B_L;\overline{B}_L\}\ .$$

Notice that the ratio (Leading/Total) = $\rho_B = \rho_{\overline{B}}$.

At ISR, in each hemisphere, the ratio (Leading/Total) is ~ 1/16 for strangeness and ~ 1/8 for "charm". In our discussion we will study the behaviour of A^0 as a function of (Leading/Total).

2.4.6 Estimates of the Asymmetry A^0.

In order to estimate the lepton Asymmetry parameter A^0, we have considered the case: lepton ≡ muon.

The angular and momentum distributions of the muons have been evaluated by means of a Monte Carlo simulation, with the conditions set in the previous sections. Figures 9a to 9d shows the angular distribution of the muons from the primary decay of "superbeauty", "top", "beauty" and "charm" [baryon and meson states]. For further reference, also the distribution of muons from the decay $t \to b\mu\nu$ with m_t=35 GeV/c^2 is shown in Fig. 9e.

For the "superbeauty" case, a choice of $\theta_{cut}=30^\circ$ gives a good acceptance for the detection of muons from baryons, which contribute to the asymmetry, while keeping low the acceptance for muons from mesons, which destroy it.

Figures 10a to 10c show the (θ vs p_μ) plots for muons coming from the "superbeauty" (m_{sb}=55 GeV/c^2), "top" (m_t=25 GeV/c^2) and "top" (m_t=35 GeV/c^2); all being baryon decays.

The detection acceptances ε have been computed for 5 values of θ_{cut} ($\theta_{cut}=10^\circ$, 20°, 30°, 40° and 90°) as will be seen in Figs. 14 and 15.

Figures 11a to 11t show the $\mu^\pm$ acceptances for $\theta_{cut}=30^\circ$ for baryons, mesons and antimesons. The acceptances for $\mu^\pm$ originated by the decay of antibaryons are, of course, negligible, because of the central nature of the production mechanism.

Fig. 12 shows the behaviour of $A^0(p_T,30^\circ)$, for (Leading/Total)=0.25. There are two main peaks, one positive around p_T=10 GeV/c, due to the "top" baryon decay into μ^+, and one negative around p_T=19 GeV/c, due to "superbeauty" baryon decay into μ^-.

It is interesting to note that the separation between the two peaks depends only on the mass differences in the semileptonic decays of "superbeauty" and "top" states. In fact, in the 3-body semileptonic decay, the transverse momentum spectrum of the muons scales with $p_T/\Delta m$, where Δm is the difference between the parent mass and the mass of the hadronic particle produced in the decay. This is shown in Fig. 13 where the normalized $p_T/\Delta m$ spectra of the muons produced in the decays :

i) $\Lambda^0_{sb} \rightarrow \Lambda^+_t \mu^- \nu$;

ii) $\Lambda^+_t \rightarrow \Lambda^0_b \mu^+ \nu$;

iii) $\Lambda^0_b \rightarrow \Lambda^+_c \mu^+ \nu$;

iv) $\Lambda^+_c \rightarrow \Lambda^0_s \mu^+ \nu$;

are reported.

The mass differences Δm have the following values:

i) $\Delta m = m(\Lambda^0_{sb}) - m(\Lambda^+_t) \approx 30$ GeV/c^2 for the "sb" baryon decay ;

ii) $\Delta m = m(\Lambda^+_t) - m(\Lambda^0_b) \approx 19.5$ GeV/c^2 for the "t" baryon decay ;

iii) $\Delta m = m(\Lambda^0_b) - m(\Lambda^+_c) \approx 3.2$ GeV/c^2 for the "b" baryon decay ;

vi) $\Delta m = m(\Lambda^+_c) - m(\Lambda^0_s) \approx 1.2$ GeV/c^2 for the "c" baryon decay ;

The amplitude of the two peaks, for "top" and "superbeauty", as a function of θ_{cut} and (Leading/Total), is shown in Figs. 14 ("top") and 15 ("superbeauty"). The strong difference in the longitudinal momentum production distributions between baryons and mesons does produce a charge asymmetry which remains high, even with low values of the ratio (Leading/Total). We will assume a value of (Leading/Total)=0.25 in most of the graphs , showing the expected asymmetry versus different parameters . However the way in which the asymmetry changes with the quantity (Leading/Total) is easily derivable from Figs. 14 and 15.

3. THE APPARATUS.

A layout of the proposed apparatus is shown in Fig. 16.

The apparatus has been designed with the limitations imposed by planned UA2 extensions and by the experimental hall. This leads to some compromises being necessary on the background level in the experiment, in the efficiency of the trigger, and in the momentum resolution, but it does not affect the general feasibility of the experiment. However, the following points had to be borne in mind in the planning:

- The effect on the precision of the incident track and the smearing of the incident track direction by multiple scattering.
- Energy losses, leading to a reduction in momentum at the magnet.
- Background from decay of π and K.

3.1 THE UA2 CALORIMETER.

In this section we will give some relevant parameters of the UA2 layout before describing the lepton asymmetry analyser.

In the forward/backward direction they consist of a pre-shower converter which has a negligible effect on muons, an electromagnetic detector of 20 radiation lengths and a hadron calorimeter of 57 radiation lengths. The space available for our apparatus starts at 330 cm. from the interaction.

3.2 THE HADRON ABSORBER.

Since there is still an appreciable rate of pion punch-through from the UA2 apparatus and to avoid putting a magnetic field immediately by existing photomultiplier bases, we place 60 cm of non-magnetized iron close behind the hadron calorimeter. Two drift chambers are incorporated for defining the incident muon direction and for recognizing interactions. The absorber is followed by an air gap and a third drift chamber to obtain a good lever arm for the track direction entering the magnet. It will be possible to displace this part of the apparatus, mass approximately 85 tons, along the beam line by the length of the air gap so as to give access to the UA2 calorimeter electronics.

3.3 THE IRON TOROID MAGNETS.

Momentum analysis around each outgoing beam direction is made with two toroidal magnet assemblies. Each of these is made of five circular iron plates, 30 cm thick and with radii varying from 3.0 to 4.0 metres. The plates are separated by 10 cm spaces in which we insert planes of Limited Streamer Tubes. The design parameters of each magnet assembly are:

Field	20 K gauss
Weight	450 tons
Power	500 KW.
Windings	Two Cu windings, water cooled, common to the five plates.
Resolution	~14% $\Delta p/p$ (limited by multiple scattering).

3.4 THE TRACKING CHAMBERS.

Two types of chamber are used: Limited Streamer Tubes, LST, for selecting transverse momentum in a fast decision logic and for coarse tracking in the magnet to avoid ambiguous momentum measurements; Drift Chambers, DC, for final reconstruction to provide more accurate measurements of the incident and emergent track positions and directions.

3.4.1 Drift Chambers.

Each of the first three chamber planes provides three measurements in the directions x and y. The fourth chamber, following the magnet, is double this so as to give the exit point of the track and a sufficient information on the emergent track direction. Space limitations prevent increasing the lever arm.

The characteristics of each drift cell (Fig. 17) are:

Track length sampled	3 cm
Cell width	6 cm
Cathode Voltage	-6000 V
Field wire voltage	-1000 V
Field wire diameter	100 μm
Sense wire diameter	20 μm
Sense wire field	330 KV/cm(*)
Typical drift field	~1.5 KV/cm(*)
Average drift velocity	47μm/nsec(*) (Ar/CO2 90/10)
Spatial resolution	300 μm(*)
Read-out channels	5800

The quantities marked with an asterisk have been calculated with a Monte Carlo program written by J. Va'Vra at SLAC [20]. In particular the spatial

resolution obtained was 100 μm. We estimate however that systematic errors will worsen it to the quoted value.

Elimination of ghost points will be achieved by charge division or by delay line read-out, but, if possible, by extrapolation of the LST information. This point is being studied.

3.4.2 Limited Streamer Tubes.

The construcion will be of 1 cm square PVC tubes with high resistance cathodes. The read-out system will take full advantage of the properties of this type of tube which allow read-out by external pick-up electrodes whose shapes are independent of the wire configuration.

Before the magnet, there is a pair of chamber planes with orthogonal wires, and their pick-up electrodes are concentric circles centred on the beam line so that the electrode number directly measures the muon production angle. Corresponding electrodes on the two planes are connected in OR configuration for the fast trigger to remove most of the 14% inefficiency which is caused by the side walls of the tubes.

Following the magnet is a similar pair of chambers so that the difference in radial electrode position between the first and last chambers gives the magnetic deflection.

Tube planes within the magnet will be fitted with rectangular or sector-shaped read-out pads with analog read-out to detect interactions in the magnet and to reduce ambiguities.

On each plane of the first and fourth chambers, there will be 116 anular electrodes, each divided into 12 azimuthal segments, giving a total of approximately 11000 data channels for this type of chambers. The pick-up pads will require a similar number of electronic channels.

4. μ IDENTIFICATION.

4.1 μ/π REJECTION.

A basic level of decay muons and punch through pions emerges from the UA2 apparatus. As described previously, 60cm of iron is placed immediately after the UA2 calorimeter to remove residual hadrons before they decay.

Background muon rates from pions and K have been calculated in two steps. In the first step, a decay and hadron shower Monte Carlo [21] has been used to find the background from π and K of fixed energy. Two groups of muons show up in the simulation: muons of the full energy range from decay in flight; muons from decay during the hadron shower development. The latter group has an energy spectrum scaled down by 30% relative to the decay spectrum. Approximately equal numbers of muons in the two groups were sufficiently energetic to penetrate to the end of the toroid.

In the second step of the calculation, the single particle distributions from the UA1 results [22] were used with the results of the first step (scaled proportional to energy) to obtain the muon flux in our apparatus as function of p_T. Figure 18 shows the ratio of background muon flux to parent hadron flux as a function of p_T after integration over the apparatus.

The total rate of muons penetrating to the end of the magnet, without any cut in p_T is 1 muon/300 interactions. The effect of this background on the asymmetry parameter is given in section 5.2.

4.2 MOMENTUM RESOLUTION.

The influence of chamber resolution and multiple scattering on the muon momentum measurement has been simulated with a Monte Carlo program, for the configuration of the magnetic spectrometer shown in Fig. 16. The main detector parameters relevant for this study were:

- calorimeter thickness in radiation lentghs : 74 X_0
- iron absorber thickness in radiation lengths: 34 X_0
- magnetized iron (toroid) thickness in rad. lengths : 85 X_0
- magnetic field inside iron : 20 KG
- single wire overall positional accuracy for drift chambers in front of and behind the toroid : 300 μm
- distance between the two chambers in front of the toroid: 80 cm.

The range of muon momenta under study was determined by the angular acceptance of the spectrometer ($5^0 \leq \theta \leq 30^0$) and the transverse momentum (p_T) interval where the maximum asymmetry effect was expected for muons from "top" decay. Assuming a "top" flavour mass of 35 GeV/c^2 and the production plus decay distributions discussed in section 2.4, the relevant p_T range is 4÷15 GeV/c (p=8÷172 GeV/c), as shown in Fig. 10c. Muons were generated in the Monte Carlo with p_T=4, 9.5 and 15 GeV/c and θ=5,10,20,30°.

The contributions from ionization, bremsstrahlung, pair production and nuclear interactions to the mean total energy loss of the muon (see Figs. 19a,b) inside the calorimeter, the first iron absorber and the toroid were taken into account [23]. Fluctuations around the mean value were then allowed according to a Landau distribution. For multiple scattering, the gaussian approximation was used [24].

The momentum determination was based on the measurement of the ingoing muon angle θ, provided by all the drift chambers placed before the toroid, and of the exit point of the muon track, obtained by extrapolating back to the toroid end face the outgoing track fitted in the planes of the last drift chamber. The information from the LST planes inside the toroid was not used for track fitting.

The results of our simulation are expressed in terms of the muon p_T accuracy, which is relevant for the charge asymmetry measurement. The $\Delta p_T/p_T$ resolution values given here are the r.m.s. relative to the distributions of the quantity

$$[\, p_{generated} - (p_{measured} + \text{energy loss correction})] \,/\, p_{generated}$$

obtained in the Monte Carlo. The energy loss correction refers to the total momentum degradation of the particle before and inside the toroid. Since these distributions are not gaussian, if the FWHM/2.36 is used instead of the r.m.s., the improvement of the quoted resolution is ~2 %. The behaviour of the transverse momentum resolution as a function of the total momentum is shown in Figs. 20a to 20c for fixed p_T values of 4.0, 9.5 and 15.0 GeV/c, respectively. For each value of p_T, the effect of the drift chamber intrinsic resolution σ_{DC} was studied. The curves shown in Figs. 20a to 20c correspond to σ_{DC}=300 and 600 μm, respectively. The expected value of the proposed drift chamber system is ~300 μm. In this case the p_T resolution obtained in the whole momentum range relevant to the asymmetry measurement is better than ~20%. When σ_{DC}=600 μm, the resolution exceeds 20% only at p_T=15 GeV/c for p>75 GeV/c.

The uncertainty on the vertex determination when tracing back the muon track to the origin was also studied. Examples of Δx, Δy, Δz distributions, corresponding to p_T=9.5 GeV/c, θ=10° and σ_{DC}=300 μm, are shown in Figs. 21a to 21c. The error on the vertex coordinate along the colliding beams direction (y) is ~11 cm (the jitter of the interaction point in the Monte Carlo generation was ±10 cm), while the errors on the transverse coordinates are ~1.5 cm. The boundary values of the errors at the vertex in the p_T and θ region considered in our exercise, are 10.5÷17 cm along y and 1÷6 cm along x or z.

5. ESTIMATE OF THE ASYMMETRY PARAMETER IN EXPERIMENTAL CONDITIONS.

5.1 THE EFFECT OF THE ANGULAR CUT.

We have already shown in Figs. 9a to 9e the angular distributions of the muons originating from the semileptonic decays of the heavy-flavour particles, as they are computed by our Monte Carlo.

When taking into account the lower cut in the angular coverage of the apparatus described in chapter 3, $\theta \geq 5^0$, the acceptance for muons from baryon decay decreases very much for low quark masses. This is due both to phase-space limits - the maximum x_F of the baryon decreases with increasing quark mass - and to the transverse momentum of the muon in the decay - it decreases with decreasing quark mass. Figure 22 shows the Asymmetry A^0 computed with the angular cut $5^0 \leq \theta \leq 30^0$.

By comparing Figs. 12 and 22 it can be seen that the $\theta \geq 5^0$ cut makes disappear the asymmetry at low p_T due to charm and beauty, and decreases by a small amount the asymmetry at higher p_T due to "top" and "superbeauty".

5.2 THE BACKGROUND.

In what has been described so far, the background contamination in the sample of prompt muons has not been considered. As discussed in capter 4, the background is mainly due to muons produced by π and K decay. This contribution can be computed from the inclusive pion cross-section as measured by the UA1 experiment [22], using the fit to their data:

$$E(d^3\sigma/dp^3) = A \times p^n{}_0/(p_0+p_T)^n \qquad (4)$$

with $A=0.37\pm0.06$ mb c^2 GeV^{-2}, $p_0=1.3\pm0.18$ GeV c^{-1} and $n=8.99\pm0.15$.

Formula (4) is relative to charged hadrons (averaged over the two charges) and is given in unit of rapidity. The rapidity interval over which we integrated the background is given by the angular acceptance of the apparatus:

$$5^{\circ} \leq \theta \leq 90^{\circ} \Rightarrow \Delta y \approx 1.8.$$

The extrapolated background rate should be multiplied by the rejection in the experimental apparatus, given in Fig. 18.

Another source of background, which will be discussed later, is the prompt muons sources other than open heavy flavoured states i.e. $W^{\pm}$, Z^{0}. It will be shown that this kind of background is relevant only above very high values of p_T (p_T > 20 GeV/c).

Due to the background source previously described, the experimental Asymmetry parameter is given by:

$$A^{exp}(p_T, \theta_{cut}) = \frac{[N(e^+)+N_{bg}(e^+)] - [N(e^-)+N_{bg}(e^-)]}{[N(e^+)+N_{bg}(e^+)] + [N(e^-)+N_{bg}(e^-)]}$$

where $N_{bg}(e^{\pm})$ is the number of background muons.

In order to have an estimate for the experimental errors on A^{exp}, we assume a total integrated luminosity L=10 pb^{-1}, i.e. 3000 hours of running with a luminosity L=10^{30} cm^{-2} sec^{-1}.

Figure 23a shows, for the case of simultaneous production of "top" (25 GeV/c^2) and "superbeauty" (55 GeV/c^2), the expected number of produced muons as a function of p_T. Superimposed is the computed background.

Figure 23b shows the plot of A^{exp} as a function of p_T. The errors are purely statistical.

5.3 THE MOMENTUM RESOLUTION.

We have studied the amplitude and the position of the peaks in the experimental asymmetry A^{exp} as a function of the finite momentum resolution of the proposed apparatus.

The results are shown in Figs. 24a and 24b for the "top" peak, and in Figs. 25a and 25b for the "superbeauty" peak. The smearing effect of the momentum resolution decreases the absolute amplitude of A^{exp} and shifts the peaks upward by a relatively small amount.

Figures 26a and 26b show the number of events and the experimental asymmetry as a function of p_T, for a momentum resolution $\Delta p/p=20\%$, as expected in the proposed apparatus (see section 4.2).

5.4 OTHER HYPOTHESES ON THE NEW HEAVY FLAVOUR MASSES AND ON THE PRODUCTION CROSS-SECTIONS.

With our Monte Carlo program, we have tested the capability of the proposed apparatus to cope with different heavy flavour masses and with lower cross sections for heavy flavour production.

We have repeated our analysis turning off the "superbeauty" signal and using two assumptions for the "top" mass:

i) $m_t=25$ GeV/c^2, as in the previous analysis;

ii) $m_t=35$ GeV/c^2.

The cross-section for a "top" mass of 35 GeV/c^2 , $\sigma_t\sim0.05$ μb, is the result of extrapolation using the same method as the one outlined in sections 2.3 and 2.4.1.

Figures 27a and 27b, 28a and 28b show the number of expected events and the experimental asymmetry A^{exp} for case (i) and, respectively, (ii).

The effect of different cross-section values has been studied for the three hypotheses:

i) m_t=25 GeV/c^2, m_{sb}=55 GeV/c^2 (simultaneous production of two flavours);

ii) m_t=25 GeV/c^2, no "superbeauty" (only one flavour);

iii) m_t=35 GeV/c^2, no "superbeauty" (only one flavour).

The values of the experimental Asymmetry peaks and the statistical significance of the measurements for the three hypotheses indicated above , are reported in Figs. 29 to 32: the experimental asymmetry remains measurable for values of the heavy flavour production cross-sections even a factor ten lower than those expected from QCD extrapolations.

5.5 EFFECTS FROM $W^{\pm}\rightarrow\mu^{\pm}\nu$ AND $W^{\pm}\rightarrow tb\rightarrow\ell\nu X$.

As it is well known, the direct leptons from $W^{\pm}$ have a pronounced asymmetry which is opposite to the one we are looking for in the case of "up-like" baryonic and antibaryonic states. A detailed calculation shows that the maximum effect expected from the $W^{\pm}\rightarrow\mu^{\pm}\nu$ decay does not exceed the 10% level with 50% efficiency for $W^{\pm}$ identification in the UA2 central detector.

As nothing is known on the process $W^{\pm}\rightarrow tb\rightarrow\ell\nu X$, we assume that all the leptons it produces behave similarly to the direct leptons from $W^{\pm}$. We can evaluate an upper limit to this effect if we know its total cross-section. Various estimates exist in the literature: for example, with a "top" mass m_t=40 GeV/c^2 and for leptons with p_T>10 GeV/c:

$$B(W\rightarrow tb\rightarrow\ell\nu X)\times\sigma_W = 36 \text{ pb (ref. [26])};$$

$$B(W\rightarrow tb\rightarrow\ell\nu X)\times\sigma_W = 29 \text{ pb (ref. [27])}.$$

From the above figures we can conclude that the background from this source is at most one half of the background from the muons directly produced by $W^{\pm}$.

6. TRIGGER LOGIC AND TRIGGER RATES.

The maximum trigger rate which is acceptable to the UA2 data acquisition system is 1 Hz and the decision of whether to accept or reject an individual event must be reached within a time delay of 1 μsec. This can be done by applying a cut in p_T around 2 GeV and this cut must be made with little loss in efficiency above p_T=5 GeV/c where the interesting events lie. Clearly any system which requires a wire-by-wire read out is excluded. What is needed is a fast parallel logic .

As indicated in the LST description, a suitable method is to make coincidences between one circular strip of the first chamber with a suitable group of circular strips in the last chamber.

6.1 TRIGGER RATE WITH PERFECT SELECTION.

To evaluate the trigger rates, the ISAJET Monte Carlo [28] was used to simulate event production at the $p\bar{p}$ Collider at 540 GeV. Each track produced in the angular intervals $5^0 \leq \theta \leq 30^0$ and $150^0 \leq \theta \leq 175^0$ was then followed through all the apparatus using a Monte Carlo [21] in which particles are allowed to produce showers and to decay; energy loss and multiple scattering are taken into account. The average number of particles reaching the toroids was evaluated to be .08 per event on each side. All particles traversing the toroids were found to be muons mostly produced by the decay in flight of primary particles in the central detector and partially by the decay of particles produced in the hadronic showers inside the calorimeters. Trigger rates were estimated for a luminosity of 10^{30} cm^{-2} sec^{-1} for different p_T cuts on particles traversing the toroids. In Table V the 90% C.L. upper limits for the trigger rates are given. Trigger conditions are defined for each side of the detector and the rate is given by the OR of the two sides.

6.2 DESIGN OF TRIGGER CONDITIONS.

The Monte Carlo results were used to find out the strip correlations between the first and the last chamber planes. Particles produced at a fixed angle and fixed transverse momentum were tracked through one strip of the first plane and through the last plane. The radial spread on the back plane to be accepted for 100% efficiency at that p_T and angle was thus determined and is shown in Fig. 33. We use the curve for $p_T \geq 5$ GeV/c in our design.

In the next step, these strip coincidence configurations are assumed fixed and the acceptance for lower values of p_T was determined using the same program. Figure 34 shows the results. For example, at $\theta = 5^0$, $p_T = 2$ GeV/c, the efficiency is 30% . The important point is that full efficiency is reached for $p_T \geq 5$ Gev/c. A more detailed simulation is to be made when the design is made final.

The best way to realize the hardware coincidence conditions is being studied. Each strip-sector of the first plane has to be put in coincidence with between 3 and 20 sectors of the last plane, and the OR of all coincidences must be taken.

7. COSTS AND TIME SCALE .

An estimate of costs is shown in the table below:

		KSFr.	KSFr.
Magnet		3000	4400
Magnet chariots		1000	
Preabsorber and chariots		400	
Drift chambers	Construction Supplies Head Electronics Cables	1300	3050
	Mechanical supports	250	
	TDC system	1500	
LST	Construction	600	2800
	Pads	200	
	Mechanical support	200	
	Head electronics (pads)	680	
	Head electronics (x,y,strips)	200	
	Trigger and read-out	620	
	Cables	300	
General fast electronics		250	550
Crates and Controllers		300	
TOTAL			10800

The foreseen time table for the experiment is as follows:

1984 : Full design of the various parts of the apparatus and in particular of the iron absorber and the toroid; tendering and contracts.

1984-1985 : Prototypes construction and tests for DC and LST.

1985 : Complete design and construction for DC and LST; material delivery.

1985-1986 : Calibrations.

1986-1987 : Final assembling.

REFERENCES

[1] S. Ferrara, private comunication.

[2] A. Martin, The masses of the Heavy Flavoured Hadrons, CERN Preprint TH-3314, 28 May 1982.

[3] M. Basile et al., Nuovo Cimento Lett. 30 (1981) 487.

[4] M. Basile et al., Nuovo Cimento Lett. 33 (1982) 33.

[5] R. Odorico, Phys. Lett. 107B (1981) 231.

[6] V. Barger, F. Halzen and W.Y. Keung, Phys. Rev. D24 (1981) 1428.

[7] F. Halzen, W.Y. Keung and D.M. Scott, Madison Rep. MAD/PH/63 (1982).

[8] M. Basile et al., Proceedings of the Third Topical Workshop on Proton-Antiproton Collider Physics, Rome , Jan-1983, p.435.

[9] F. Halzen, Rapp. Talk, XXI Int. Conf. on High Energy Physics, Paris

[10] M. Basile et al., Nuovo Cimento 63A (1981) 230.

[11] M. Basile et al., Nuovo Cimento 65A (1981) 457.

[12] M. Basile et al., Nuovo Cimento 67A (1982) 40.

[13] D. Drijard et al., Phys. Lett. 85B (1979) 452;
K. Giboni et al., Phys. Lett. 85B (1979) 437;
W. Lockman et al., Phys. Lett. 85B (1979) 443;
J. Eickmeyer et al., XX ICHEP (Madison, 1981);
D. Drijard et al., Phys. Lett. 81B (1979) 250;
P. F. Jacques et al., Phys. Rev. D21 (1980) 1206;
P. Coteus et al., Phys. Rev. Lett. 42 (1979) 1438;
A. Soukas et al., Phys. Rev. Lett. 44 (1980) 564;
A.E. Asratyan et al., Phys. Lett. 74B (1978) 497;
P. Alibran et al., Phys. Lett. 74B (1978) 134;
T. Hansl et al., Phys. Lett. 74B (1978) 139;
A. Bosetti et al., Phys. Lett. 74B (1978) 143;
M. Fritze et al., Phys. Lett. 96B (1980) 427;
D. Jonker et al., Phys. Lett. 96B (1980) 435;
H. Abramowicz et al., Cern Preprint CERN-EP/82-17;
M. Aguilar-Benitez et al., CERN Preprint CERN-EP/81-131;

T. Aziz et al., Nucl. Phys. B199 (1982) 424;

J. Sandweiss et al., Phys. Rev. Lett. 44 (1980) 1104.

[14] M. Basile et al., Nuovo Cimento 65A (1981) 391.

[15] J. Badier et al., XXI Int. Conf. on High Energy Physics, Paris 1982.

[16] K. Chadwick et al., preprint CLNS/82/546.

[17] M. Basile et al., Nuovo Cimento Lett. 30 (1981) 481.

[18] M. Basile et al., Nuovo Cimento Lett. 33 (1982) 17.

[19] L. Olsen, Moriond workshop on New Flavours, Les Arcs 1982.

[20] J. Va'Vra, Proceedings of the Vienna Wire Chamber Conference (1983).

[21] A. Baroncelli, Nucl. Instr. Meth. 188 (1974) 445.

[22] G. Arnison et al., UA1 Collaboration, Preprint CERN-EP/82-171.

[23] C. Richard-Serre, CERN report 71-18.

[24] B. Rossi, High Energy Particles (Prentice-Hall), p.63-77.

[25] T. Hansl and Kozaneka, Preprint CERN-EP/83-193.

[26] R. Odorico, Preprint CERN TH-3678/83.

[27] R. Kinnunen, Preprint CERN-EP/84-19.

[28] F.E. Paige and S.D. Protopopescu, BNL 31987, September 1982.

TABLE I.

The four families of quarks and leptons.

The dashed circles indicate the main objectives of this proposal.

Families:	1^{st}	2^{nd}	3^{rd}	4^{th}
Quarks:	$\begin{pmatrix} u \\ d \end{pmatrix}$	$\begin{pmatrix} c \\ s \end{pmatrix}$	$\begin{pmatrix} t \\ b \end{pmatrix}$	$\begin{pmatrix} u_H \\ d_H \end{pmatrix}$
Leptons:	$\begin{pmatrix} \nu_e \\ e \end{pmatrix}$	$\begin{pmatrix} \nu_\mu \\ \mu \end{pmatrix}$	$\begin{pmatrix} \nu_\tau \\ \tau \end{pmatrix}$	$\begin{pmatrix} \nu_H \\ L_H \end{pmatrix}$

TABLE II.

Experimental findings versus theoretical predictions for "charm" production.

	experiment	models		
		diffractive	flavour excitation	fusion
Leading effect	yes	yes	yes	no
threshold behaviour	steeper then $\ln^2 s$	$\ln s$	steeper than $\ln^2 s$	>> steeper than $\ln^2 s$
mass dependence	?	$1/m^2$	stronger than $1/m^2$	>> stronger than $1/m^2$
cross section	large	large	large	small
A^α dependence	$\alpha<2/3$ (*)	$\alpha=2/3$	$\alpha=1$	$\alpha=...$

(*) The p_T dependence is derived from data on strangeness.

TABLE III.

The heavy-flavour decay chains producing ℓ^+ and ℓ^-.

Flavour	Decays producing ℓ^+	Decays producing ℓ^-
sb	$sb \to t \to b + \ell^+$ $sb \to t \to b \to c \to s + \ell^+$	$sb \to t + \ell^-$ $sb \to t \to b \to c + \ell^-$
t	$t \to b + \ell^+$ $t \to b \to c \to s + \ell^+$	$t \to b \to c + \ell^-$
b	$b \to c \to s + \ell^+$	$b \to c + \ell^-$
c	$c \to s + \ell^+$	

TABLE IV.

The heavy-antiflavour decay chains producing ℓ^+ and ℓ^-.

Antiflavour	Decays producing ℓ^+	Decays producing ℓ^-
$\overline{sb}$	$\overline{sb} \to \bar{t} + \ell^+$ $\overline{sb} \to \bar{t} \to \bar{b} \to \bar{c} + \ell^+$	$\overline{sb} \to \bar{t} \to \bar{b} + \ell^-$ $\overline{sb} \to \bar{t} \to \bar{b} \to \bar{c} \to \bar{s} + \ell^-$
$\bar{t}$	$\bar{t} \to \bar{b} \to \bar{c} + \ell^+$	$\bar{t} \to \bar{b} + \ell^-$ $\bar{t} \to \bar{b} \to \bar{c} \to \bar{s} + \ell^-$
$\bar{b}$	$\bar{b} \to \bar{c} + \ell^+$	$\bar{b} \to \bar{c} \to \bar{s} + \ell^-$
$\bar{c}$		$\bar{c} \to \bar{s} + \ell^-$

TABLE V.

90% C.L. upper limits for trigger rates.

Trigger	Rate (Hz)
no p_T cut	240.
$p_T \geq 2$ Gev/c	4.4
$p_T \geq 3$ Gev/c	.5

Figure captions.

Fig. 1 : The diagram illustrates how a gluino can acquire a mass from radiative processes, where a spin 1/2 quark and a spin 0 antiquark are virtually produced. The quark mass must be in the 10^2 GeV/c^2 range, in order to allow a gluino mass of the order of a few GeV/c^2.

Fig. 2 : Main trend of the muon charge Asymmetry in the proton hemisphere (a) and in the antiproton hemisphere (b).

Fig. 3 : Experimental longitudinal momentum distribution of Λ^+_c.

Fig. 4 : a) Λ^+_c and Λ^0_s leading effects compared.
b) Qualitative behaviour of the quantity (Leading/Total) as a function of the heavy flavour mass, at $\sqrt{s}$=62 GeV.

Fig. 5 : a) The six quark mixing with CP violation. $S_i=\sin\theta_i$, $C_i=\cos\theta_i$.
b) Transitions among the various states. The Cabibbo dominance opens the dashed channels. The horizontal transitions are forbidden for any value of the mixing angle. Allowed neutral currents are: $u\bar{u}$, $c\bar{c}$, $t\bar{t}$, $d\bar{d}$, $s\bar{s}$ and $b\bar{b}$.

Fig. 6 : Charm cross-section derived from strange cross-section following formula (3). The data are taken from refs. 10, 11, 12 and 13.

Fig. 7 : "Beauty" cross-section derived from strange (full line) and "charm" (dashed lines - notice the width due to the experimental uncertainties) cross-sections following formula (3). The data are taken from refs. 14 and 15.

Fig. 8 : Diagram illustrating all possible electric charge signs of the muons originating from the semileptonic decay of the flavours c, b, t and sb, and the corresponding anti-flavour states..

Fig. 9 : Angular distribution of the muons from the semileptonic decays:

a) $sb \rightarrow t\mu\nu$;

b) $t \rightarrow b\mu\nu$;

c) $b \rightarrow c\mu\nu$;

d) $c \rightarrow s\mu\nu$;

e) $t \rightarrow b\mu\nu$ (m_t=35 GeV/c^2).

The full lines refer to baryon states, the dashed/dotted lines to meson states.

The dotted vertical lines indicate the angular acceptance of the proposed apparatus (see chapter 3).

The spectra from baryons and mesons are normalized to a ratio (Leading/Total)=0.25.

Fig. 10 : θ vs. p_μ plots from the decays:

a) $\Lambda^0_{sb} \rightarrow \Lambda^+_t \mu^- \nu$;(m_{sb}=55 Gev/c^2);

b) $\Lambda^+_t \rightarrow \Lambda^0_b \mu^+ \nu$;(m_t=25 Gev/c^2);

c) $\Lambda^+_t \rightarrow \Lambda^0_b \mu^+ \nu$;(m_t=35 GeV/c^2).

Fig. 11 : (a) to (t): Acceptances ε for the various states and decay chains.

Fig. 12 : Plot of $A^0(p_T, \theta_{cut})$ as a function of p_T. The value assumed for the angular cut and for the ratio (Leading/Total) are:

θ_{cut} = 30°;

(Leading/Total) = 0.25.

The heavy flavour masses are taken to be: m_t=25 GeV/c^2 and m_{sb}=55 GeV/c^2

Fig. 13 : Normalized ($p_T/\Delta m$) spectra of the muons from the decays:

$\Lambda^0_{sb} \rightarrow \Lambda^+_t \mu^- \nu$ (m_{sb}=55 GeV/c^2);
$\Lambda^+_t \rightarrow \Lambda^0_b \mu^+ \nu$ (m_t=25 GeV/c^2);
$\Lambda^0_b \rightarrow \Lambda^+_c \mu^- \nu$;
$\Lambda^+_c \rightarrow \Lambda^0_s \mu^+ \nu$.
The Δm values relative to the four decays are indicated.

Fig. 14 : Plot of $A^0(p_T$=10 GeV/c,$\theta_{cut})$ ("top" peak, m_t=25 GeV/c^2) as a function of (Leading/Total) for different values of θ_{cut}.

Fig. 15 : Plot of $A^0(p_T$=19 GeV/c,$\theta_{cut})$ ("superbeauty" peak, m_{sb}=55 GeV/c^2) as a function of (Leading/Total) for different values of θ_{cut}.

Fig. 16 : Showing a schematic side view of the experimental apparatus.
CD and FD are the central and forward detectors of UA2 ;
DC are the drift chambers for momentum measurement;
ST are the Limited Streamer Tubes with pad read out for triggering;
HF is the iron hadron filter;
IT is the iron toroidal magnet.
Also shown is the mobile UA2 platform.

Fig. 17 : a) The equipotentials map of a drift cell is shown. Two sets of seven guard wires define the cell. The middle plane contains seven wires: four field and three sense wires alternated. The three sense wires are staggered by ±500 μm relative to the field wire plane to resolve left-right ambiguity.
b) The drift of electrons generated by a track and reaching wires: 2(sense), 3(field), 4(sense).

Fig. 18 : The ratio of background muons to parent hadrons as function of p_T, and integrated over the angular acceptance of the apparatus.

Fig. 19 : The mean energy loss of muons in iron (I=ionization, B=bremsstrahlung, P=pair creation, N=nuclear interaction). The horizontal scale refers to the muon kinetic energy. [(a):different contributions to the mean energy loss, (b):total mean energy loss].

Fig. 20 : The muon transverse momentum resolution as a function of the total momentum, for p_T=4, 9.5 and 15 GeV/c, $5^0<\theta<30^0$ and two values of drift chamber resolution.

Fig. 21 : Distributions of the reconstructed vertex coordinates transverse to the beams direction [(a):DX and (b):DZ] and along the beams direction [(c):DY]. The vertex jitter along y was $\mp$10 cm in the Monte Carlo generation.

Fig. 22 : Plot of A^0 as a function of p_T in the angular acceptance defined by the apparatus ($5^0\leq\theta\leq30^0$).

Fig. 23 : a) Expected number of produced μ^+ (black points) and μ^- (white points), as a function of p_T and for an integrated lumnosity of 10 pb^{-1}, with the conditions set in the text and for m_t=25 GeV/c^2 and m_{sb}=55 GeV/c^2. The estimated background for each charge sign is indicated by the full line. The errors are purely statistic.
b) The expected asymmetry A^{exp} as a function of p_T

Fig. 24 : a) Position in p_T of the peak of the experimental Asymmetry coming from "top" (m_t=25 GeV/c^2) decay as a function of the momentum measurement error $\Delta p/p$.
b) Absolute value of the A^{exp} peak position given in (a) as a function of $\Delta p/p$.

Fig. 25 : Same as Fig. 24 for "superbeauty" peaks (m_{sb}=55 GeV/c^2).

Fig. 26 : Same as Fig. 23, with the smearing in p_T due to the expected momentum resolution $\Delta p/p=20\%$.

Fig. 27 : Same as Fig. 23 for a "top" mass $m_t=25$ GeV/c^2 and no "superbeauty".

Fig. 28 : Same as Fig. 23 for a "top" mass $m_t=35$ GeV/c^2 and no "superbeauty".

Fig. 29 : a) "Top" peak experimental Asymmetry amplitude;
b) statistical significance of the measurement.
Both quantities are plotted versus the production cross-section for the hypotesis (i) defined in the text (simultaneous production of "up-like" and "down-like" flavours). The curves correspond to a p_T integration in the interval specified in the figure. The arrows indicate the cross-section value used so far (see section 2.4.1).

Fig. 30 : Same as Fig. 29 but for "superbeauty" peak (simultaneous production of "up-like" and "down-like" flavours).

Fig. 31 : Same as Fig. 29 but for hypothesis (ii) in the text (only one flavour produced).

Fig. 32 : Same as Fig. 29 but for hypothesis (iii) in the text (only one flavour produced).

Fig. 33 : Number of circular pads in the last LST plane projected by one pad in the first LST plane as function of θ and p_T of the muons. This number corresponds to full efficiency for μ of both charge signs.

Fig. 34 : Trigger efficiency vs. θ for different values of p_T, for a trigger configuration 100% efficient at $p_T \geq 5$ GeV/c.

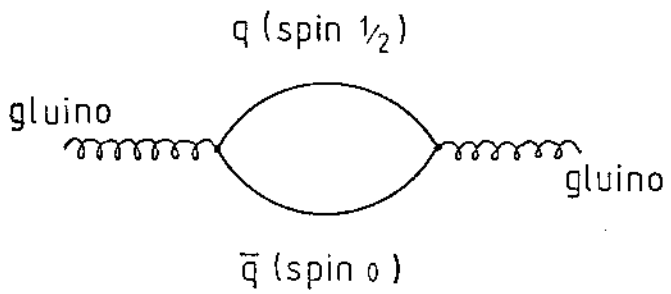

FIG. 1

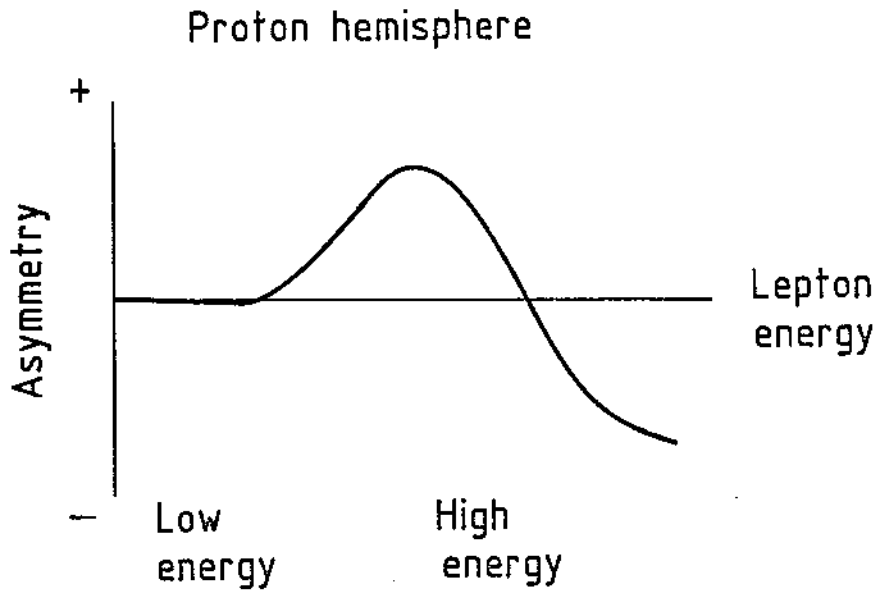
Proton hemisphere
+
Asymmetry
Lepton
energy
−
Low
energy
High
energy

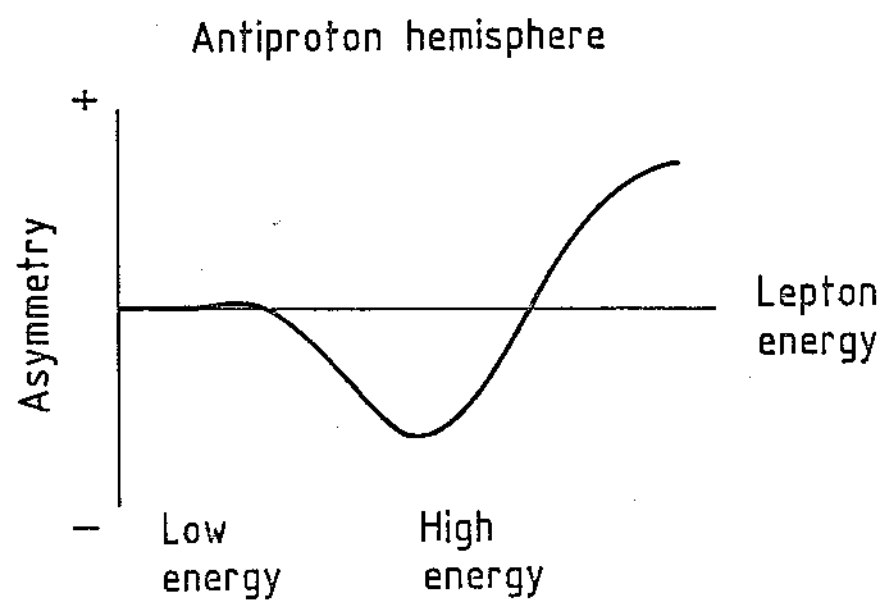
Antiproton hemisphere
+
Asymmetry
Lepton
energy
−
Low
energy
High
energy

FIG. 2

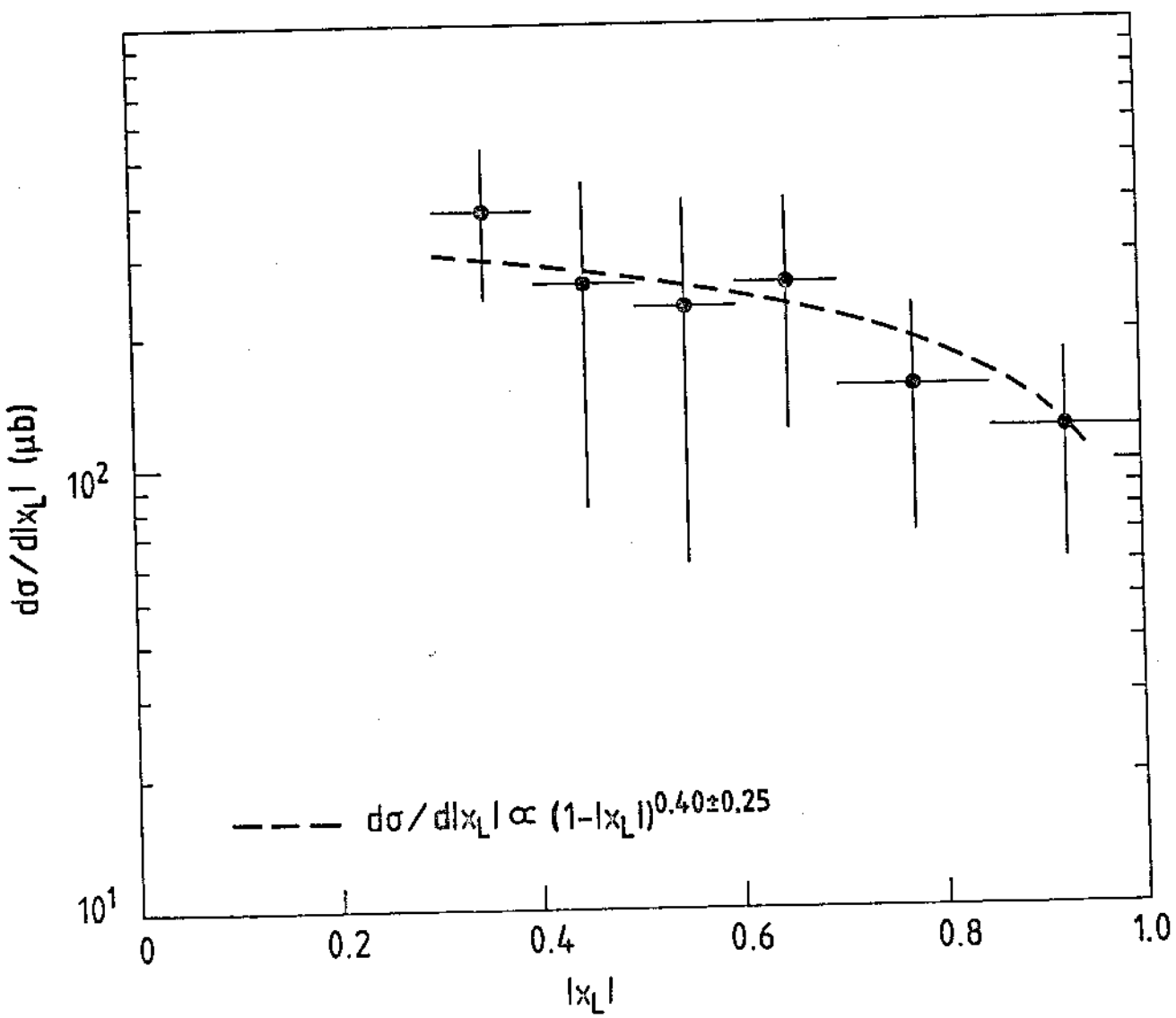

FIG.3

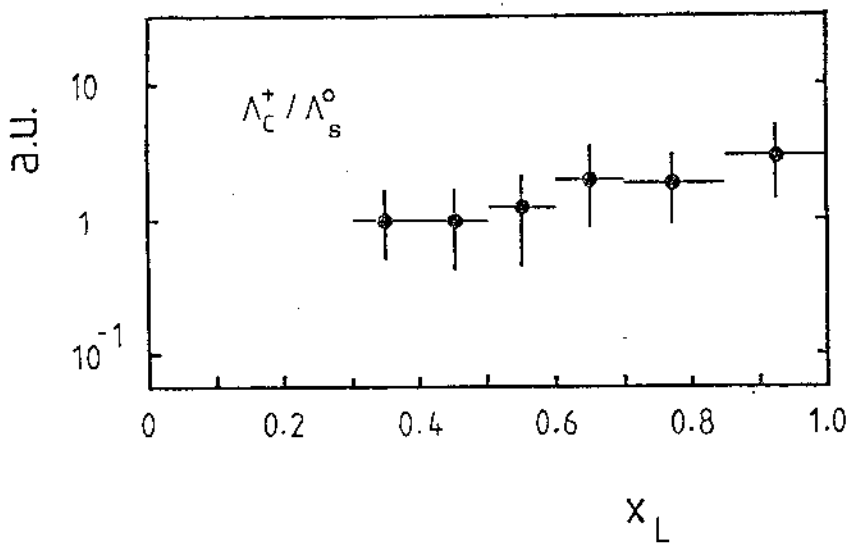
a.u.
10
1
10^{-1}
$\Lambda_c^+ / \Lambda_s^\circ$
0
0.2
0.4
0.6
0.8
1.0
x_L

(a)

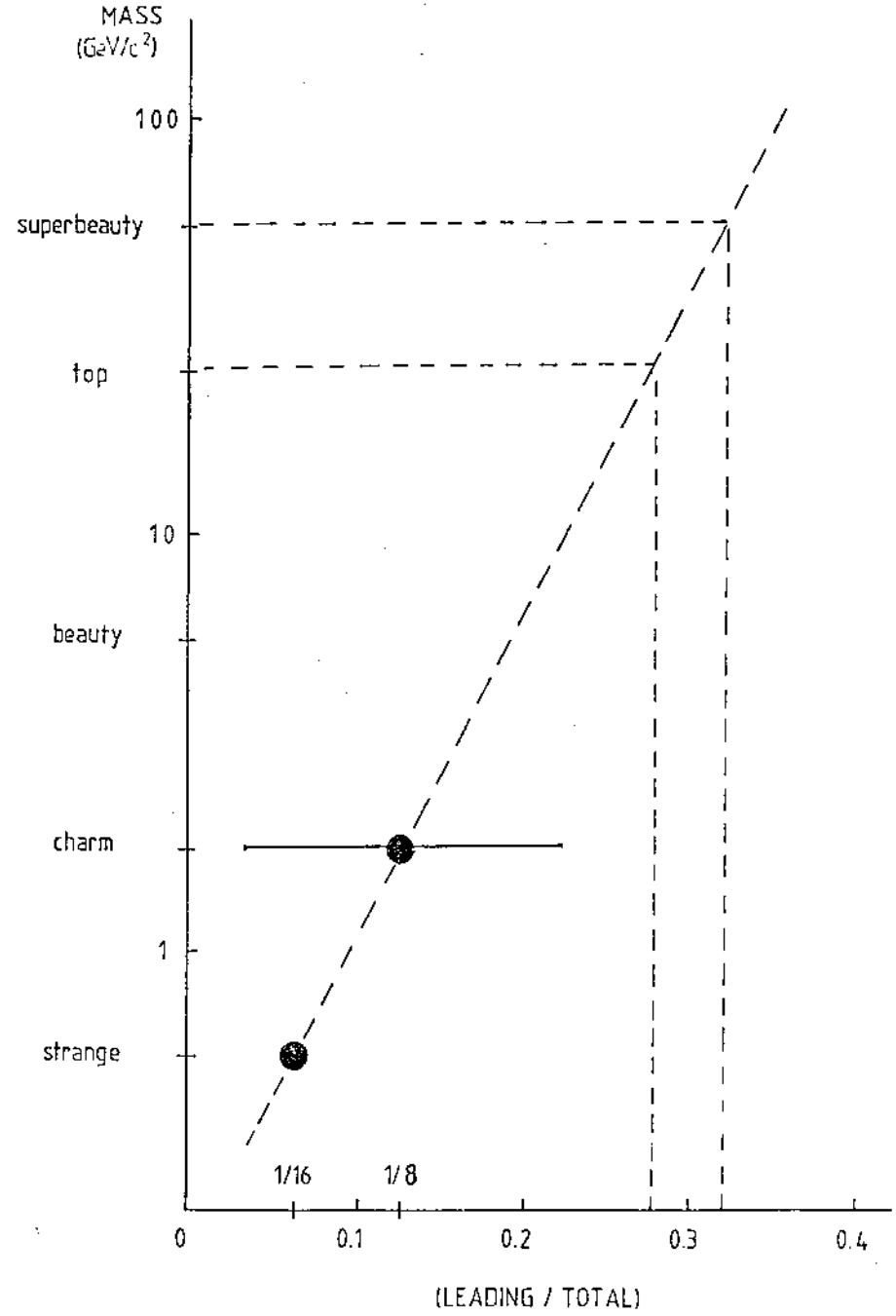
MASS
(GeV/c²)
100
superbeauty
top
10
beauty
charm
1
strange
1/16
1/8
0
0.1
0.2
0.3
0.4
(LEADING / TOTAL)

(b)

FIG. 4

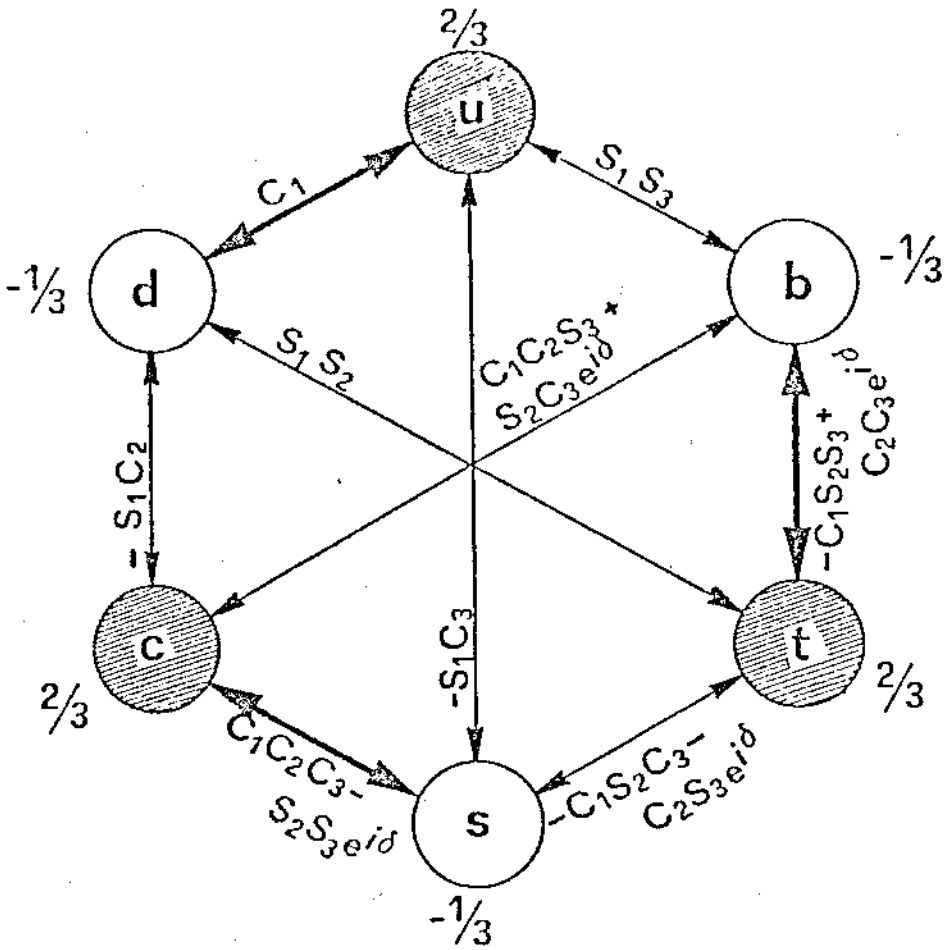
2/3
u
C1
S1 S3
-1/3
d
b
-1/3
S1 S2
C1C2S3* S2C3eiδ
-S1C2
-C1S2S3* C2C3eiδ
c
t
2/3
2/3
-S1C3
C1C2C3- S2S3eiδ
-C1S2C3- C2S3eiδ
s
-1/3

(a)

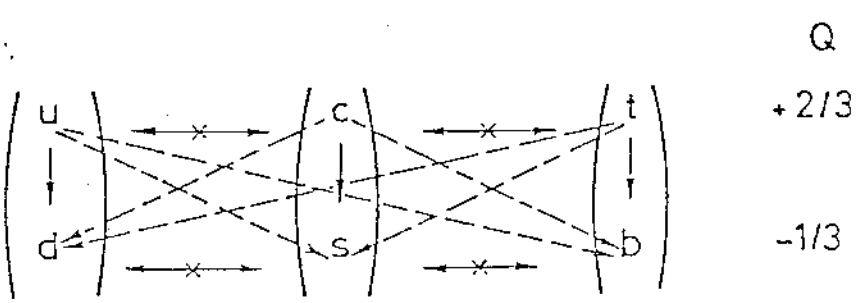
Q
u
c
t
+2/3
d
s
b
-1/3

(b)

FIG. 5

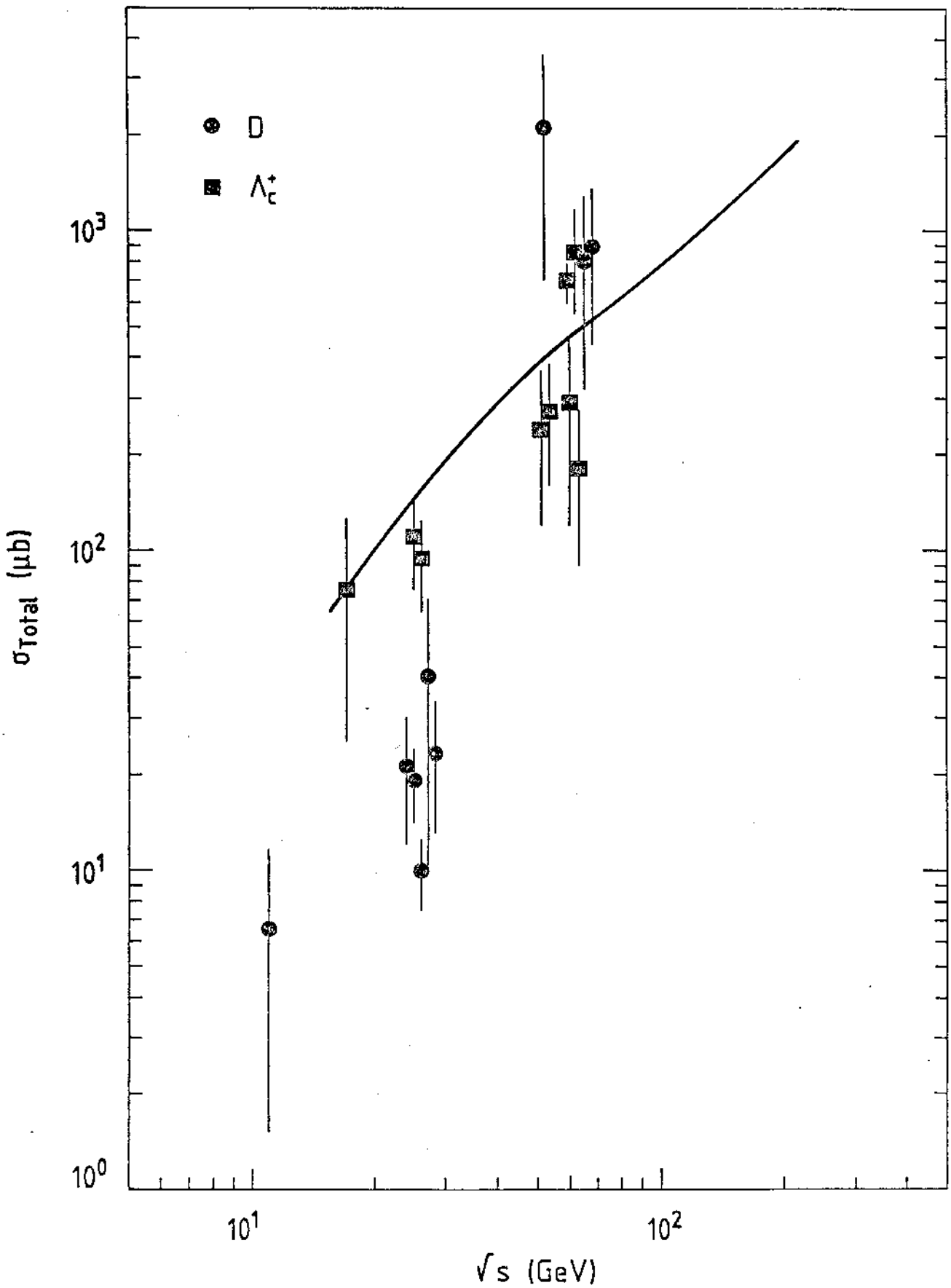

FIG. 6

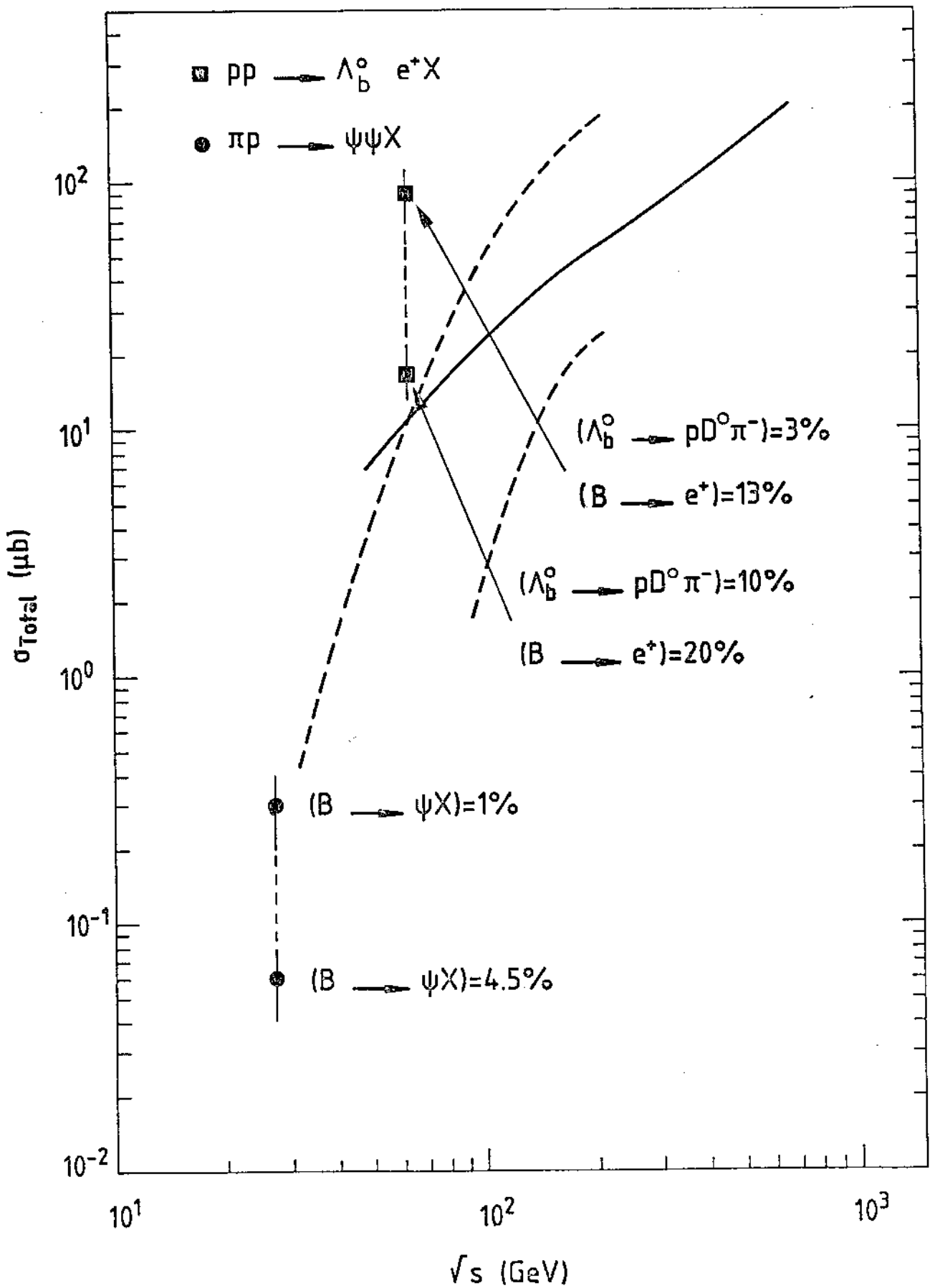
pp → Λ°b e⁺X
πp → ψψX
(Λ°b → pD°π⁻)=3%
(B → e⁺)=13%
(Λ°b → pD°π⁻)=10%
(B → e⁺)=20%
(B → ψX)=1%
(B → ψX)=4.5%
σTotal (μb)
√s (GeV)
10²
10¹
10⁰
10⁻¹
10⁻²
10¹
10²
10³

FIG.7

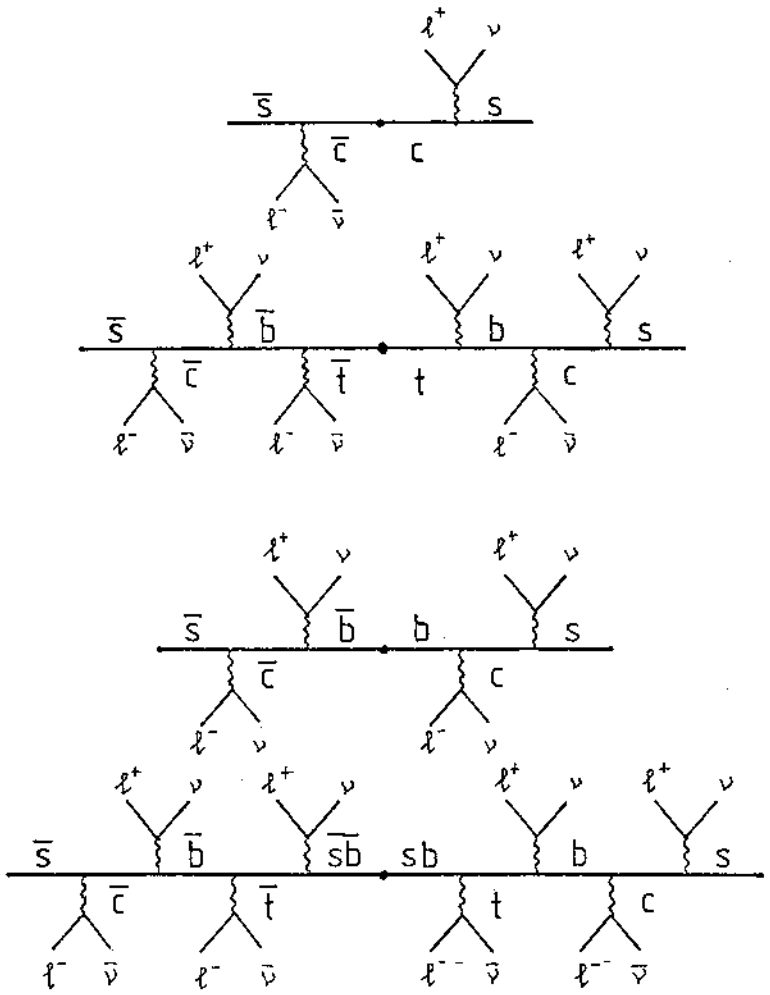
ℓ^+ ν
$\bar{s}$ s
$\bar{c}$ c
ℓ^- $\bar{\nu}$
$\bar{s}$ $\bar{b}$ b s
$\bar{c}$ $\bar{t}$ t c
$\bar{s}$ $\bar{b}$ b s
$\bar{c}$ c
$\bar{s}$ $\bar{b}$ $\bar{sb}$ sb b s
$\bar{c}$ $\bar{t}$ t c

FIG. 8

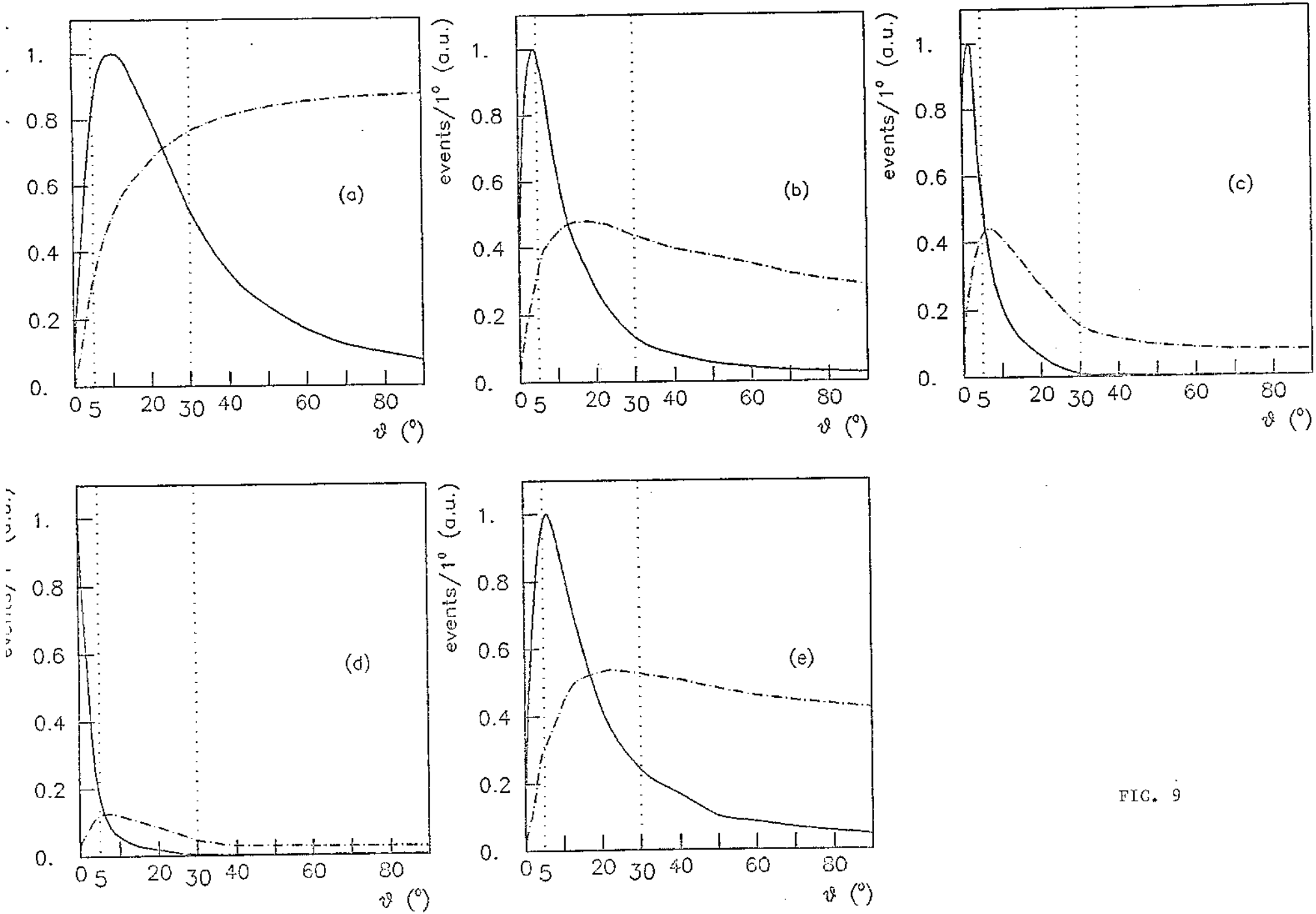

FIG. 9

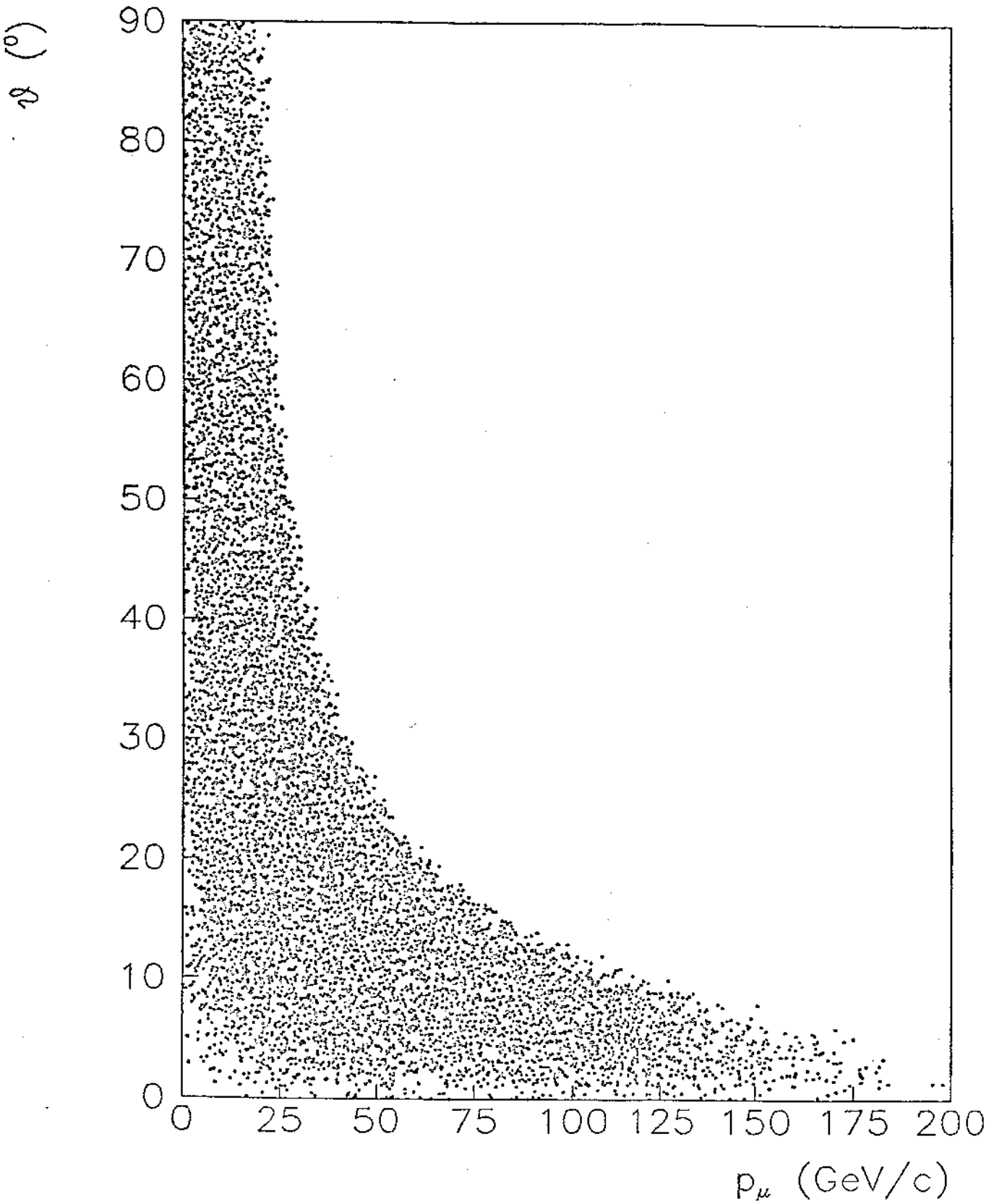

FIG. 10 a)

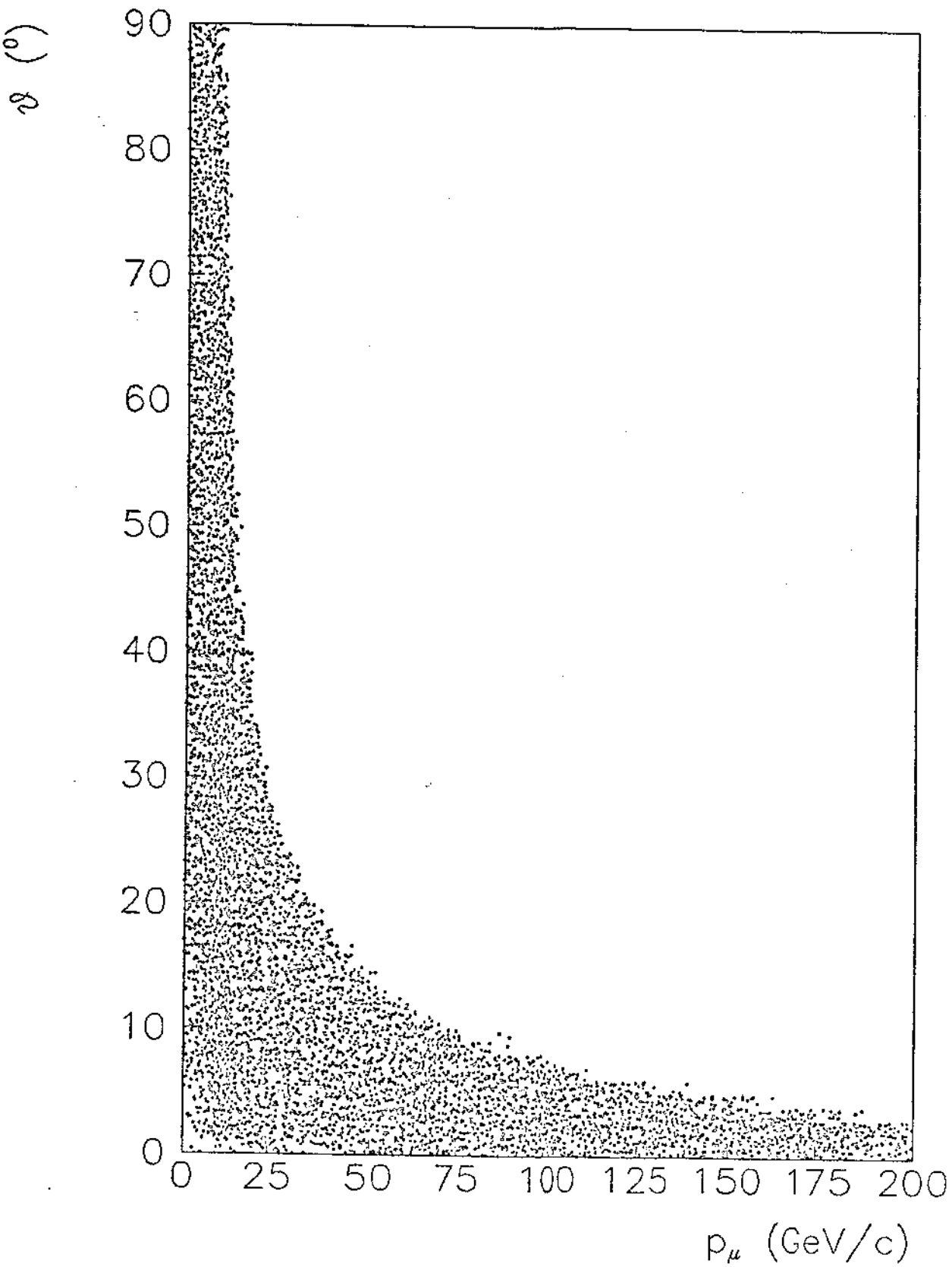

FIG. 10 b)

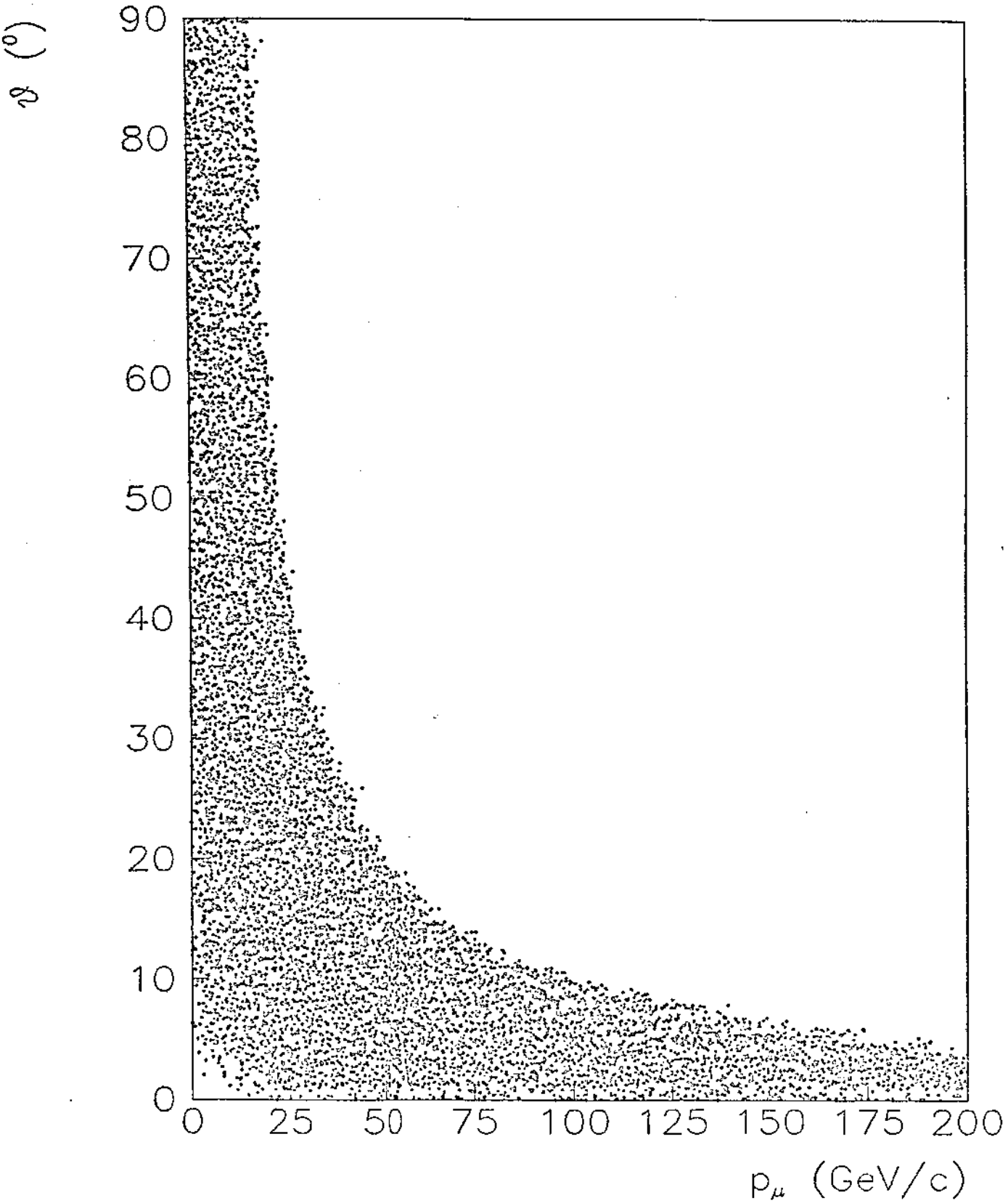

FIG. 10 c)

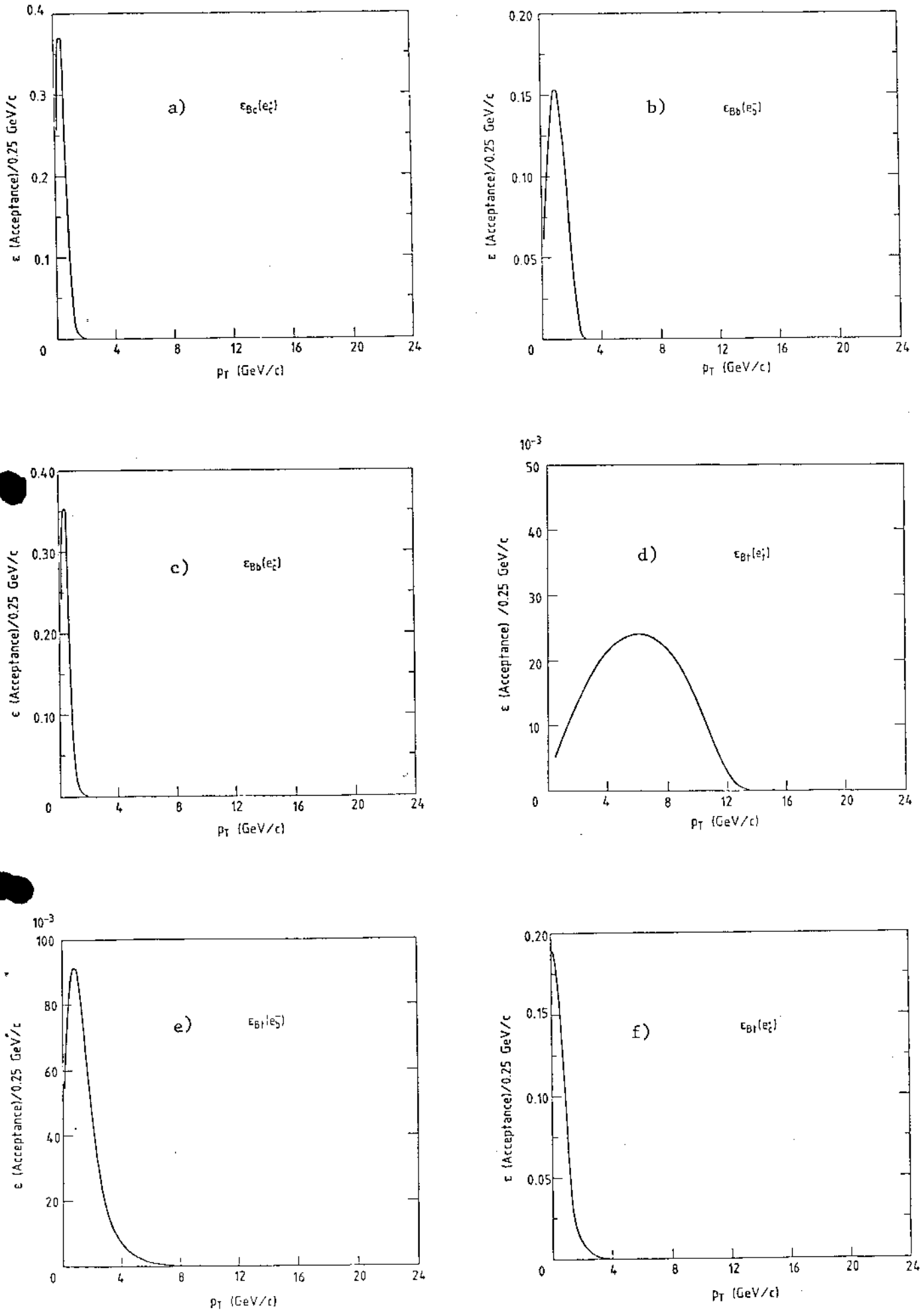
a)
$\varepsilon_{Bc}(e_c^-)$
b)
$\varepsilon_{Bb}(e_b^-)$
c)
$\varepsilon_{Bb}(e_c^-)$
d)
$\varepsilon_{Bf}(e_f^-)$
e)
$\varepsilon_{Bf}(e_b^-)$
f)
$\varepsilon_{Bf}(e_c^-)$
ε (Acceptance)/0.25 GeV/c
ε (Acceptance) /0.25 GeV/c
p_T (GeV/c)
10^{-3}

FIG. 11 a) to f)

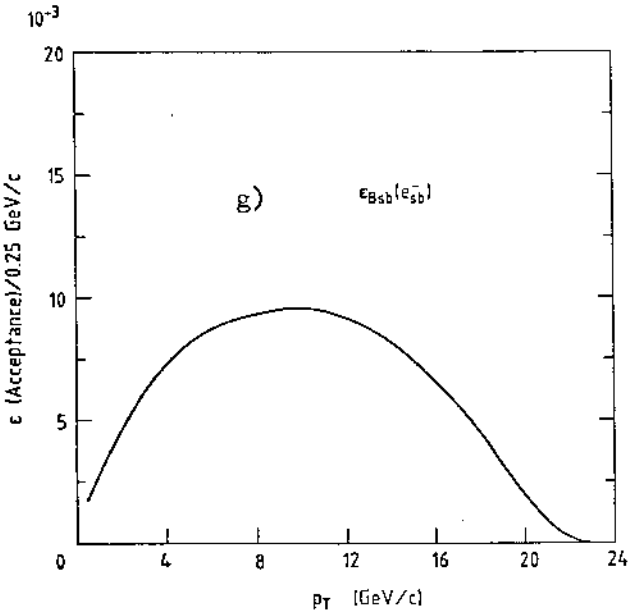
10^{-3}
20
15
10
5
0
g)
$\varepsilon_{Bsb}(e^-_{sb})$
ε (Acceptance)/0.25 GeV/c
4
8
12
16
20
24
p_T (GeV/c)

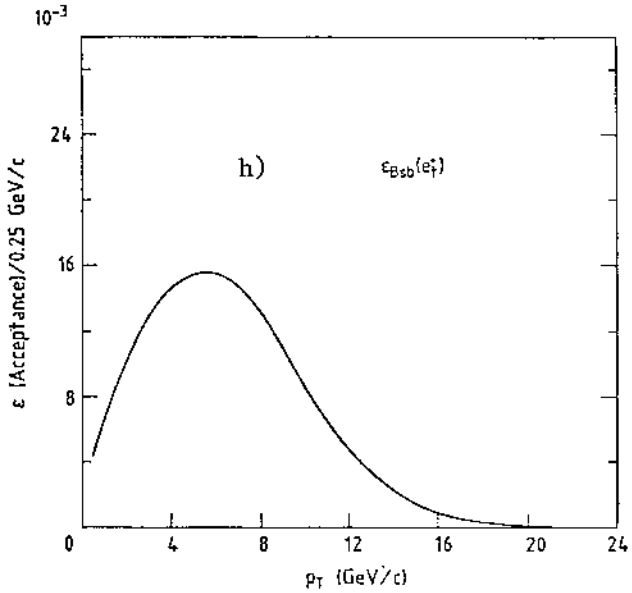
10^{-3}
24
16
8
0
h)
$\varepsilon_{Bsb}(e^+_s)$
ε (Acceptance)/0.25 GeV/c
4
8
12
16
20
24
p_T (GeV/c)

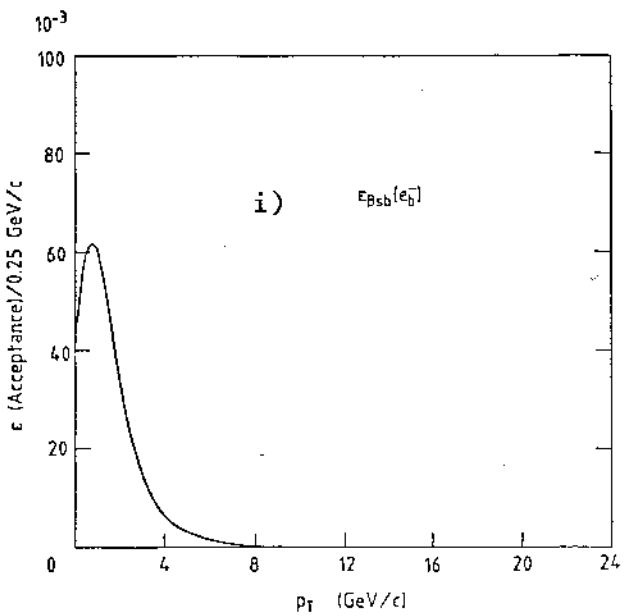
10^{-3}
100
80
60
40
20
0
i)
$\varepsilon_{Bsb}(e^-_b)$
ε (Acceptance)/0.25 GeV/c
4
8
12
16
20
24
p_T (GeV/c)

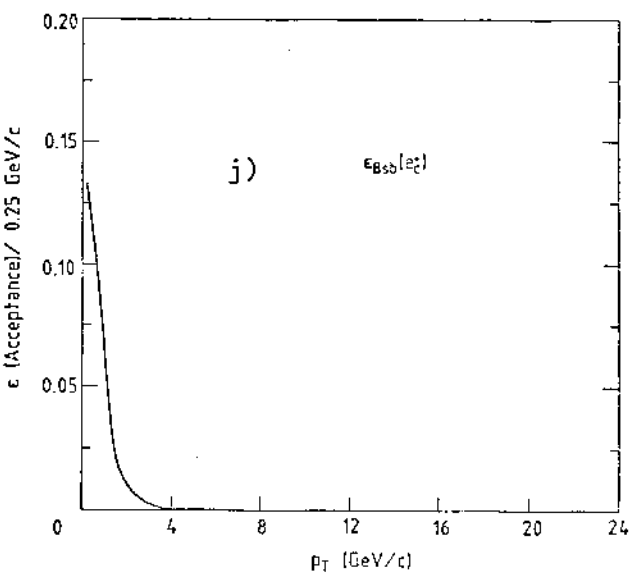
0.20
0.15
0.10
0.05
0
j)
$\varepsilon_{Bsb}(e^+_c)$
ε (Acceptance)/ 0.25 GeV/c
4
8
12
16
20
24
p_T (GeV/c)

FIG. 11 g) to j)

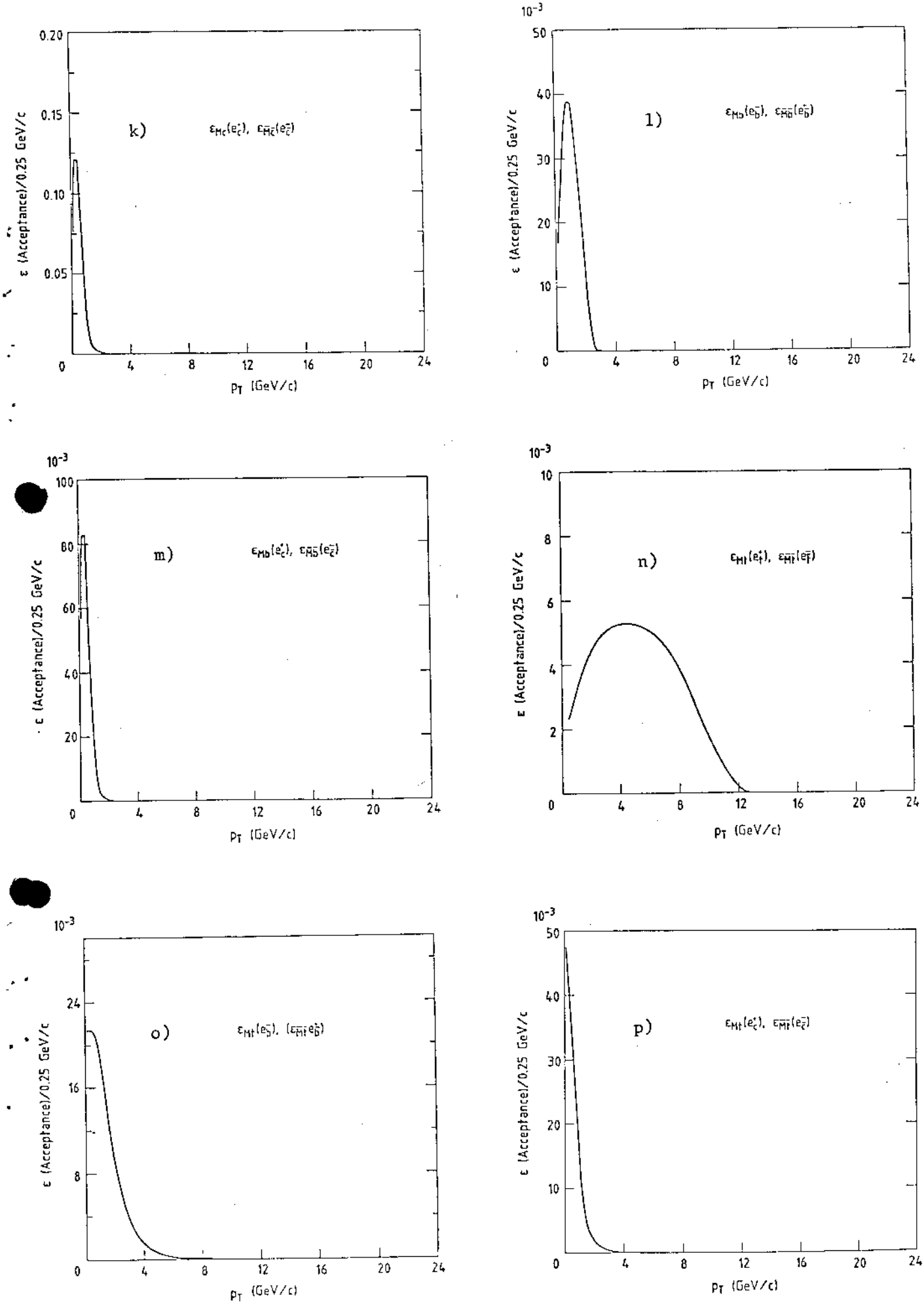
k)
$\varepsilon_{Mc}(e_c^+)$, $\varepsilon_{\overline{Mc}}(e_c^-)$
l)
$\varepsilon_{Mb}(e_b^-)$, $\varepsilon_{\overline{Mb}}(e_b^+)$
m)
$\varepsilon_{Mb}(e_c^+)$, $\varepsilon_{\overline{Mb}}(e_c^-)$
n)
$\varepsilon_{Mt}(e_t^+)$, $\varepsilon_{\overline{Mt}}(e_t^-)$
o)
$\varepsilon_{Mt}(e_b^-)$, $(\varepsilon_{\overline{Mt}} e_b^+)$
p)
$\varepsilon_{Mt}(e_c^+)$, $\varepsilon_{\overline{Mt}}(e_c^-)$
ε (Acceptance)/0.25 GeV/c
p_T (GeV/c)
10^{-3}

FIG. 11 k) to p)

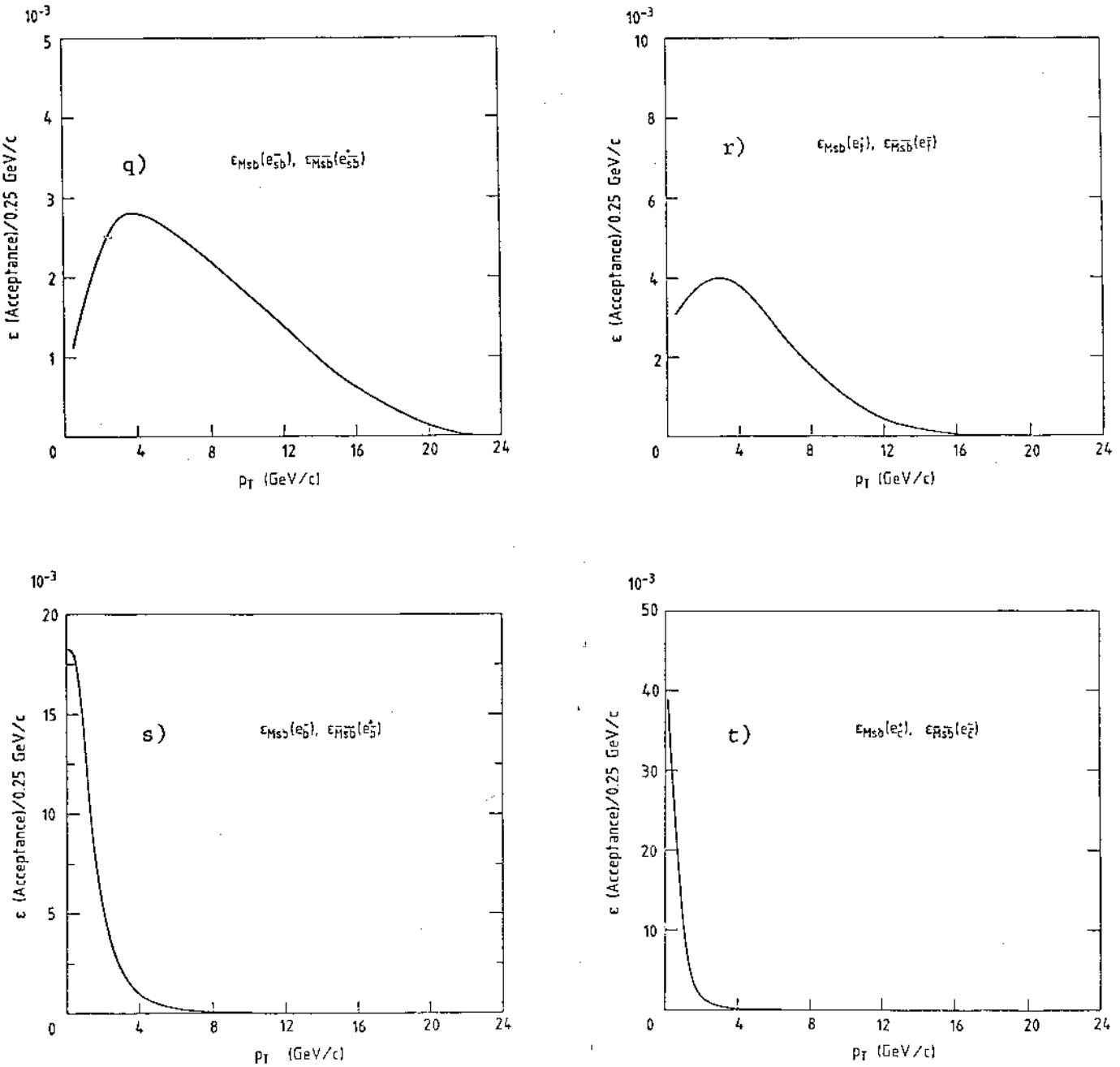
q)
$\varepsilon_{Msb}(e^-_{sb})$, $\varepsilon_{\overline{Msb}}(e^+_{sb})$
r)
$\varepsilon_{Msb}(e_j)$, $\varepsilon_{\overline{Msb}}(e_j)$
s)
$\varepsilon_{Msb}(e^-_b)$, $\varepsilon_{\overline{Msb}}(e^+_b)$
t)
$\varepsilon_{Msb}(e^+_c)$, $\varepsilon_{\overline{Msb}}(e^-_c)$
ε (Acceptance)/0.25 GeV/c
p_T (GeV/c)
10^{-3}

FIG. 11 q) to t)

ϑ_{cut}= 30°, (Leading/Total)= 0.25

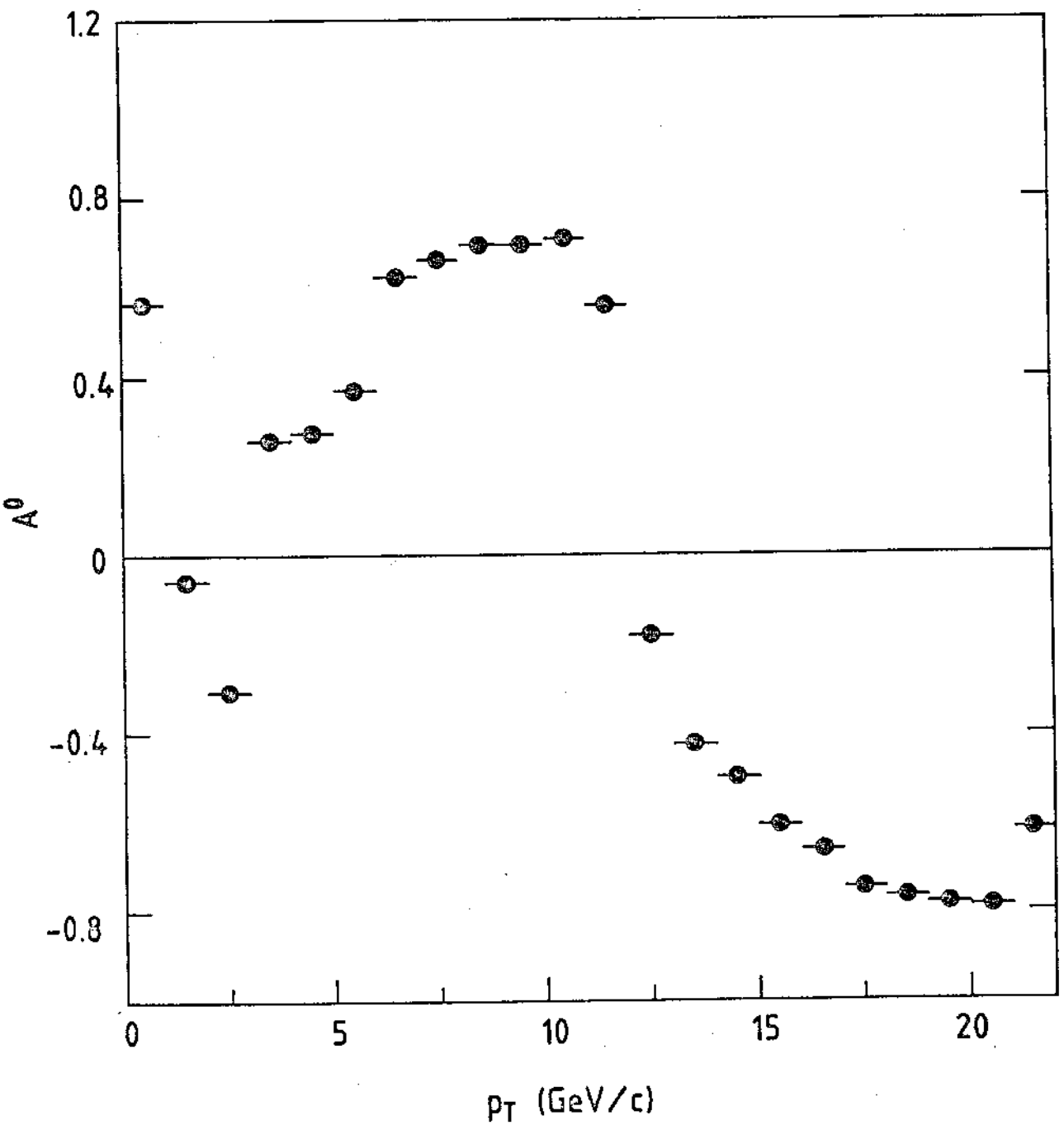

FIG. 12

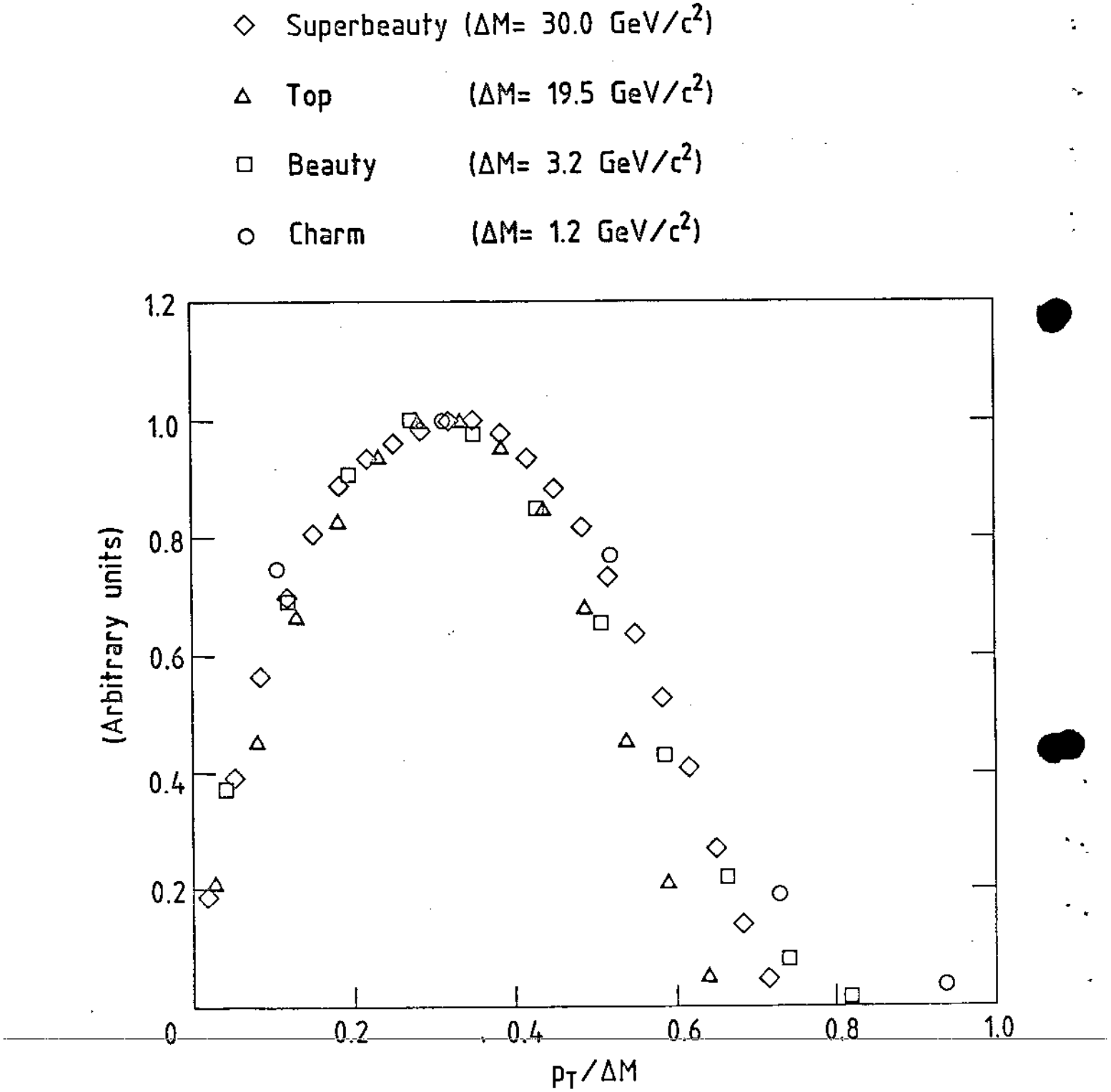
◇ Superbeauty (ΔM= 30.0 GeV/c²)
△ Top (ΔM= 19.5 GeV/c²)
□ Beauty (ΔM= 3.2 GeV/c²)
○ Charm (ΔM= 1.2 GeV/c²)
(Arbitrary units)
1.2
1.0
0.8
0.6
0.4
0.2
0
0.2
0.4
0.6
0.8
1.0
pT/ΔM

FIG. 13

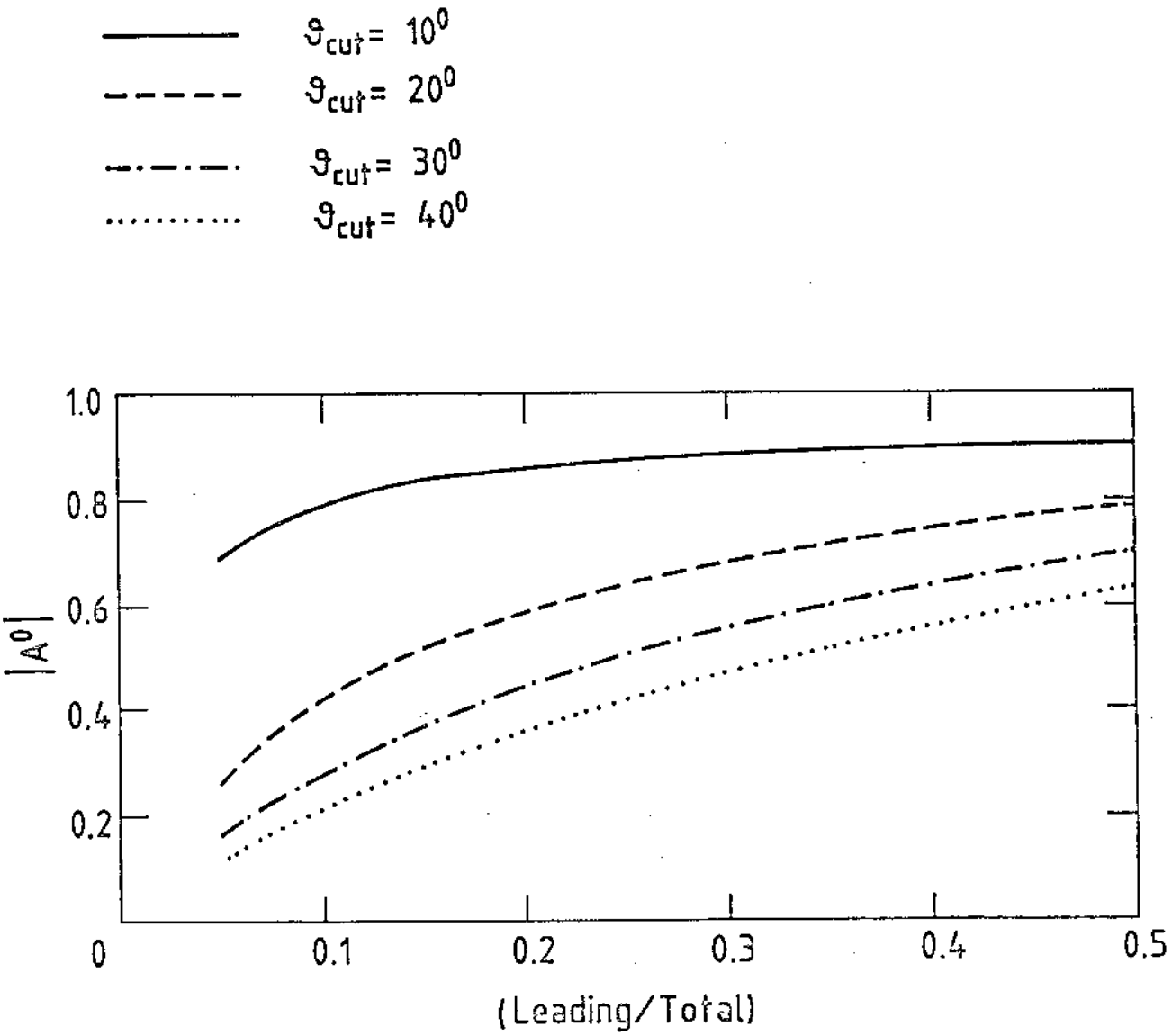
ϑ_{cut}= 10°
ϑ_{cut}= 20°
ϑ_{cut}= 30°
ϑ_{cut}= 40°
1.0
0.8
0.6
0.4
0.2
0
|A°|
0.1
0.2
0.3
0.4
0.5
(Leading/Total)

FIG. 14

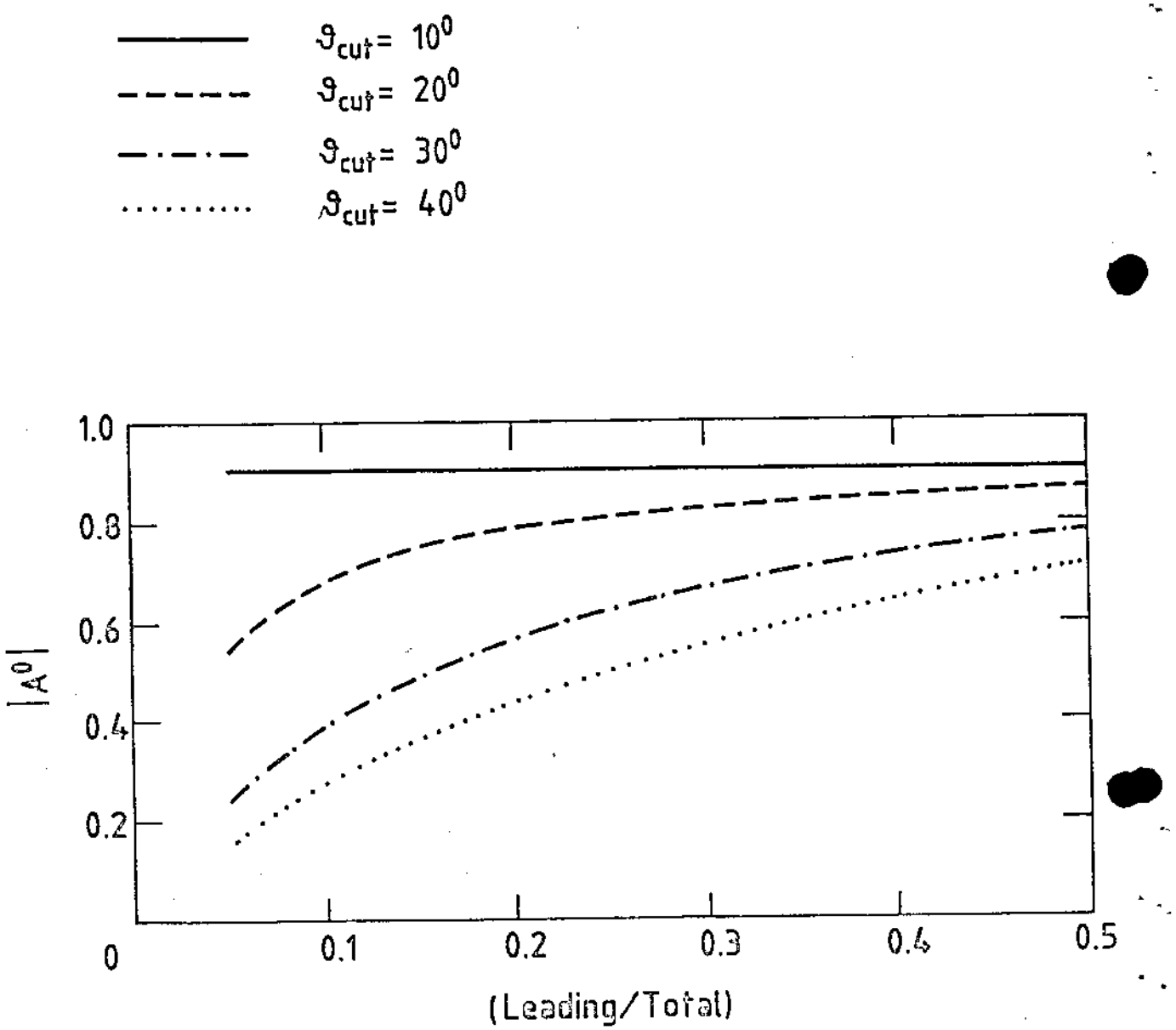
ϑ_{cut}= 10°
ϑ_{cut}= 20°
ϑ_{cut}= 30°
ϑ_{cut}= 40°
1.0
0.8
0.6
0.4
0.2
0
|A⁰|
0.1
0.2
0.3
0.4
0.5
(Leading/Total)

FIG. 15

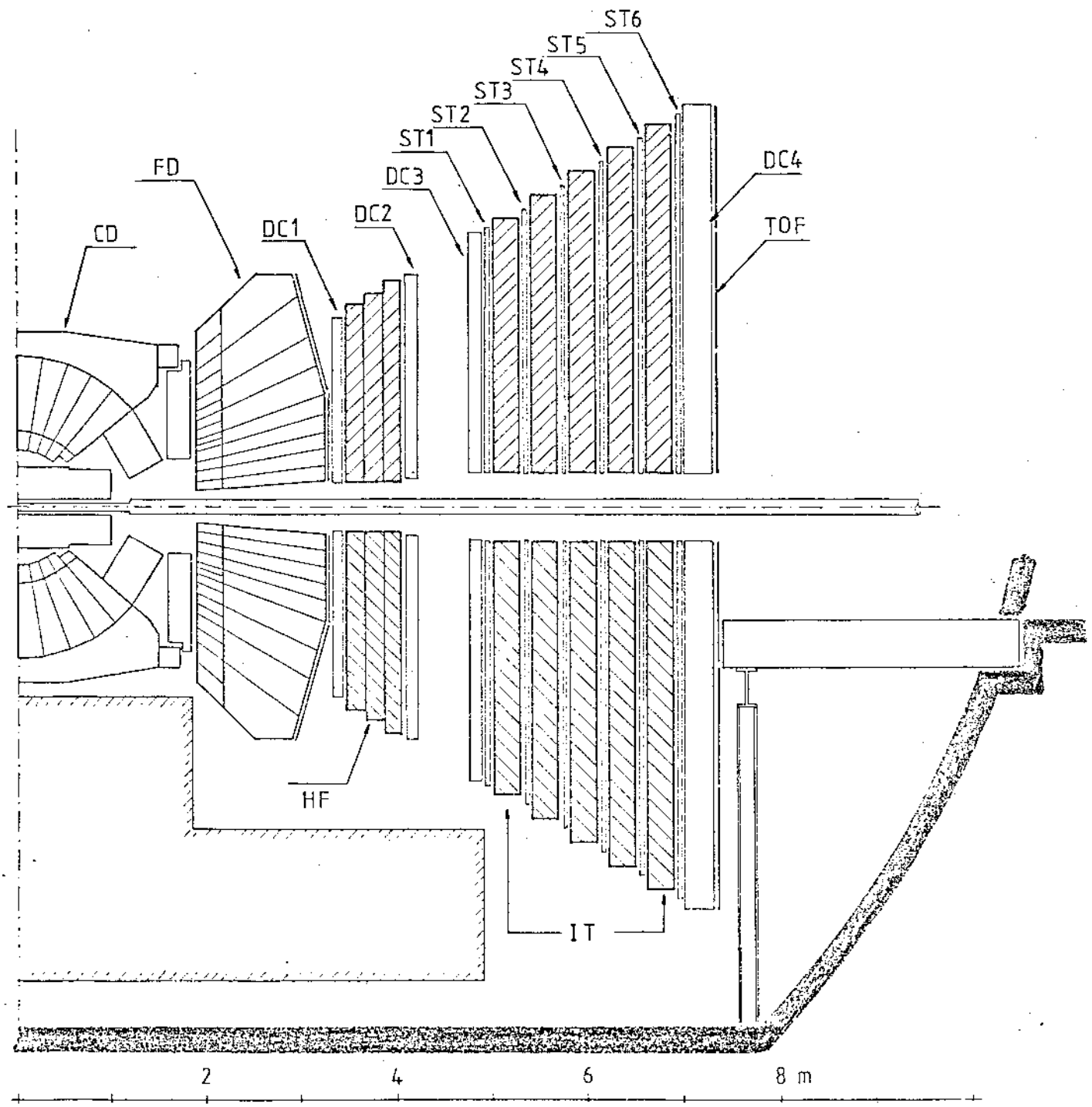

FIG. 16

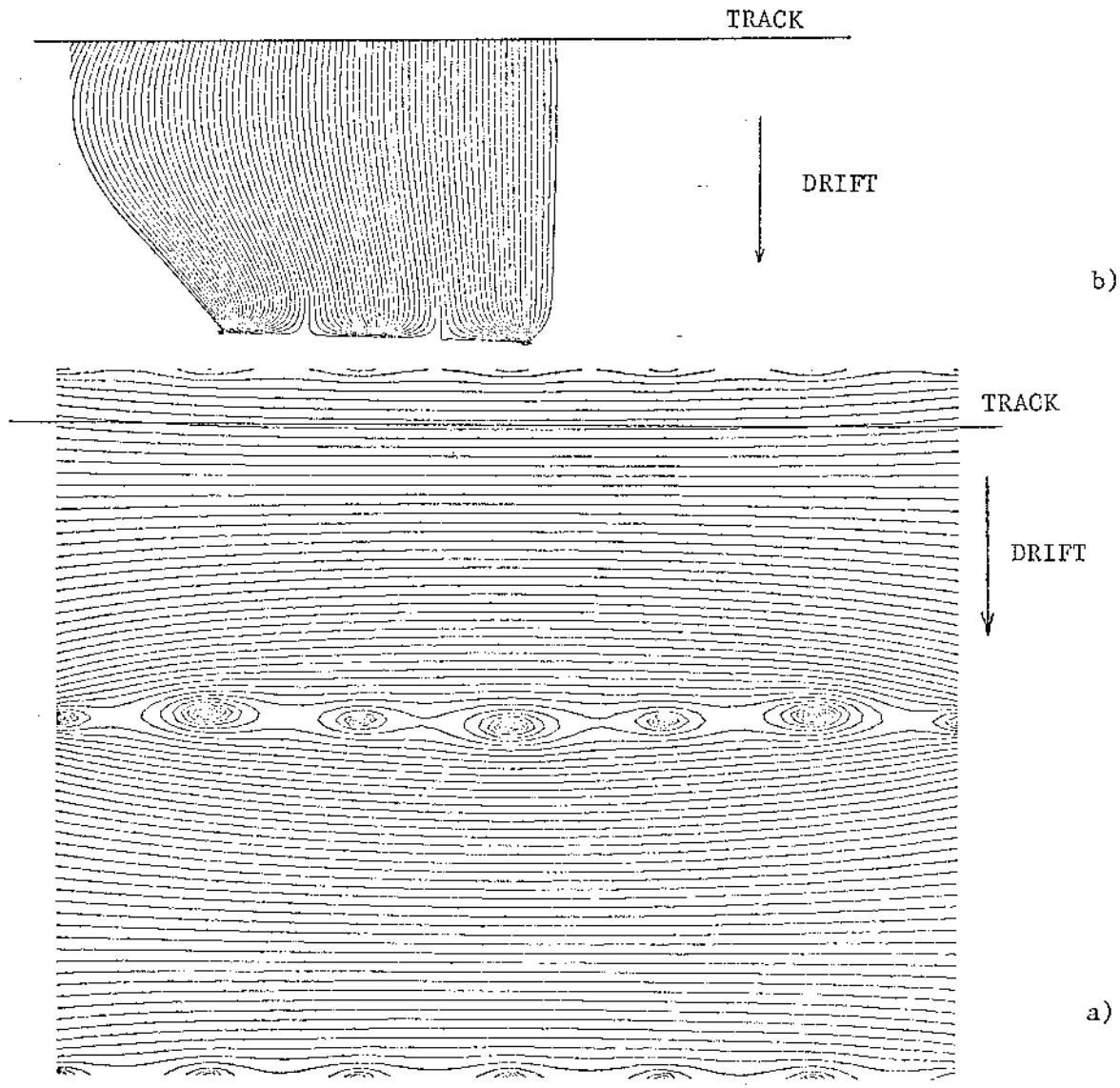

FIG. 17

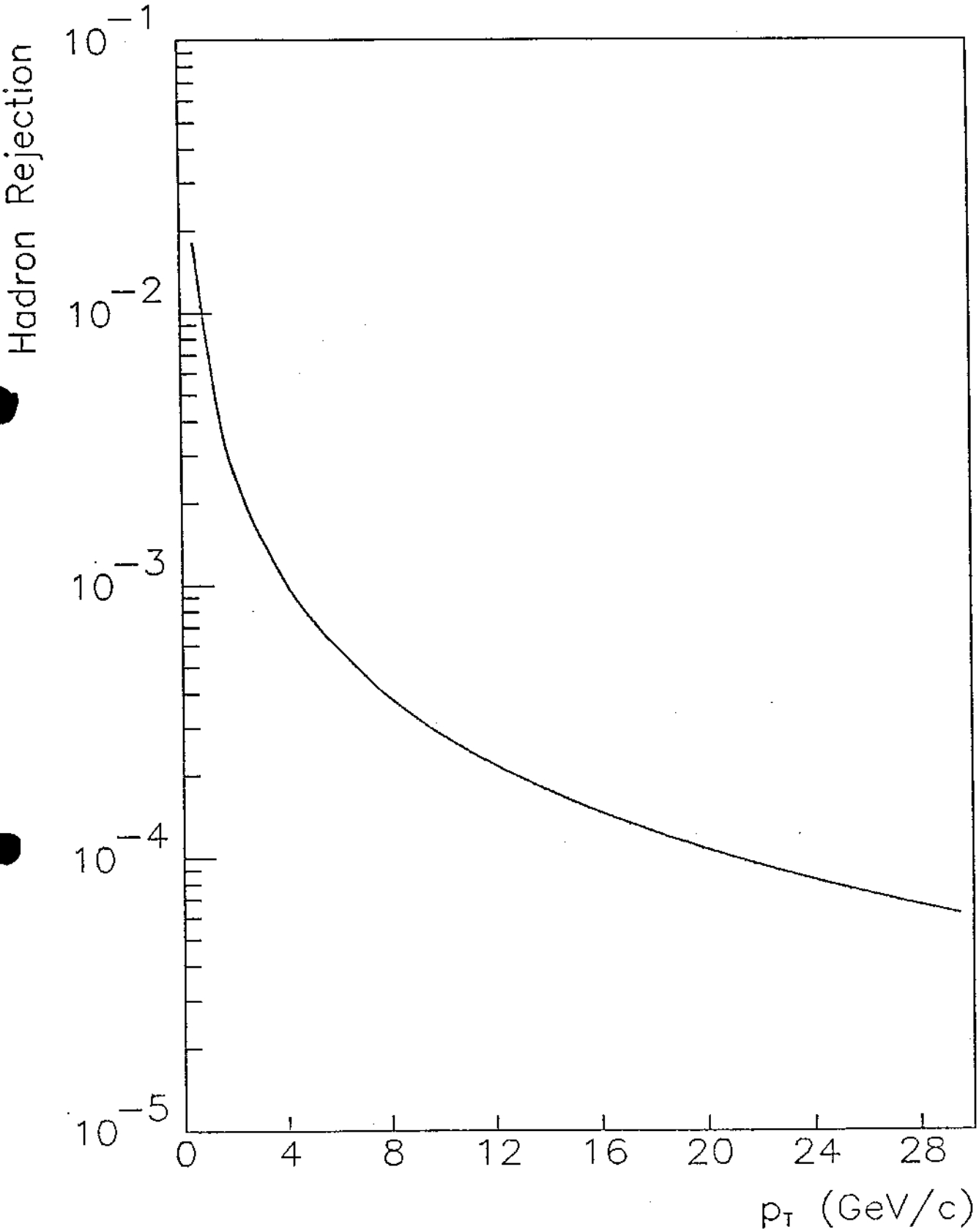

FIG. 18

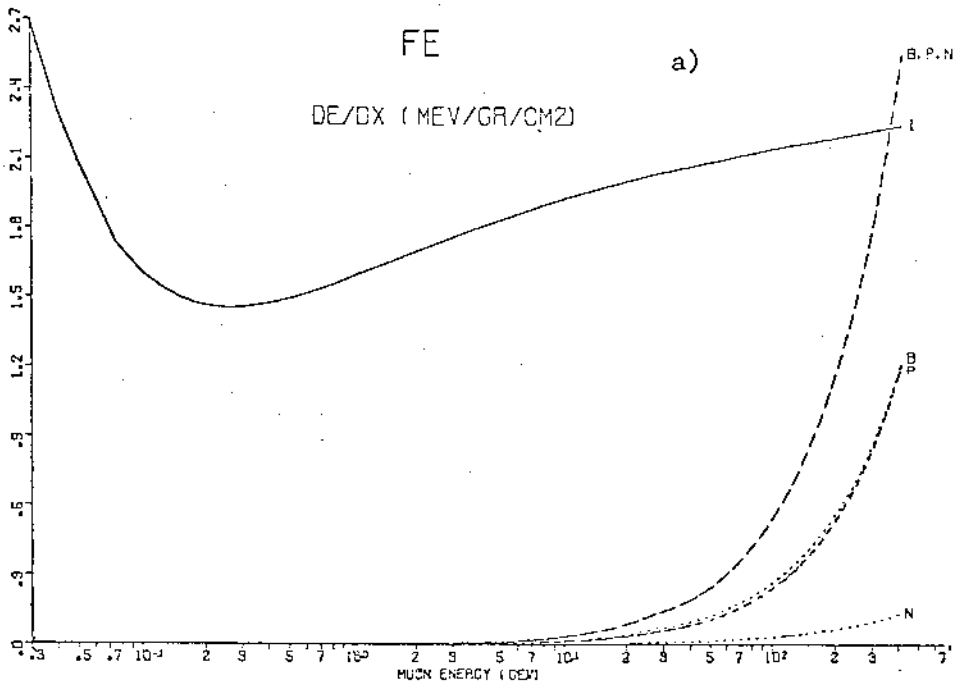
FE
a)
DE/DX (MEV/GR/CM2)
B, P, N
L
B
P
N
MUON ENERGY (GEV)

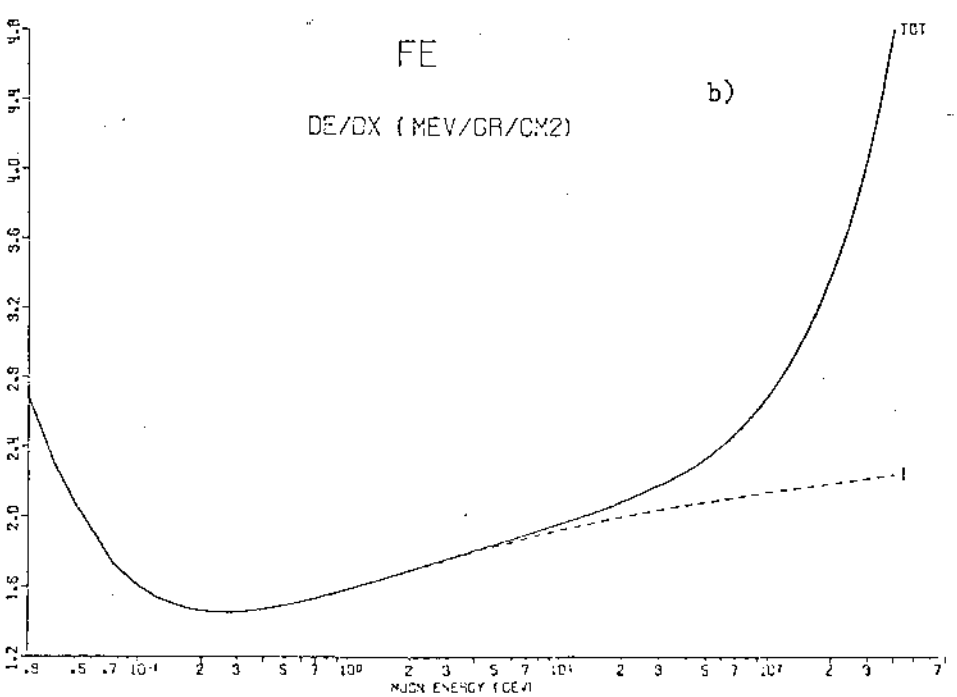
FE
b)
DE/DX (MEV/GR/CM2)
TOT
I
MUON ENERGY (GEV)

FIG. 19

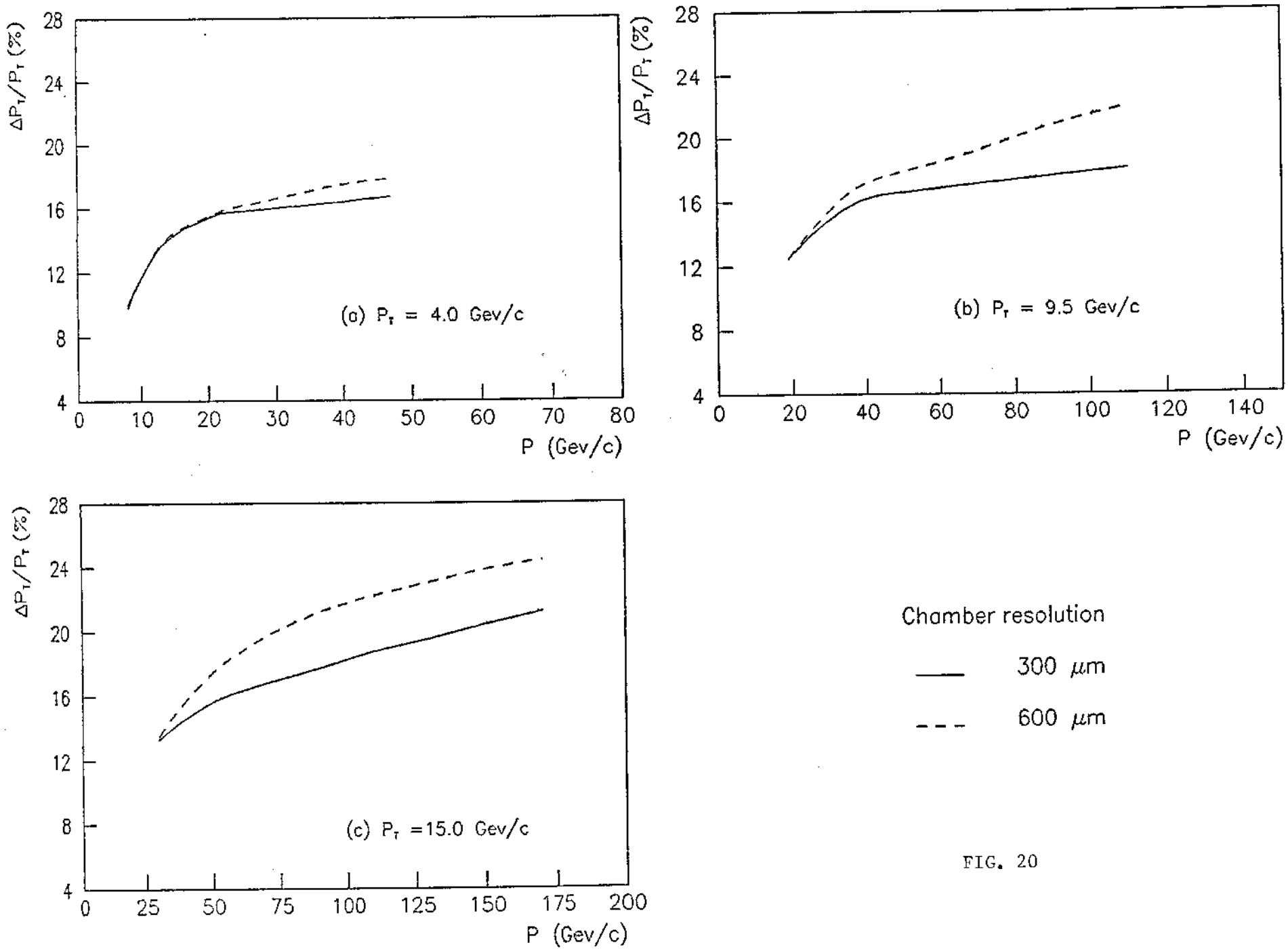
ΔP_T/P_T (%)
28
24
20
16
12
8
4
0
10
20
30
40
50
60
70
80
P (Gev/c)
(a) P_T = 4.0 Gev/c
ΔP_T/P_T (%)
28
24
20
16
12
8
4
0
20
40
60
80
100
120
140
P (Gev/c)
(b) P_T = 9.5 Gev/c
ΔP_T/P_T (%)
28
24
20
16
12
8
4
0
25
50
75
100
125
150
175
200
P (Gev/c)
(c) P_T =15.0 Gev/c
Chamber resolution
300 μm
600 μm

FIG. 20

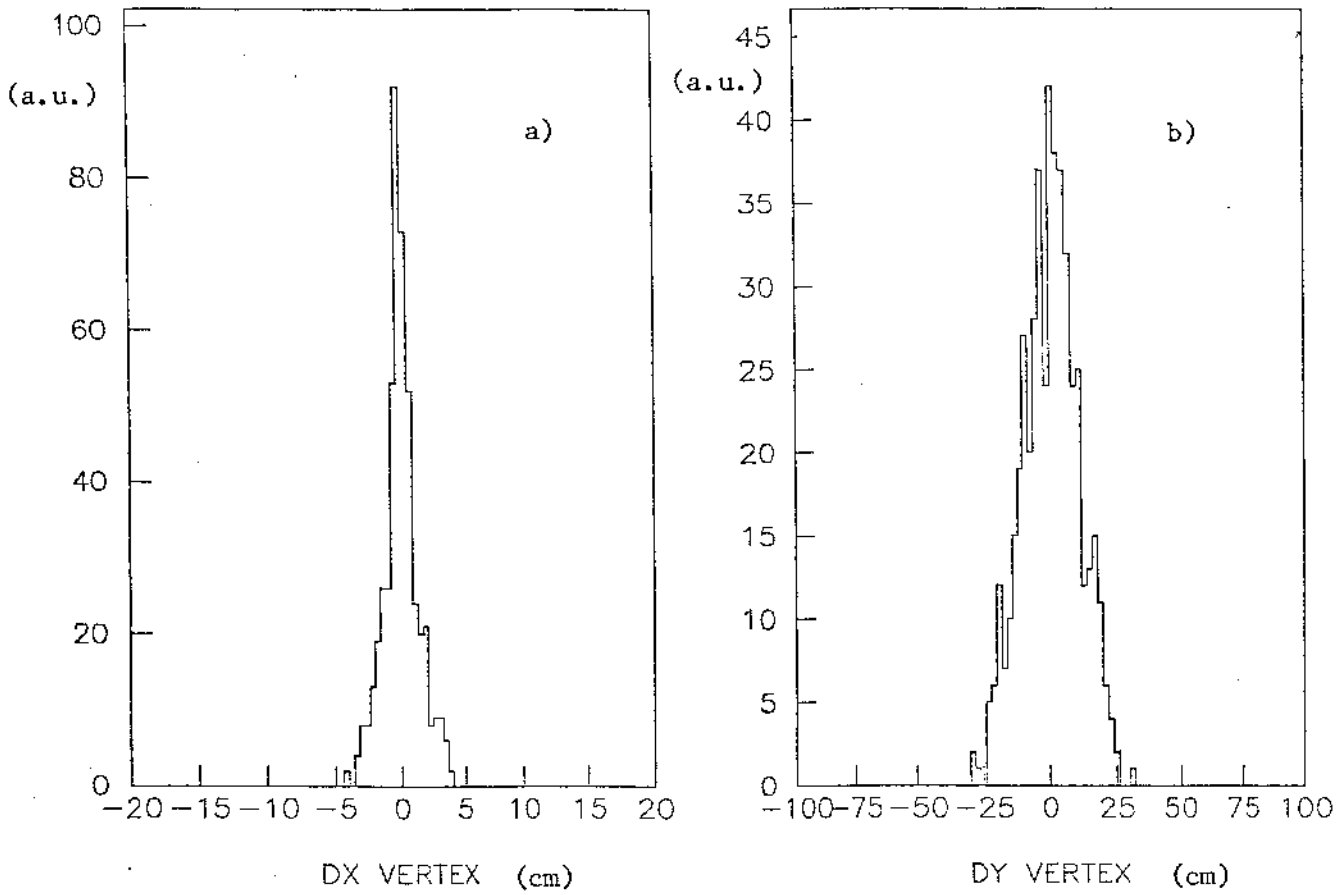
(a.u.)
a)
100
80
60
40
20
0
−20 −15 −10 −5 0 5 10 15 20
DX VERTEX (cm)
(a.u.)
b)
45
40
35
30
25
20
15
10
5
0
−100 −75 −50 −25 0 25 50 75 100
DY VERTEX (cm)
(a.u.)
c)
100
80
60
40
20
0
−20 −15 −10 −5 0 5 10 15 20
DZ VERTEX (cm)

FIG. 21

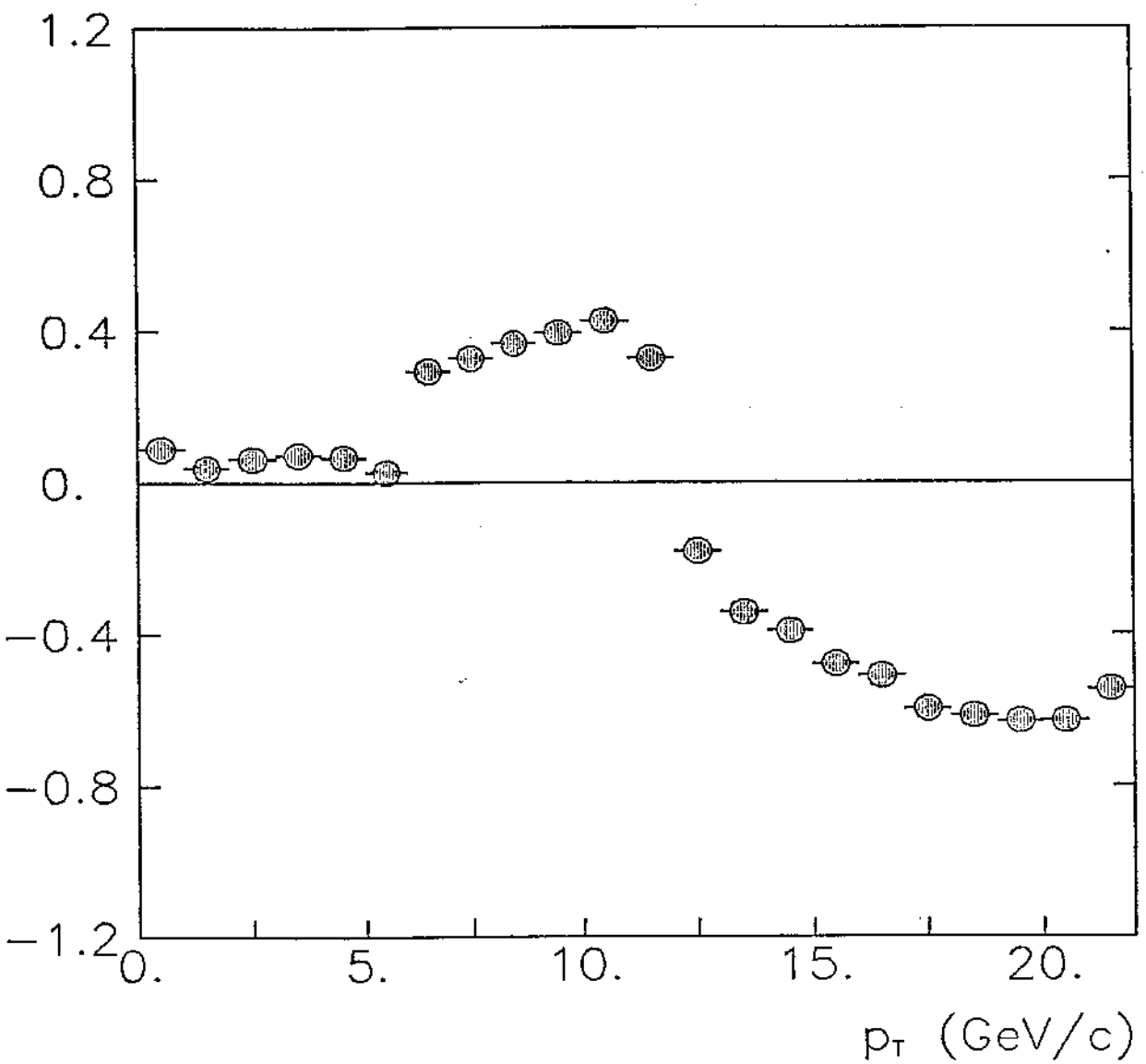

FIG. 22

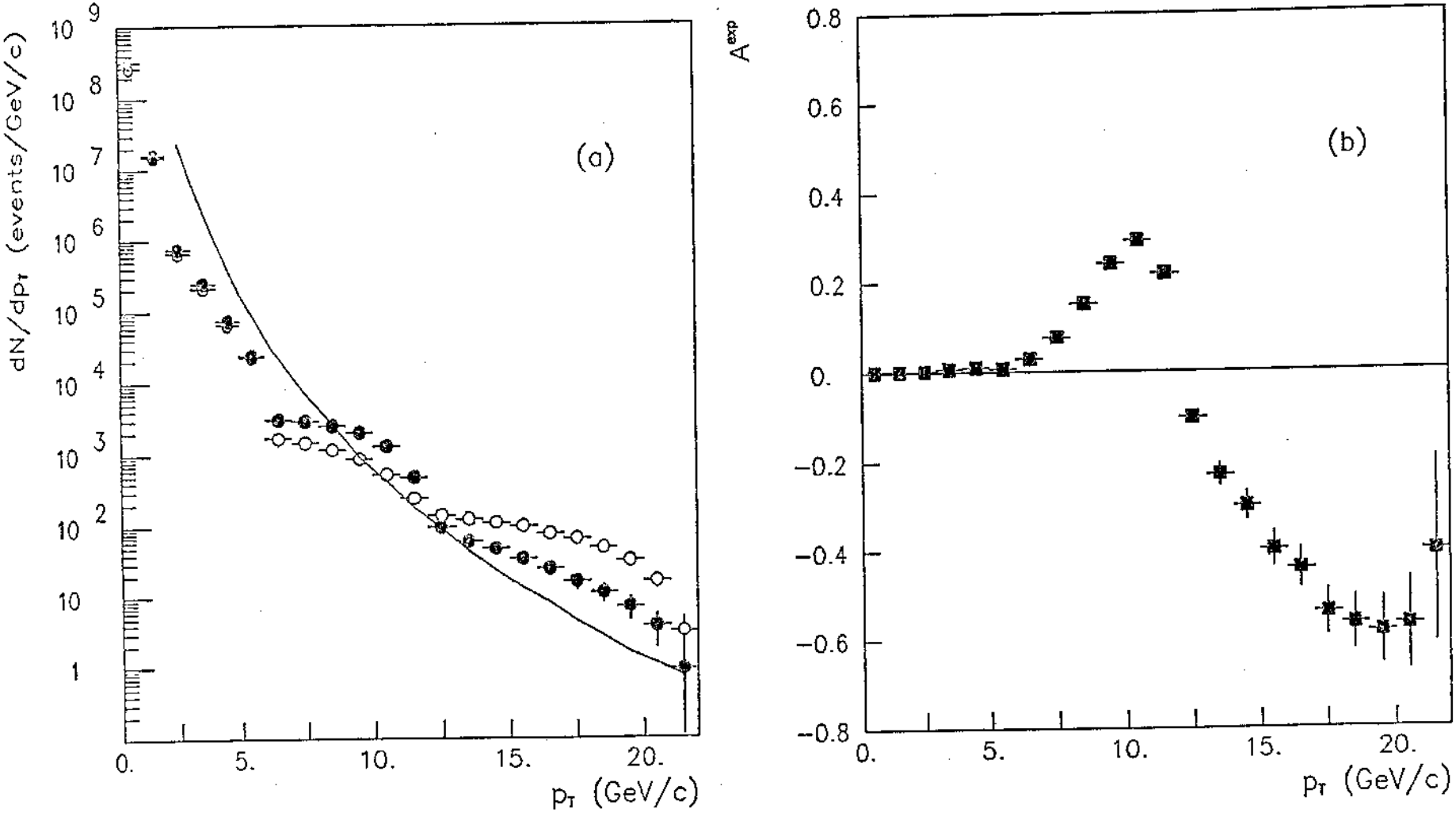

FIG. 23

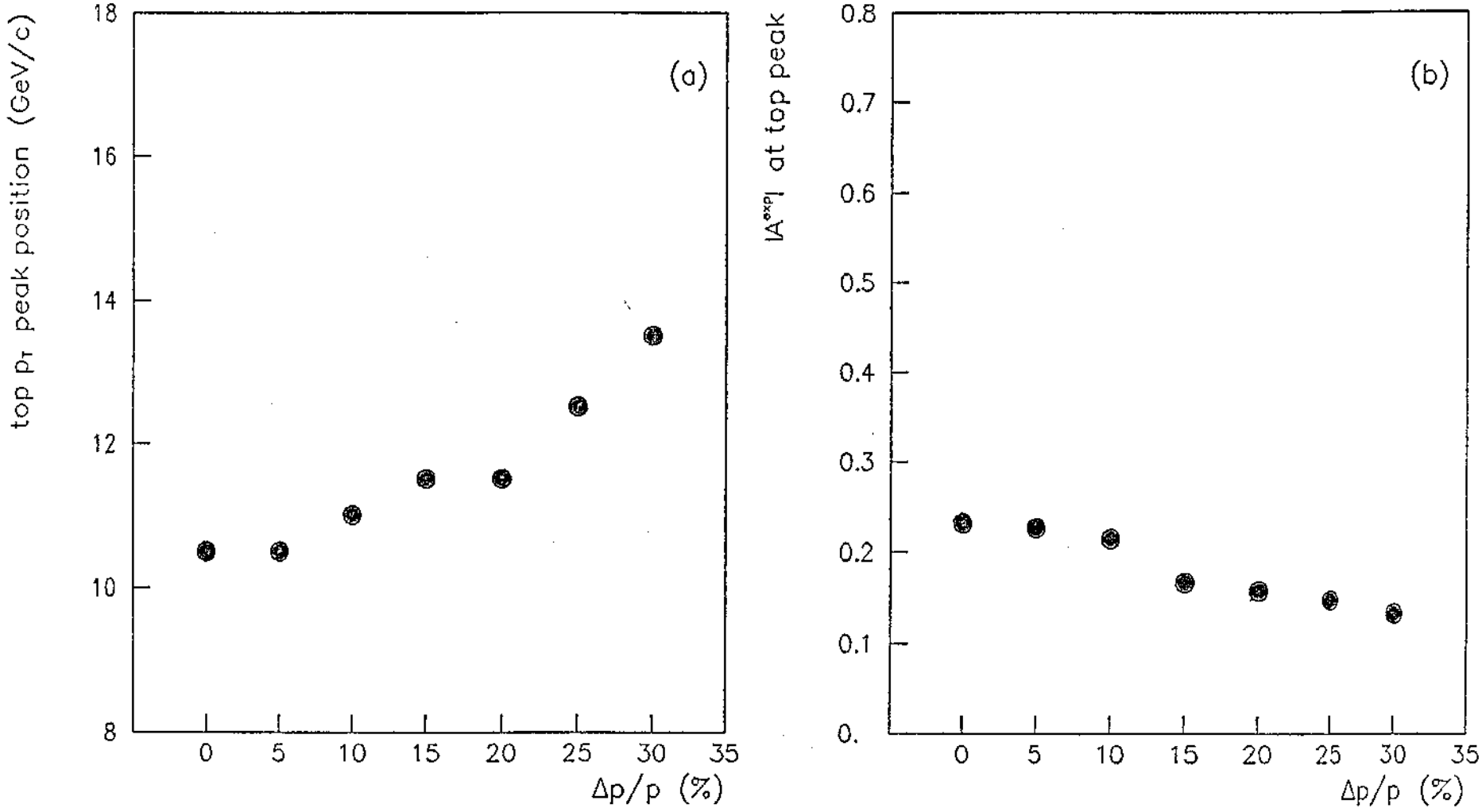
(a)
top p_T peak position (GeV/c)
18
16
14
12
10
8
0
5
10
15
20
25
30
35
Δp/p (%)
(b)
$|A^{exp}|$ at top peak
0.8
0.7
0.6
0.5
0.4
0.3
0.2
0.1
0.
0
5
10
15
20
25
30
35
Δp/p (%)

FIG. 24

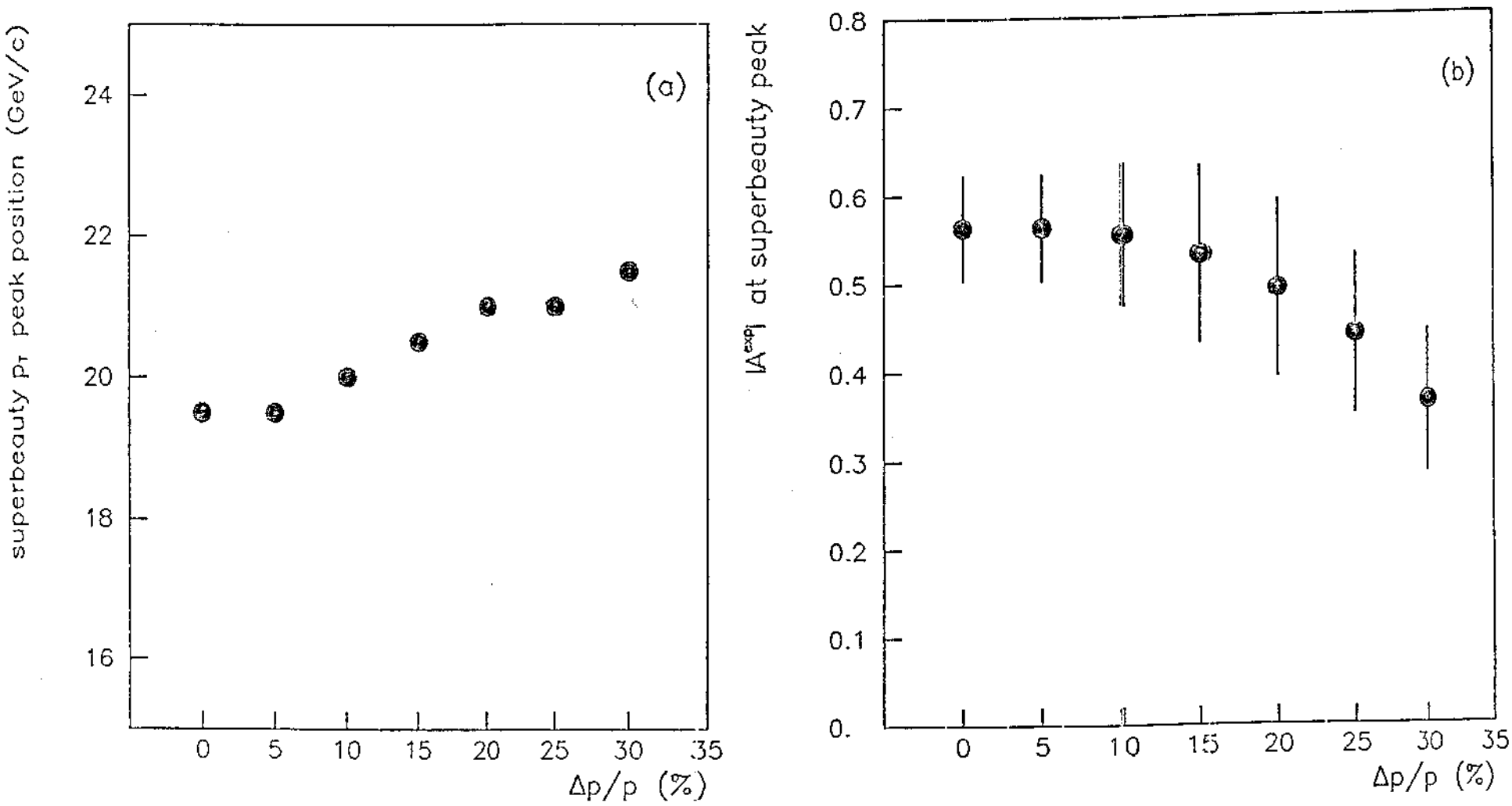
superbeauty p_T peak position (GeV/c)
24
22
20
18
16
(a)
0
5
10
15
20
25
30
35
Δp/p (%)
$|A^{exp}|$ at superbeauty peak
0.8
0.7
0.6
0.5
0.4
0.3
0.2
0.1
0.
(b)
0
5
10
15
20
25
30
35
Δp/p (%)

FIG. 25

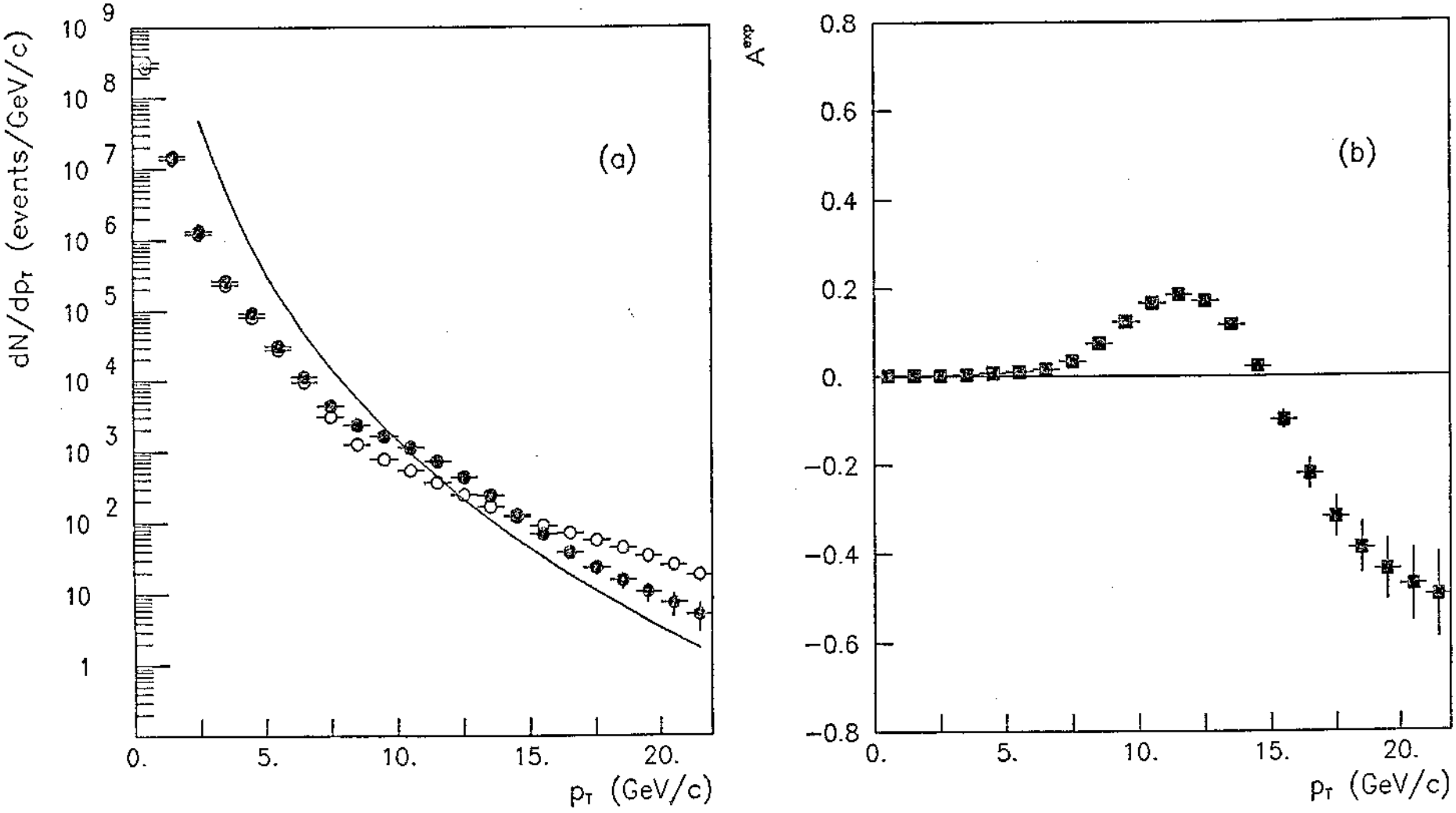

FIG. 26

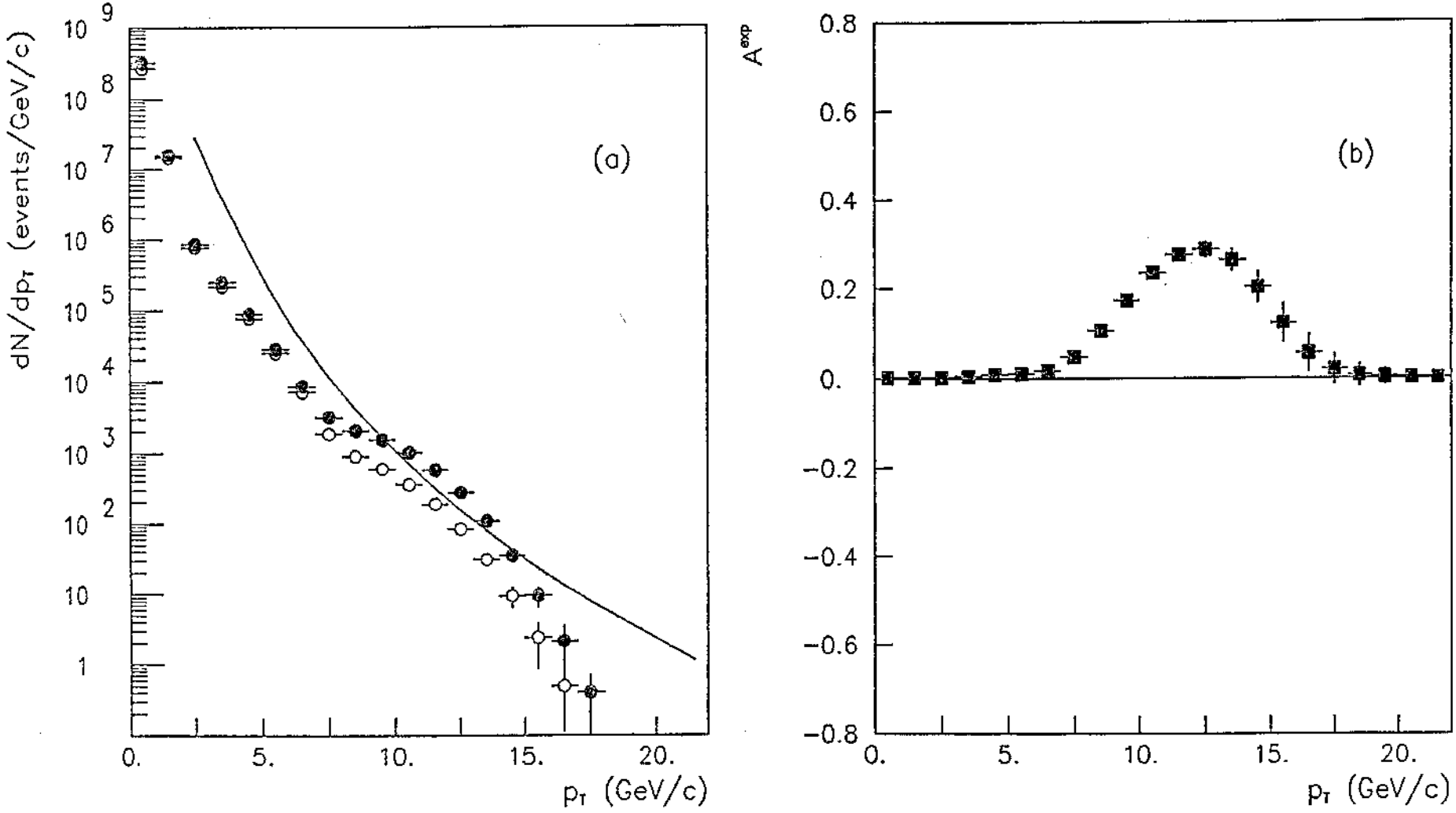

FIG. 27

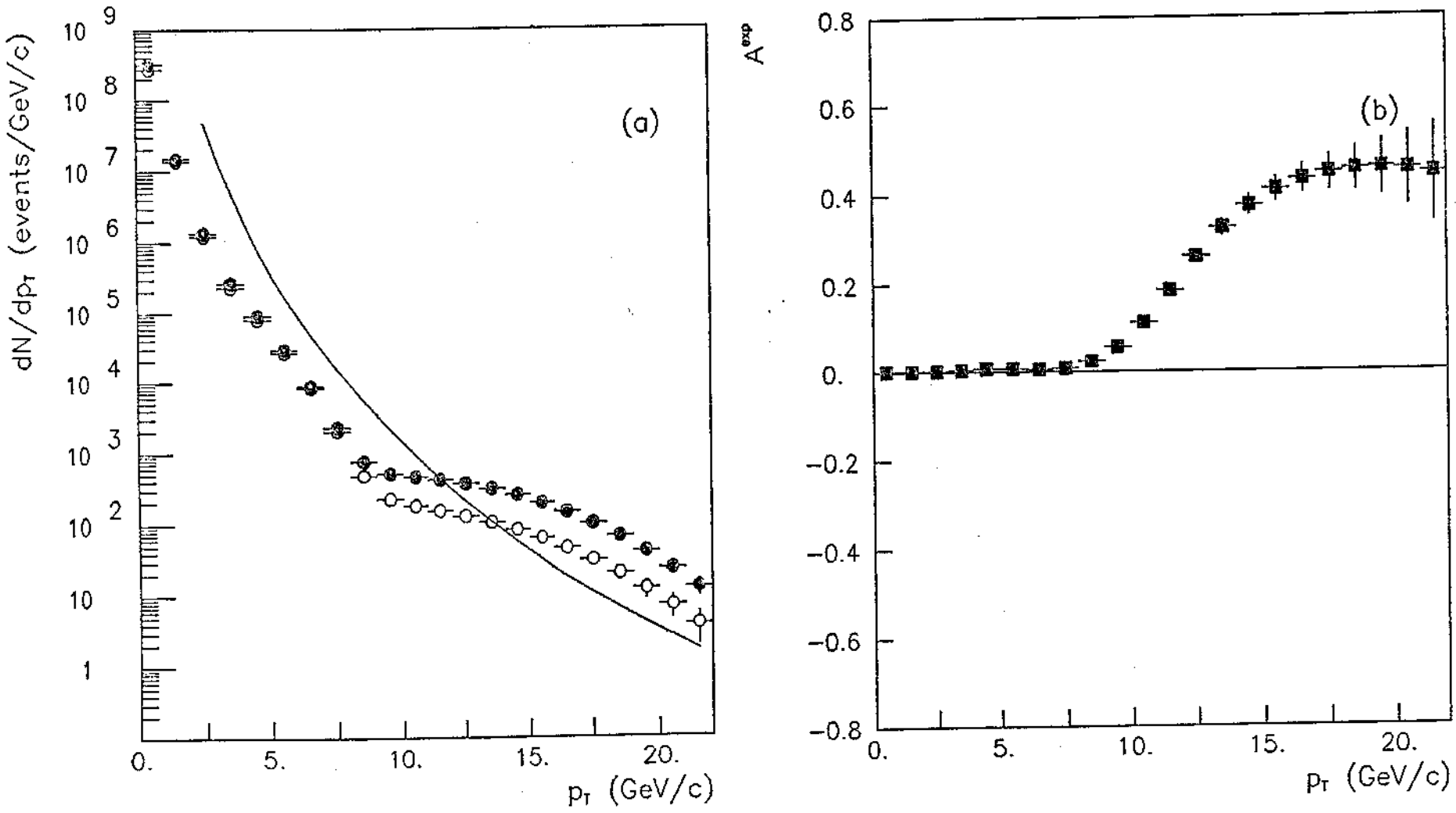

FIG. 28

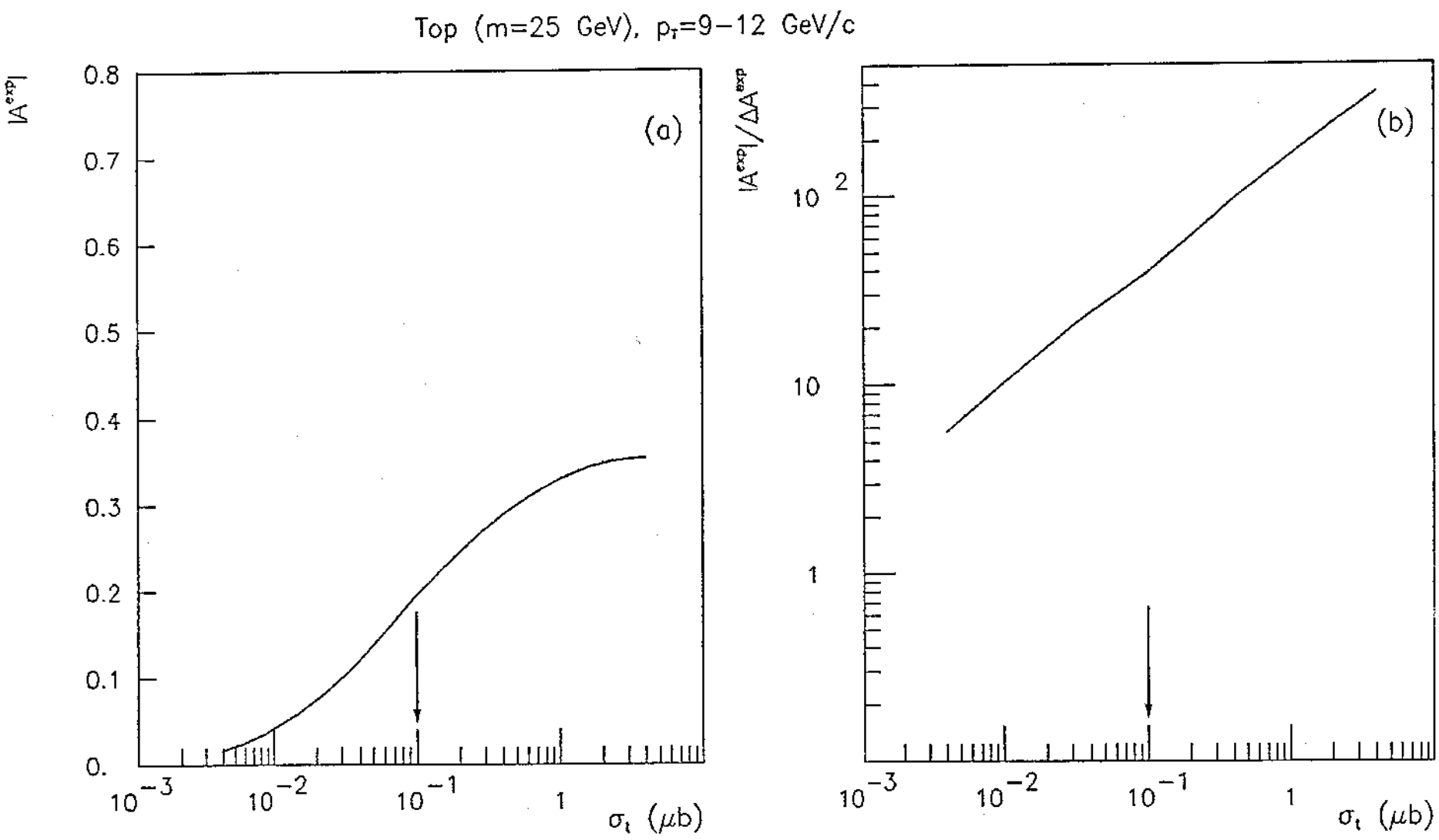
Top (m=25 GeV), p_T=9–12 GeV/c
$|A^{exp}|$
0.8
0.7
0.6
0.5
0.4
0.3
0.2
0.1
0.
(a)
10^{-3}
10^{-2}
10^{-1}
1
σ_t (μb)
$|A^{exp}|/\Delta A^{exp}$
10^2
10
1
(b)
10^{-3}
10^{-2}
10^{-1}
1
σ_t (μb)

FIG. 29

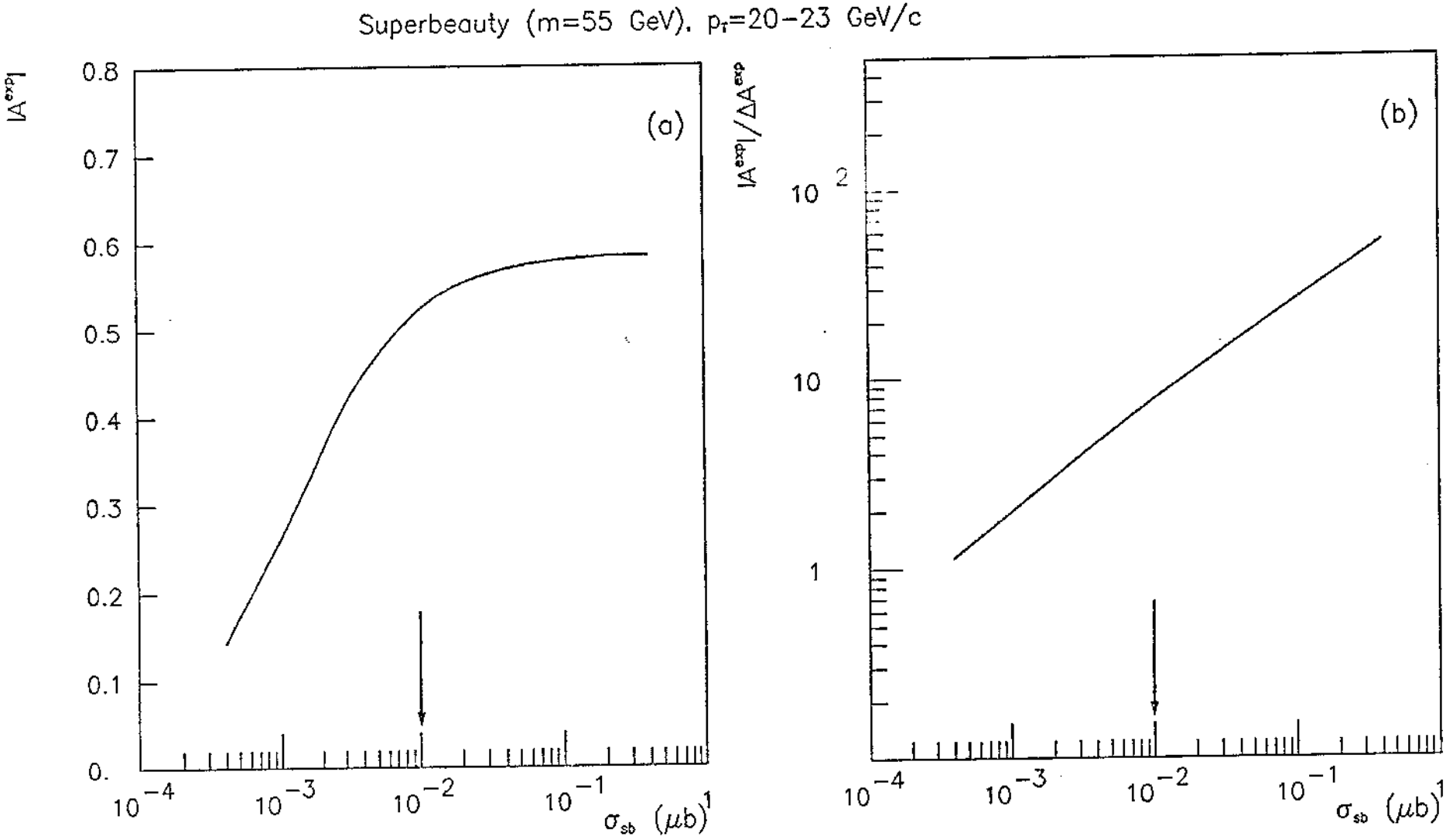
Superbeauty (m=55 GeV), p_T=20-23 GeV/c
$|A^{exp}|$
0.8
0.7
0.6
0.5
0.4
0.3
0.2
0.1
0.
(a)
10^{-4}
10^{-3}
10^{-2}
10^{-1}
1
σ_{sb} (μb)
$|A^{exp}|/\Delta A^{exp}$
10^2
10
1
(b)
10^{-4}
10^{-3}
10^{-2}
10^{-1}
1
σ_{sb} (μb)

FIG. 30

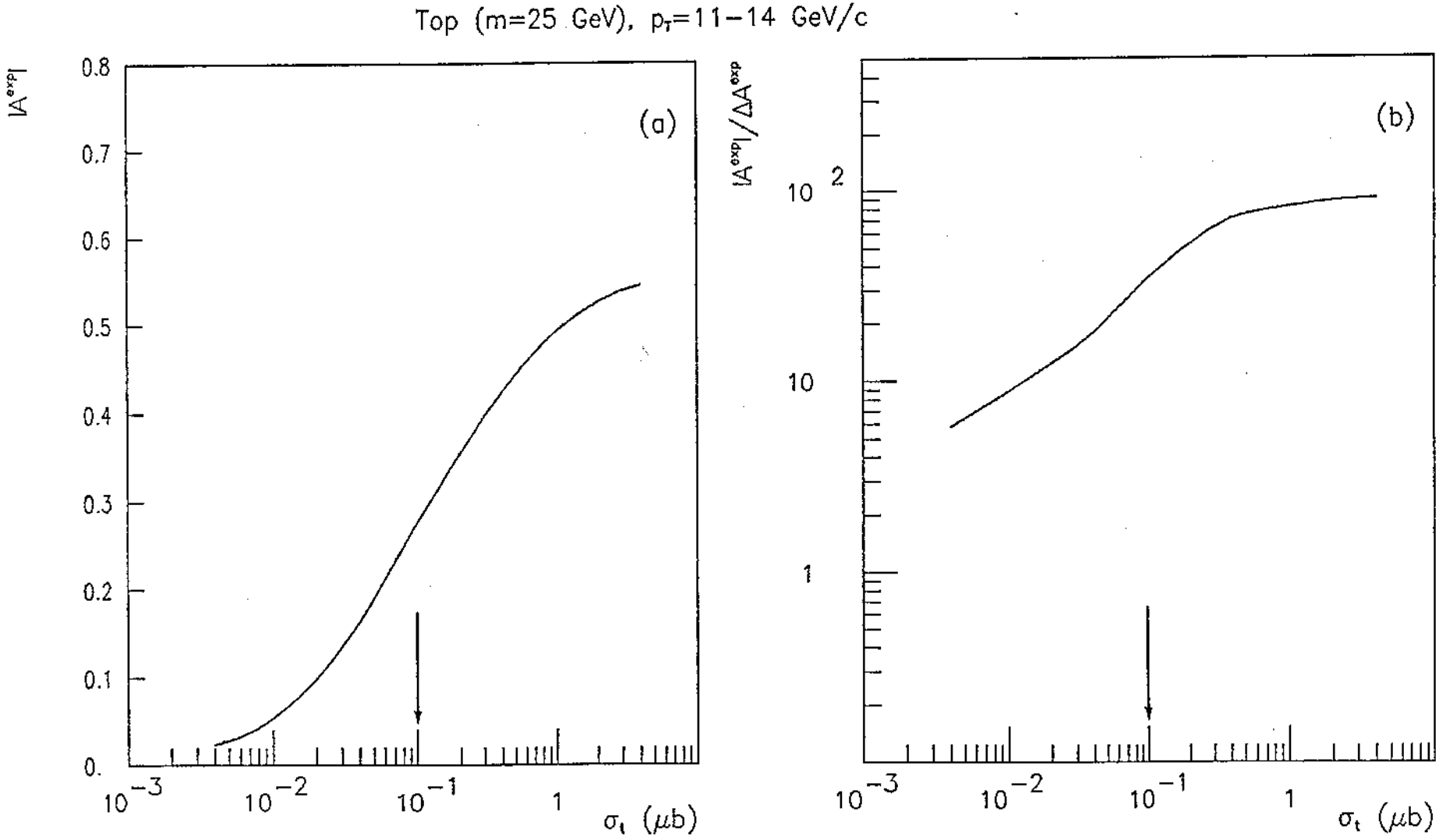
Top (m=25 GeV), p_T=11−14 GeV/c
$|A^{exp}|$
0.8
0.7
0.6
0.5
0.4
0.3
0.2
0.1
0.
(a)
10^{-3}
10^{-2}
10^{-1}
1
σ_t (μb)
$|A^{exp}|/\Delta A^{exp}$
10^2
10
1
(b)
10^{-3}
10^{-2}
10^{-1}
1
σ_t (μb)

FIG. 31

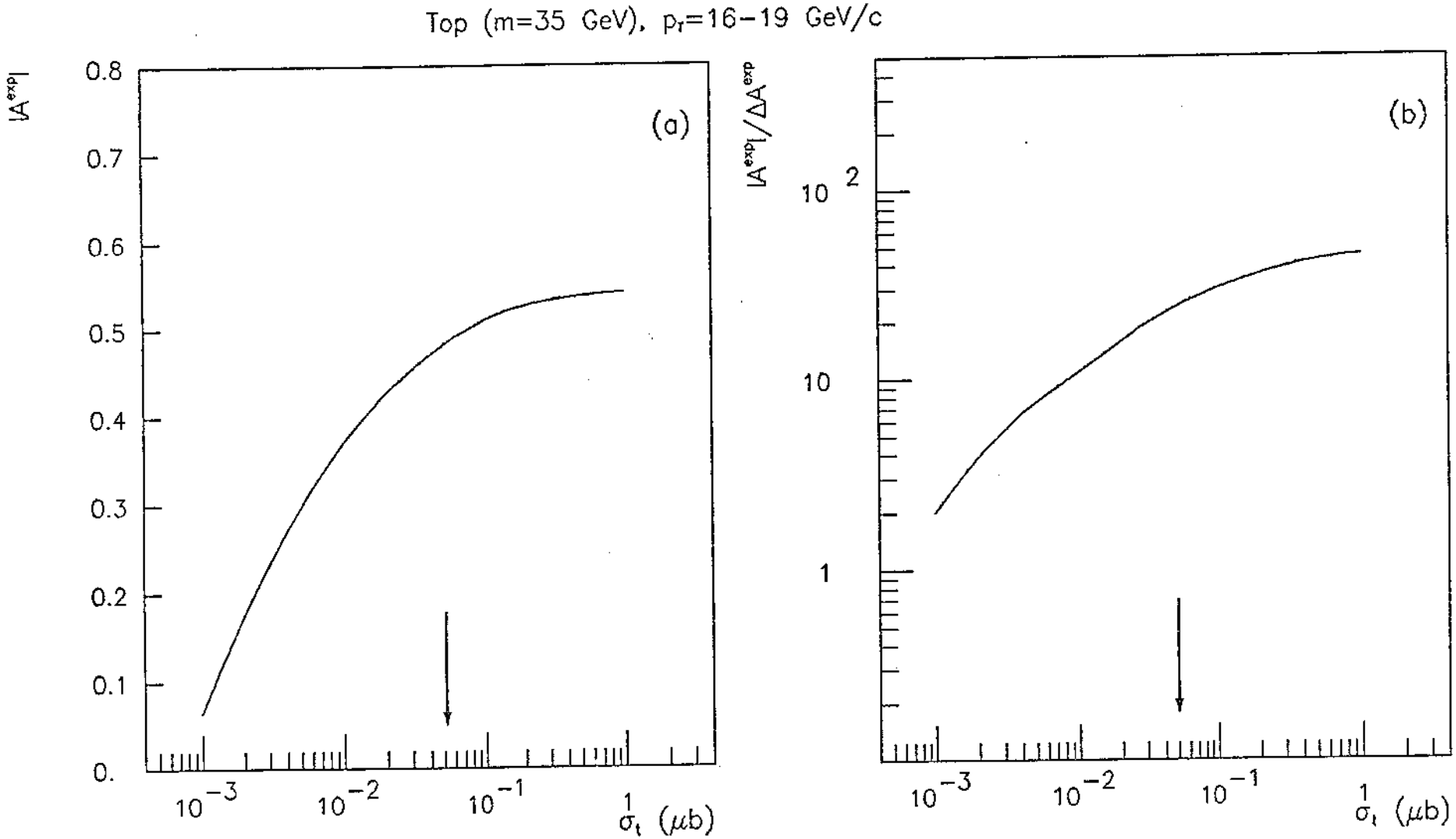
Top (m=35 GeV), p_T=16-19 GeV/c
$|A^{exp}|$
0.8
0.7
0.6
0.5
0.4
0.3
0.2
0.1
0.
(a)
10^{-3}
10^{-2}
10^{-1}
$\frac{1}{\sigma_t}$ (μb)
$|A^{exp}|/\Delta A^{exp}$
10^2
10
1
(b)
10^{-3}
10^{-2}
10^{-1}
$\frac{1}{\sigma_t}$ (μb)

FIG. 32

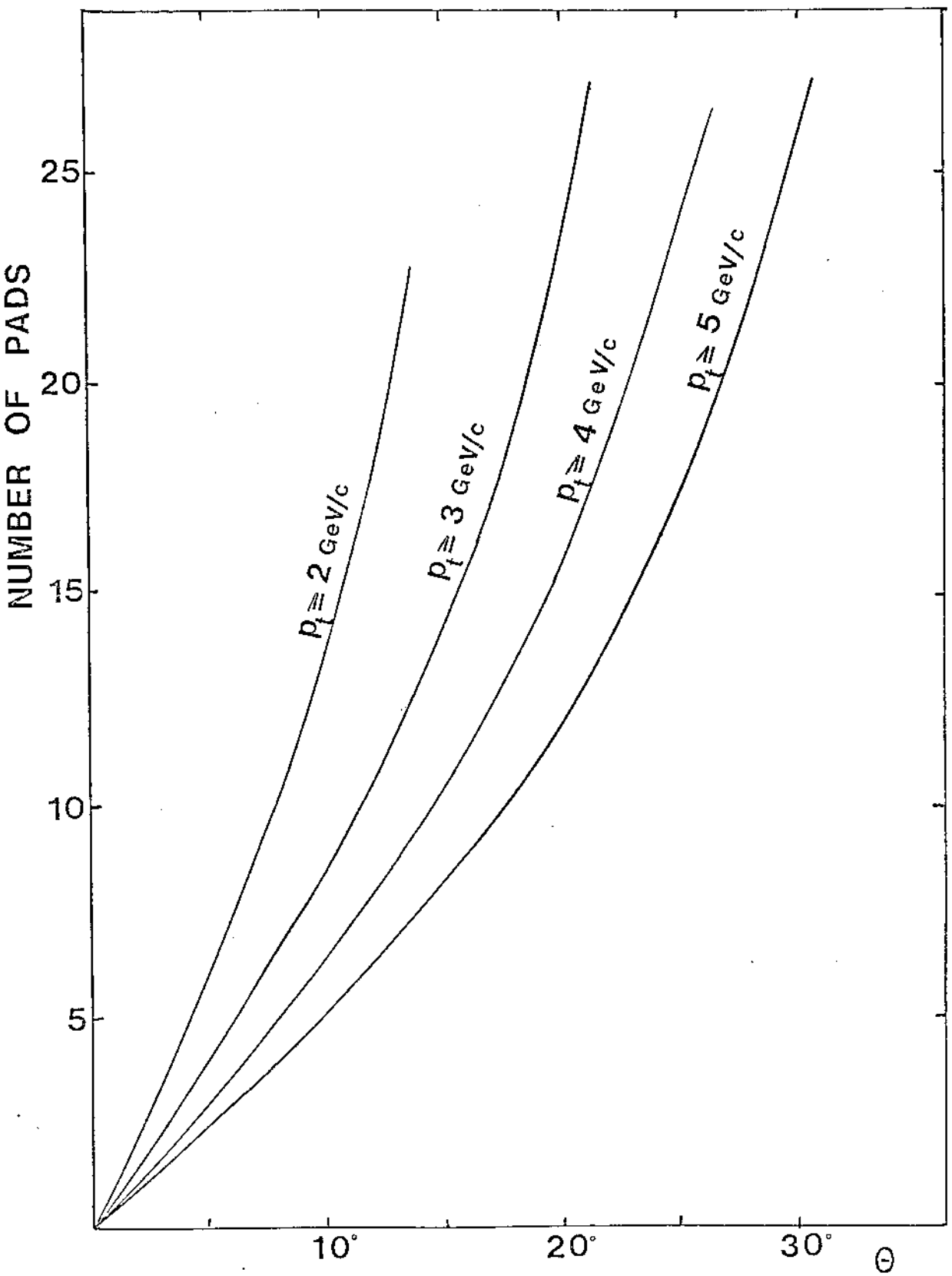
NUMBER OF PADS
25
20
15
10
5
10°
20°
30°
Θ
$p_t \geq 2$ GeV/c
$p_t \geq 3$ GeV/c
$p_t \geq 4$ GeV/c
$p_t \geq 5$ GeV/c

FIG. 33

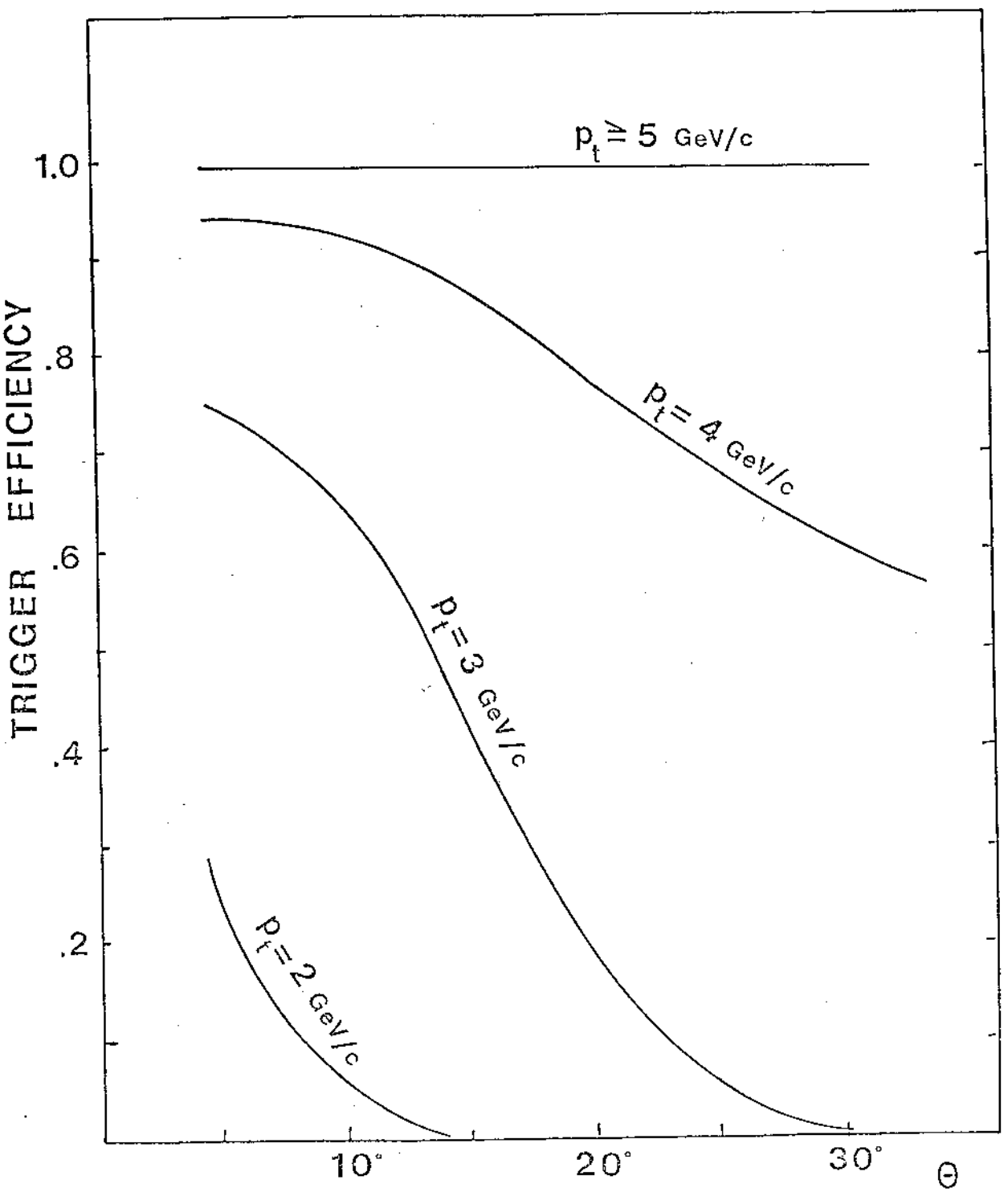
TRIGGER EFFICIENCY
1.0
.8
.6
.4
.2
$p_t \geq 5$ GeV/c
$p_t = 4$ GeV/c
$p_t = 3$ GeV/c
$p_t = 2$ GeV/c
10°
20°
30°
Θ

FIG. 34